

SANDIA REPORT

SAND2015-8886
Unlimited Release
September 2015

Criteria for initiation of delamination in quasi-static punch-shear tests of a carbon-fiber composite material

Eric B. Chin
Shawn A. English
Timothy M. Briggs

Prepared by
Sandia National Laboratories
Albuquerque, New Mexico 87185 and Livermore, California 94550

Sandia National Laboratories is a multi-program laboratory managed and operated by Sandia Corporation, a wholly owned subsidiary of Lockheed Martin Corporation, for the U.S. Department of Energy's National Nuclear Security Administration under contract DE-AC04-94AL85000.

Approved for public release; further dissemination unlimited.



Issued by Sandia National Laboratories, operated for the United States Department of Energy by Sandia Corporation.

NOTICE: This report was prepared as an account of work sponsored by an agency of the United States Government. Neither the United States Government, nor any agency thereof, nor any of their employees, nor any of their contractors, subcontractors, or their employees, make any warranty, express or implied, or assume any legal liability or responsibility for the accuracy, completeness, or usefulness of any information, apparatus, product, or process disclosed, or represent that its use would not infringe privately owned rights. Reference herein to any specific commercial product, process, or service by trade name, trademark, manufacturer, or otherwise, does not necessarily constitute or imply its endorsement, recommendation, or favoring by the United States Government, any agency thereof, or any of their contractors or subcontractors. The views and opinions expressed herein do not necessarily state or reflect those of the United States Government, any agency thereof, or any of their contractors.

Printed in the United States of America. This report has been reproduced directly from the best available copy.

Available to DOE and DOE contractors from

U.S. Department of Energy
Office of Scientific and Technical Information
P.O. Box 62
Oak Ridge, TN 37831

Telephone: (865) 576-8401
Facsimile: (865) 576-5728
E-Mail: reports@osti.gov
Online ordering: <http://www.osti.gov/scitech>

Available to the public from

U.S. Department of Commerce
National Technical Information Service
5301 Shawnee Rd
Alexandria, VA 22312

Telephone: (800) 553-6847
Facsimile: (703) 605-6900
E-Mail: orders@ntis.gov
Online order: <http://www.ntis.gov/search>



SAND2015-8886
Unlimited Release
September 2015

Criteria for initiation of delamination in quasi-static punch-shear tests of a carbon-fiber composite material

Eric B. Chin
Shawn A. English
Timothy M. Briggs
Sandia National Laboratories
P.O. Box 969
Livermore, CA 94551-0969

Abstract

Various phenomenological delamination initiation criteria are analyzed in quasi-static punch-shear tests conducted on six different geometries. These six geometries are modeled and analyzed using elastic, large-deformation finite element analysis. Analysis output is post-processed to assess different delamination initiation criteria, and their applicability to each of the geometries. These criteria are compared to test results to assess whether or not they are appropriate based on what occurred in testing. Further, examinations of CT scans and ultrasonic images of test specimens are conducted in the appendix to determine the sequence of failure in each test geometry.

ACKNOWLEDGMENTS

The authors are appreciative to those that contributed to this work and would like to specifically recognize the efforts of Tim Gilbertson and Alan Moore for composite laminate consolidation, Kevin Nelson for conducting the experiments, Karin Krafcik for performing the ultrasonic imaging, David Moore, Kyle Thompson, Carl Jacques and Burke Kernan for the computed tomography imaging, as well as Stacy Nelson for aid with experimental planning.

CONTENTS

1. Introduction.....	9
2. Testing.....	11
2.1 Material.....	11
2.2. Test procedure.....	11
2.3. Results.....	12
2.4. Discussion.....	16
2.4.1. Failure in SPR = 8, N = 6 test specimens	16
2.4.2. Failure in remaining test specimens.....	17
2.4.3. Failure mode at proportional limit	18
3. Analysis.....	21
3.1. Model information	21
3.1.1. Geometry.....	21
3.1.2. Material properties	22
3.1.3. Boundary conditions and loading	23
3.1.4. Element type	24
3.1.5. Constitutive model.....	24
3.1.6. Mesh refinement	25
3.2. Results.....	27
3.3. Failure criteria analysis	31
3.3.1. von Mises stress criterion.....	32
3.3.2. Maximum principal stress and strain criterion.....	33
3.3.3. Hashin/Rotem quadratic criterion.....	36
3.3.4. Yen/Caiazzo quadratic stress criterion.....	37
3.3.5. Yen/Caiazzo quadratic strain criterion.....	42
3.4. Discussion.....	45
4. Conclusion	47
5. References.....	49
Appendix A: Non-destructive evaluation of test specimens.....	51
A.1. Testing and evaluation	51
A.1.1. SPR = 2, N = 6 specimens	52
A.1.2. SPR = 2, N = 12 specimens	55
A.1.3. SPR = 2, N = 24 specimens	60
A.1.4. SPR = 8, N = 6 specimens	67
A.1.5. SPR = 8, N = 12 specimens	70
A.1.6. SPR = 8, N = 24 specimens	75
A.2. Example CT images.....	89
A.3. Observations and Trends.....	90
Distribution	91

FIGURES

Figure 1. Schematic of experimental setup.....	11
Figure 2. Force/displacement curves for SPR = 2, N = 6 test specimens.....	13
Figure 3. Force/displacement curves for SPR = 2, N = 12 test specimens.....	14
Figure 4. Force/displacement curves for SPR = 2, N = 24 test specimens.....	14
Figure 5. Force/displacement curves for SPR = 8, N = 6 test specimens.....	15
Figure 6. Force/displacement curves for SPR = 8, N = 12 test specimens.....	15
Figure 7. Force/displacement curves for SPR = 8, N = 24 test specimens.....	16
Figure 8. Typical force/displacement curve shape in SPR = 8, N = 6 geometry.....	17
Figure 9. Typical force/displacement curve shape in non-SPR = 8, N = 6 geometries.....	18
Figure 10. Example CUBIT specified geometry.....	22
Figure 11. Boundary conditions in the finite element model.....	24
Figure 12. Three levels of CFRP mesh refinement tested.....	26
Figure 13. Stress convergence with mesh refinement.....	27
Figure 14. Force/displacement curve in FEA and test results for SPR = 2, N = 6 geometry.....	28
Figure 15. Force/displacement curve in FEA and test results for SPR = 2, N = 12 geometry.....	29
Figure 16. Force/displacement curve in FEA and test results for SPR = 2, N = 24 geometry.....	29
Figure 17. Force/displacement curve in FEA and test results for SPR = 8, N = 6 geometry.....	30
Figure 18. Force/displacement curve in FEA and test results for SPR = 8, N = 12 geometry.....	30
Figure 19. Force/displacement curve in FEA and test results for SPR = 8, N = 24 geometry.....	31
Figure 20. Maximum von Mises stress at delamination initiation.....	33
Figure 21. Maximum principal stress at delamination initiation.....	34
Figure 22. Maximum principal strain at delamination initiation.....	35
Figure 23. Maximum Hashin/Rotem failure criteria at delamination initiation.....	37
Figure 24. Yen/Caiazzo failure criterion value as a function of ϕ	39
Figure 25. Yen/Caiazzo failure criterion in SPR = 2, N = 24 model with $\phi = 30^\circ$	40
Figure 26. Maximum Yen/Caiazzo stress failure criteria at delamination initiation.....	41
Figure 27. Yen/Caiazzo failure surface with max FCYC in each geometry plotted.....	42
Figure 28. Maximum Yen/Caiazzo strain failure criteria at delamination initiation.....	44
Figure 29. Yen/Caiazzo strain failure criterion value as a function of ϕ	45

TABLES

Table 1. Test specimen geometry.....	12
Table 2. Specific test specimen dimensions.....	21
Table 3. Isotropic material properties.....	22
Table 4. Orthotropic CFRP material properties.....	23
Table 5. Applied force to CFRP at delamination initiation.....	23
Table 6. Mesh refinement study on interlaminar regions of SPR = 2, N = 6 geometry.....	25
Table 7. Maximum von Mises stress value and location at delamination initiation.....	33
Table 8. Maximum principal stress value, location, and direction at delamination initiation.....	34
Table 9. Maximum principal strain value, location, and direction at delamination initiation.....	35
Table 10. Maximum Hashin/Rotem failure criterion and location at delamination initiation.....	37
Table 11. Assumed model parameters for the Yen/Caiazzo failure criterion.....	40

Table 12. Maximum Yen/Caiazzo failure criterion value at delamination initiation. 41
Table 13. Maximum Yen/Caiazzo strain failure criterion value at delamination initiation. 43

NOMENCLATURE

CFRP	carbon-fiber reinforced polymer
ILR	interlaminar region
N	number of layers of laminate
PST	punch-shear test
QS	quasi-static
S-BST	short-beam shear test
SNL	Sandia National Laboratories
SPR	span-to-punch ratio

1. INTRODUCTION

Carbon-fiber reinforced polymers (CFRP) are the material of choice in applications where structural integrity and component weight are important considerations. Compared to more traditional metal alloys, CFRPs offers similar strength and stiffness in a relatively lightweight package. However, while traditional metal alloys are generally treated as isotropic materials in analysis, carbon-fiber composites (and composite materials in general) are highly anisotropic, precluding such a treatment. Further complicating matters, there are a number of different ways composite materials can fail, requiring a variety of failure initiation criteria to be tracked as an analysis progresses. These failure initiation criteria can include fiber tensile, compressive, shear, and crush modes and delamination. While this document is limited to the understanding of delamination failure, extensive literature exists on describing and characterizing alternative modes of failure in composite materials (see References [7, 11-14], for example).

Understanding and accurately modeling the initiation of delamination failure in composite materials is critically important to ensuring the safety of composite components. Delamination causes a drastic reduction in in-plane compressive strength and shear modulus in composite materials. Further complicating the issue, delamination is difficult to detect in service, since delaminated composites generally have no change in exterior appearance. Therefore, accurate prediction of delamination analytically can speed inspection of components and lead to improved design of composite components.

A number of failure criteria exist for predicting initiation of delamination failure. Most criteria are based on quadratic interlaminar stresses. Specifically, out-of-plane tensile/compressive stress and shear stresses with an out-of-plane component. An early quadratic delamination failure criteria was developed in 1988 by Brewer and Lagace [1], based on a non-local stress criteria suggested by Kim and Soni [2]. This criteria tracks out-of-plane stresses individually, then takes the Euclidean norm of each component. This delamination failure criteria was improved by Yen and Caiazzo [3] in 2001. Their model accounts for increased shear strength when the interlaminar region experienced out-of-plane compression – an effect observed in experiments [4]. More recently, additional parameters have been proposed to the Yen and Caiazzo model by Xiao and Gillespie [5], which allow for improved fitting of test data as crush strength is approached.

To test prospective failure criteria, a number of different tests have been performed on composite materials. Hollow cylindrical specimens were used by deTeresa et al. [4] to characterize combined compressive plus shear response in interlaminar regions. Short-beam shear tests (S-BST) are another popular method of characterizing interlaminar failure resistance [6]. Xiao et al. used quasi-static (QS) punch-shear testing (PST) to characterize delamination, as well as a variety of other failure criteria, in Reference [7]. Similar to the S-BST, this geometry produces combined compression plus shear stress in interlaminar regions. However, unlike the S-BST, delamination is not accelerated by edge effects. For these reasons, QS PST is a favorable geometry to determine a delamination initiation criteria absent of edge effects and taking into account combined compression and shear loading.

In this document, finite element analyses to model a series of QS PSTs conducted at Sandia National Laboratories (SNL) are described. These analyses are compared to test results to determine an appropriate delamination initiation criteria.

2. TESTING

In order to test the validity of different delamination initiation criteria, quasi-static (QS) punch-shear tests (PST) of carbon-fiber composites are conducted. To understand failure modes present in different test specimens, high-resolution ultrasonic and CT imaging is performed. More in-depth information regarding these tests can be found in [15].

2.1 Material

The carbon-fiber reinforced polymer (CFRP) used in these tests is composed of eight-hardness satin (8HS) 3K AS4 fiber and UF3362 resin. The test fixture is machined from 6061 aluminum, the bolts are stainless steel, and the indenter is hardened steel. These items are illustrated schematically in Figure 1.

2.2. Test procedure

Renderings and pictures of the experimental apparatuses are shown in Figure 1.

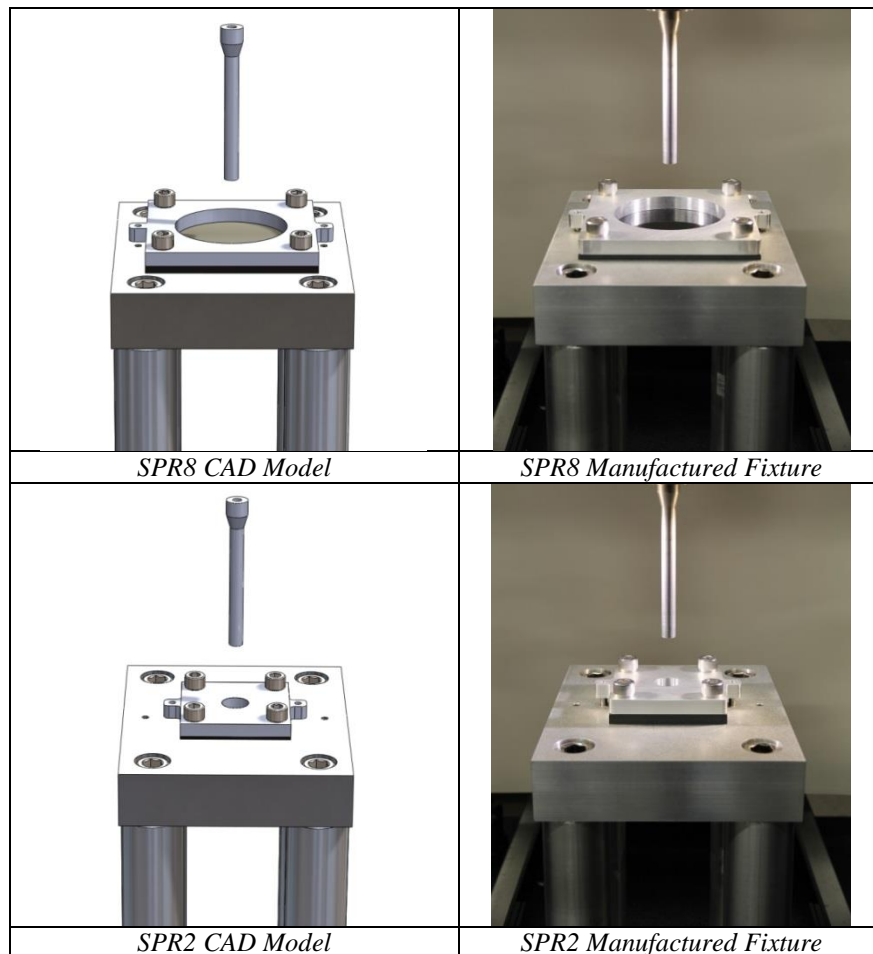


Figure 1. Schematic of experimental setup.

As each test progresses, the indenter is slowly moved down at constant rate through the CFRP. The movement of the indenter places compressive stress and shear stress in the out-of-plane direction of the CFRP. The rate of movement is sufficiently slow such that rate effects are negligible. For the duration of the test, the total displacement of the indenter, as well as the force on the indenter, are measured and recorded. While some tests are run until complete failure of the test specimen, the majority of tests are halted before complete failure occurs. In these tests, the specimens are unloaded and the force and displacement upon unloading are recorded. Since delamination does not result in complete failure of the material, the tests that are not run to complete failure provide useful information in developing delamination initiation criteria.

The tests are run on six different geometries, which are listed in Table 1. In these geometries, the span/punch ratio (SPR) varies from 2 to 8, and the number of layers of laminate (N) varies from 6 to 24. Four to eight specimens are tested for each geometry. The quantities of test specimens for each geometry are listed in Table 1.

Table 1. Test specimen geometry.

Span/punch ratio (SPR)	Layers of laminate (N)	# of test specimens
2	6	5
2	12	5
2	24	5
8	6	4
8	12	5
8	24	8

2.3. Results

The force/displacement curves for each of the test specimens in the six test geometries are displayed in Figures 2 through 7. While the curves vary slightly from specimen to specimen, for the most part they share a general shape. With the exception of the SPR = 8, N = 6 geometry, all tests begin with a linear force/displacement relationship, until a proportional limit is reached. At this point, a loss of flexural stiffness is observed, resulting in a 20 to 40 percent loss in load. From here, the stiffness rebounds and increases non-linearly to a peak load much higher than the load observed in the proportional limit (slightly more than double the loading in all cases except for the SPR = 8, N = 6 case). Following this, the load dramatically decreases, and the test specimen is considered to be completely failed. For specimens not loaded to complete failure, a smooth, non-linear force/displacement curve is observed on unloading in all specimens loaded past the proportional limit. For test specimens not loaded past the proportional limit, unloading generally occurs elastically.

The SPR = 8, N = 6 case is unique among the geometries tested. In this geometry, flexural stiffness increases with increasing displacement. No region of linear force/displacement behavior is observed. At about 5 kN of load, an extremely small region of stiffness loss is observed in all test results. This region is barely visible in Figure 5, but confirmed to exist by examining load/displacement tables generated during testing. At an indenter displacement of roughly 6.25 mm, the load dramatically decreases and the test specimen is considered completely

failed. Elastic damage, plastic deformation, and frictional forces cause the unload path to deviate from the load path in the force/displacement curve.

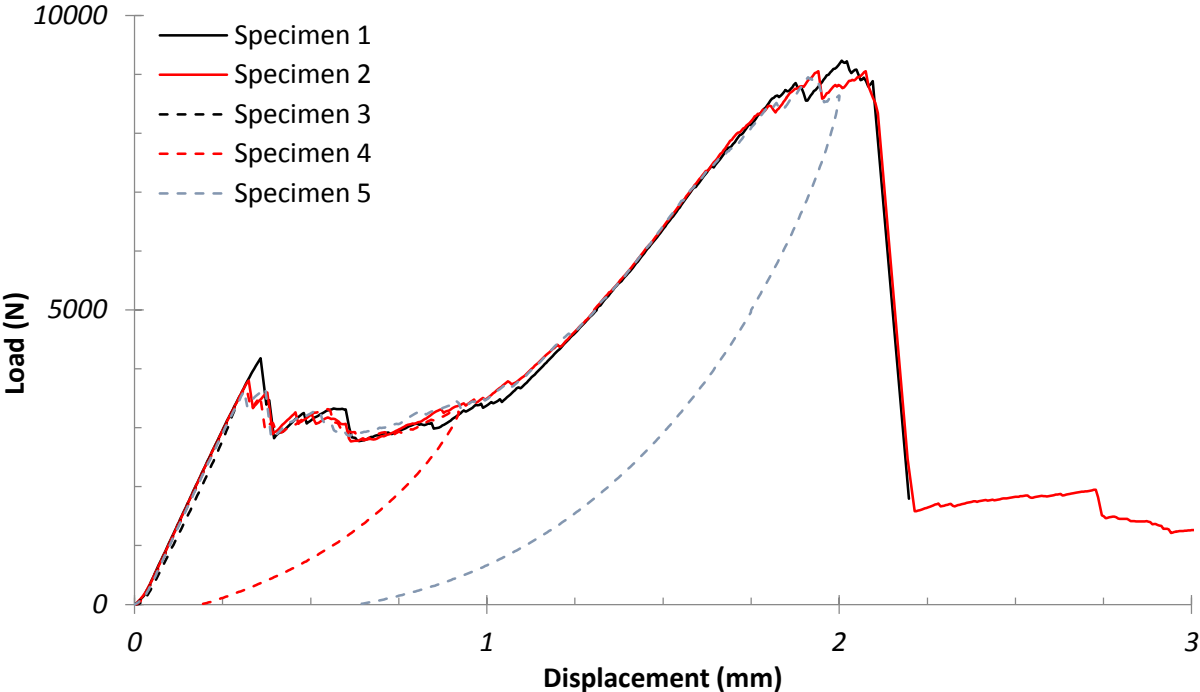


Figure 2. Force/displacement curves for SPR = 2, N = 6 test specimens.

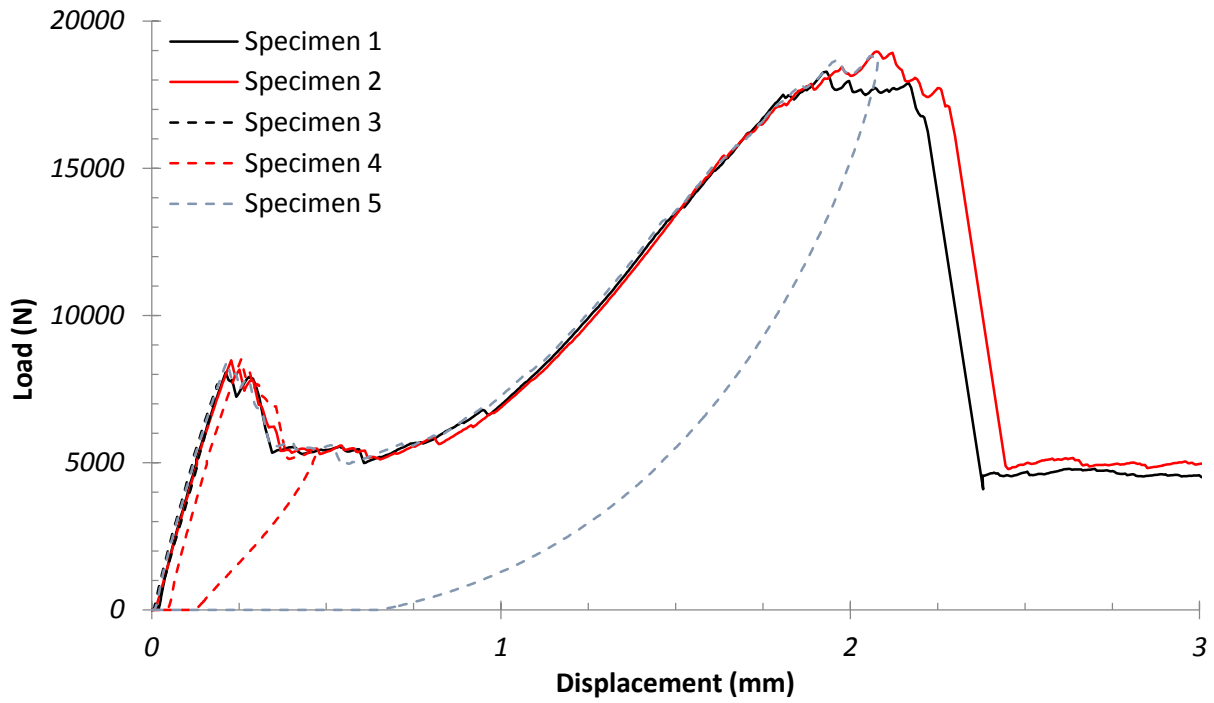


Figure 3. Force/displacement curves for SPR = 2, N = 12 test specimens.

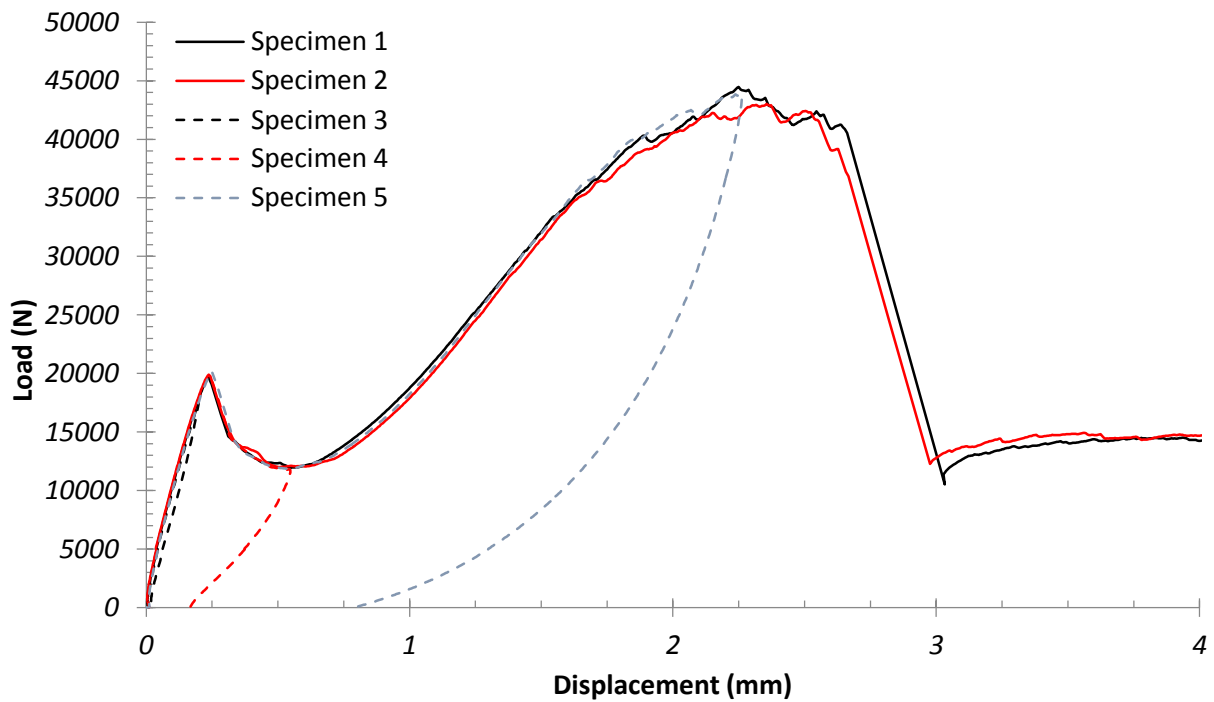


Figure 4. Force/displacement curves for SPR = 2, N = 24 test specimens.

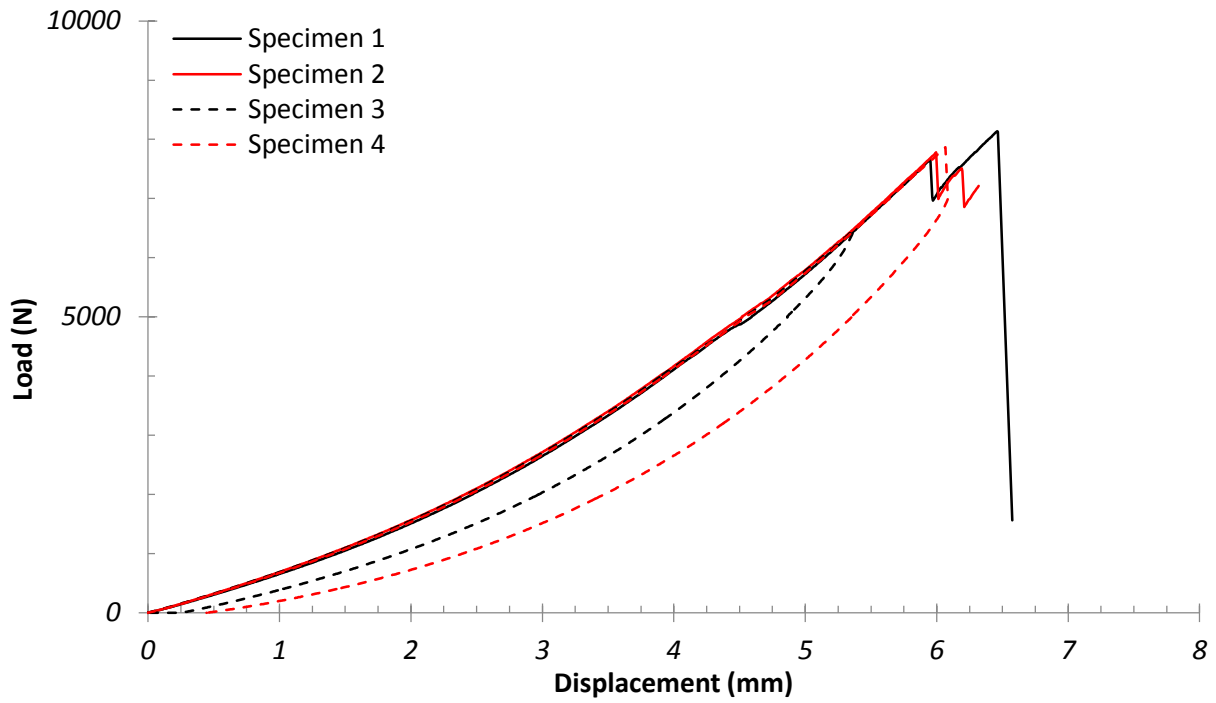


Figure 5. Force/displacement curves for SPR = 8, N = 6 test specimens.

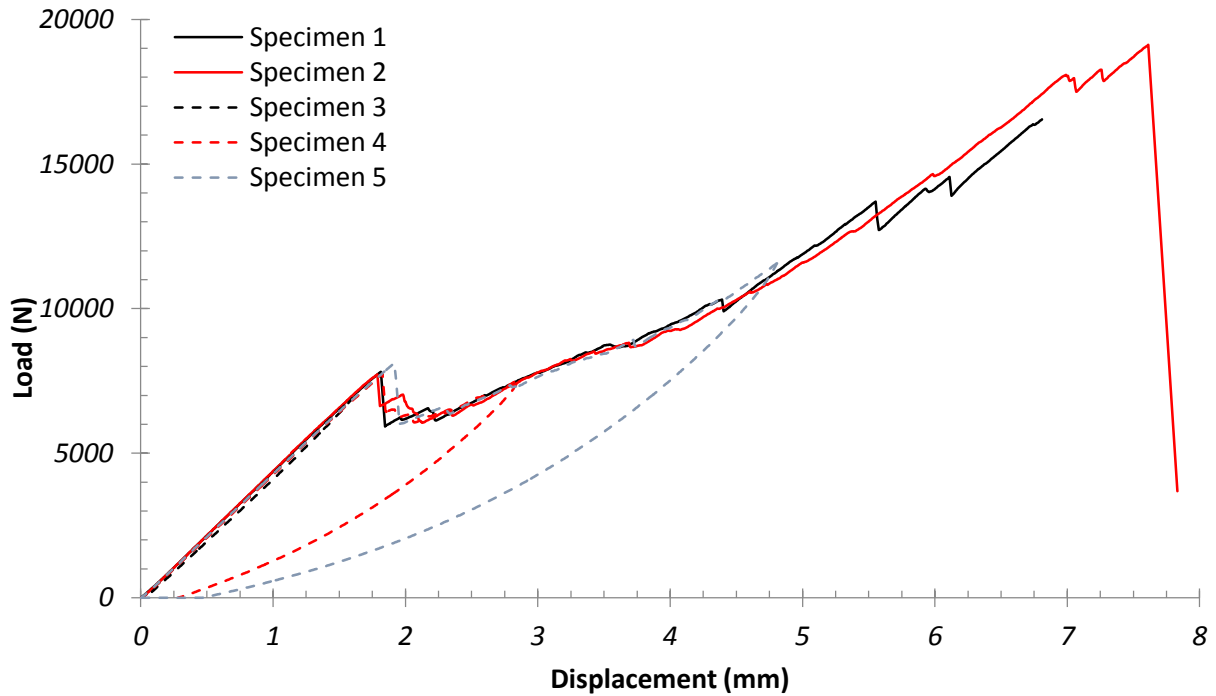


Figure 6. Force/displacement curves for SPR = 8, N = 12 test specimens.

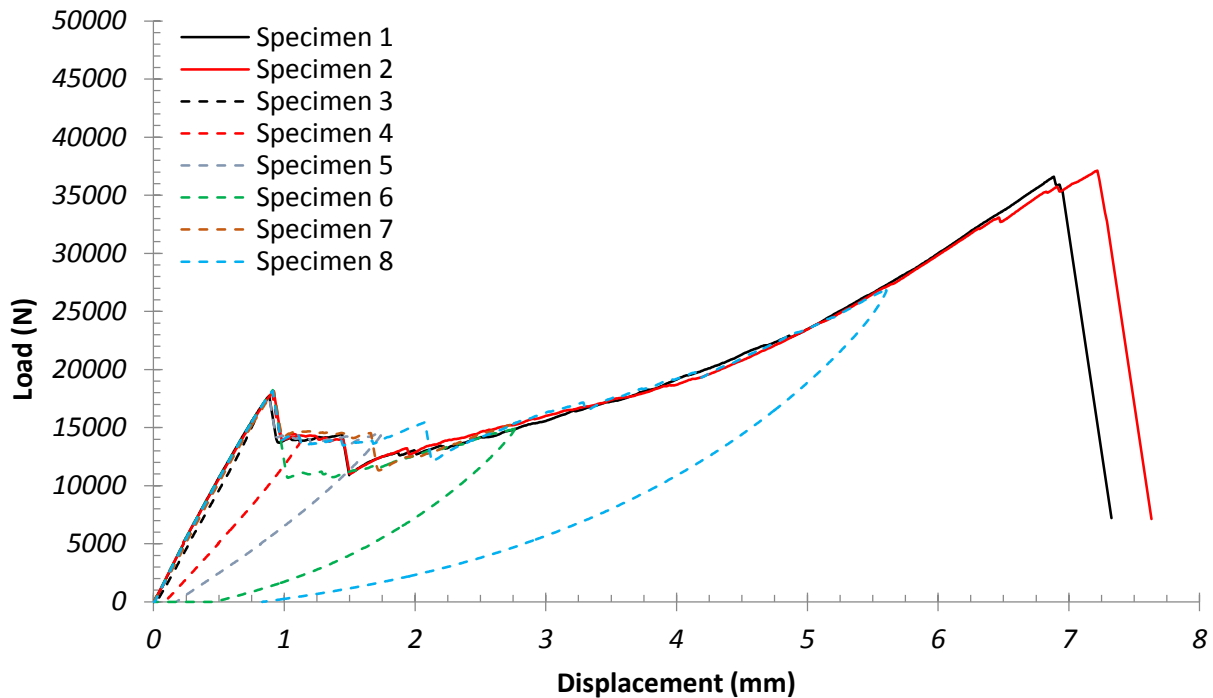


Figure 7. Force/displacement curves for SPR = 8, N = 24 test specimens.

To determine the causes behind the various critical points in the force/displacement curves, non-destructive evaluations of each test specimen were conducted. These evaluations included CT scans and ultrasonic imaging. Based on these evaluations, a general sequence of failure is compiled in each of the test specimen geometries. This failure sequence is described in Section 2.4 below. More detail on the CT scans and ultrasonic imaging can be found in Appendix A.

2.4. Discussion

In this section, possible sequences of failure, based on test results and evaluations in Appendix A, are postulated and discussed. First, the failure sequence in the SPR = 8, N = 6 test geometry (which had a unique force/displacement curve) is discussed. Then the failure sequence in the remaining test geometries is described. Finally, the exact failure mode that occurs at the proportional limit of loading is posited.

2.4.1. Failure in SPR = 8, N = 6 test specimens

A typical force/displacement curve is pictured in Figure 8 for the SPR = 8, N = 6 geometry. This was the only test specimen geometry to have a completely unique force/displacement curve. A large SPR combined with a thin test specimen resulted in relatively high in-plane tensile stresses and relatively low out-of-plane shear stresses, resulting in a different sequence of failure. Two key points in this curve are identified in Figure 8. At these points, the following occurs in the test specimen:

- **Point A** – Initial indentation, cracking, and delamination form in the immediate vicinity of the indenter. This damage only affects the first couple of layers of the laminate. The remainder of the test specimen remains intact.
- **Point B** – Damage progresses to the bottom layers of laminate in the test specimen. Punch through failure occurs, and load carrying capacity is severely diminished. Even at point B, delamination is limited to regions immediately in the vicinity of damaged regions of laminate.

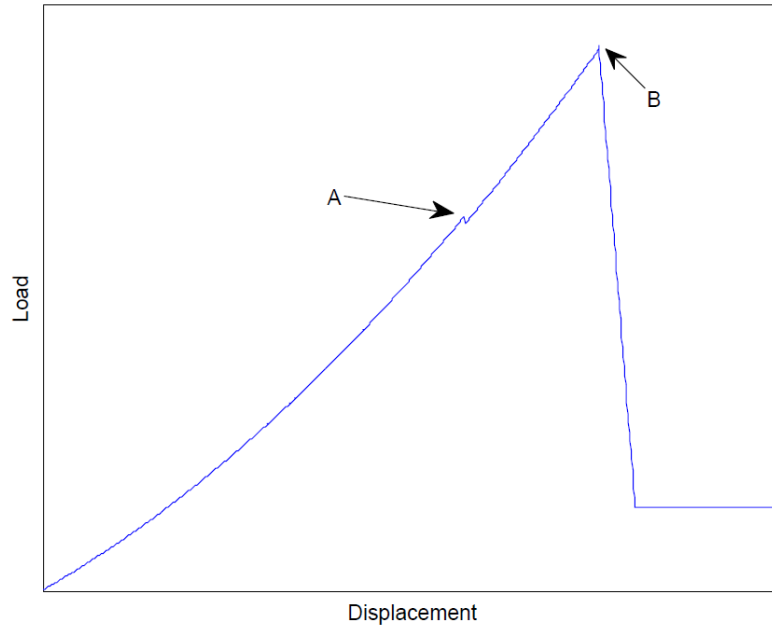


Figure 8. Typical force/displacement curve shape in SPR = 8, N = 6 geometry.

While delamination does not have a large effect on the load-carrying capacity of test specimens in this geometry, a delamination initiation criteria should be met in regions in the immediate vicinity of the indenter. Were a delamination propagation criteria implemented, it should not result in large-scale delamination in this geometry.

2.4.2. Failure in remaining test specimens

A typical force/displacement diagram is shown in Figure 9 for all test specimen geometries other than SPR = 8, N = 6. On this figure, the three critical points in the curve are labeled A, B, and C. At each of these points in the curve, the following is happening to the test specimen:

- **Point A** – Initiation of delamination failure in the test specimen and out-of-plane crush failure in fiber/matrix regions surrounding the indenter. From test results alone, it's unclear whether delamination or crush failure occurs first, or whether both occur at the same time. Based on imaging of the test specimens, large-scale delamination generally initiates in interlaminar regions about half way to two-thirds of the way through the thickness of the CFRP. Delamination also occurs in interlaminar regions immediately adjacent to regions that have undergone crush failure.
- **Point B** – Continuation of delamination failure. In SPR = 2 specimens, delamination is complete once the constant stiffness region between point B and point C is reached. In SPR = 8 specimens, delamination continues roughly until point C is reached.

- Point C** – Stiffness reduces as point C is approached in the SPR = 2 specimens. This reduction in stiffness is caused by the indenter progressing further through the sample. Matrix and fiber failure progress in the out-of-plane direction as point C is reached and passed. In comparison, the region of stiffness reduction is much smaller in the SPR = 8 specimens, indicating failure here occurs more suddenly. Eventually, a sharp drop in load carrying capacity after point C signifies the point when the indenter has punched through all layers of lamina. Residual load carrying capacity is due to friction.

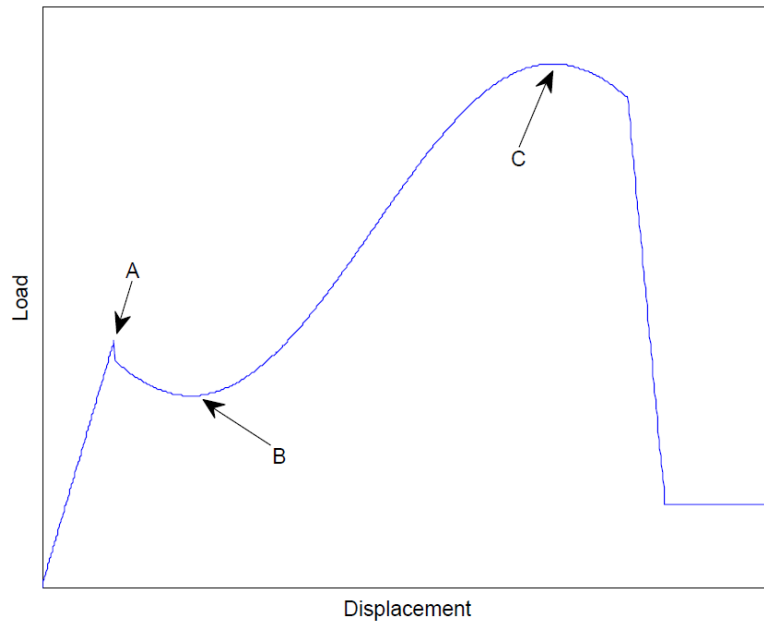


Figure 9. Typical force/displacement curve shape in non-SPR = 8, N = 6 geometries.

2.4.3. Failure mode at proportional limit

All test specimens loaded past point A in Figure 9 exhibit both matrix (and some possible fiber) crushing near the indenter radius (due to out-of-plane forces from the indenter) and delamination both around the indenter and in interlaminar regions near the center of the test specimen. Since no test specimen contained only one of these modes of failure, the hypothesized mode of failure is a combination of both failure modes. Specifically, out-of-plane failure is presumed to occur first; however, when this out-of-plane failure occurs, additional shear and tensile forces are incurred in the interlaminar regions, causing immediate delamination both around the indenter and in regions of high shear at the center of the test specimen. As evidenced by the SPR = 8, N = 6 specimen, out-of-plane punching failure from the indenter without delamination does not cause considerable loss in load carrying capacity of the test specimen. Further, in the SPR = 2, N = 24 specimen, some damage is indicated in ultrasonic imaging before point A in Figure 9 is reached. Since no out-of-plane crushing is demonstrated in CT scans, this demonstrates that local delamination near the indenter radius alone does not cause a loss in proportionality of the load/displacement curve. Therefore, large-scale delamination near the center of the test specimen caused by out-of-plane failure is most likely the specific cause for loss of proportionality in the load/displacement curve.

Assuming this hypothesis to be true, the most accurate method of analyzing delamination failure criteria would be to first accurately model out-of-plane fiber/matrix crush damage, followed by delamination. This type of analysis will be handled in a future document. In this document, finite element analysis will be conducted assuming delamination is the first failure mode in the CFRP, similar to the procedure of Reference [7]. Conducting the analysis in this fashion greatly simplifies the analysis procedure, since only linear elastic finite element analysis is needed. Furthermore, this type of analysis allows for different delamination initiation criteria to be rapidly evaluated, and a relatively accurate criterion to be developed before more complicated modeling is pursued. The analysis procedure is described in the section that follows.

3. ANALYSIS

Finite element analysis was conducted on the six test specimen geometries. The analysis procedure and results are presented herein. The section concludes with comparison of various delamination failure criteria, and their ability to match test results.

3.1. Model information

Linear elastic, large deformation finite element models were run in Sierra/SolidMechanics (Sierra/SM) version 4.36, the Lagrangian, three-dimensional, implicit code developed at SNL [8]. Linear elastic finite element models are sufficient for developing delamination initiation criteria since it is the first failure mechanism to cause non-linear behavior in geometries with delamination present. Model geometry was developed in CUBIT 14.1, a software toolkit for generation of finite element meshes developed at SNL.

3.1.1. Geometry

The testing apparatus and material anisotropy required a quarter-symmetry three-dimensional finite element model to properly capture all anticipated effects in the test. While a two-dimensional axisymmetric model would suffice to model the test setup, the orthotropic CFRP required a fully three-dimensional model to properly tabulate state variables in the model.

The CUBIT-developed quarter-symmetry geometry for the $SPR = 2, N = 6$ model is shown in Figure 10. The indenter (punch) is designed to slowly descend into the CFRP as the model is run. Fixtures on the top and bottom of the test setup hold the CFRP in place as the indenter moves. While the actual tests have much larger fixtures and bolts to hold to CFRP in place, including these in the finite element model had minimal effect on the analysis. Measurements of each of the critical dimensions of each geometry are listed in Table 2.

Table 2. Specific test specimen dimensions.

Model	Laminate thickness (mm)	Indenter radius (mm)	Indenter fillet radius (mm)	Fixture inner radius (mm)
SPR = 2, N = 6	2.12	6.35	0.25	12.70
SPR = 2, N = 12	4.21	6.35	0.25	12.70
SPR = 2, N = 24	8.50	6.35	0.25	12.70
SPR = 8, N = 6	2.13	6.35	0.25	50.80
SPR = 8, N = 12	4.25	6.35	0.25	50.80
SPR = 8, N = 24	8.50	6.35	0.25	50.80

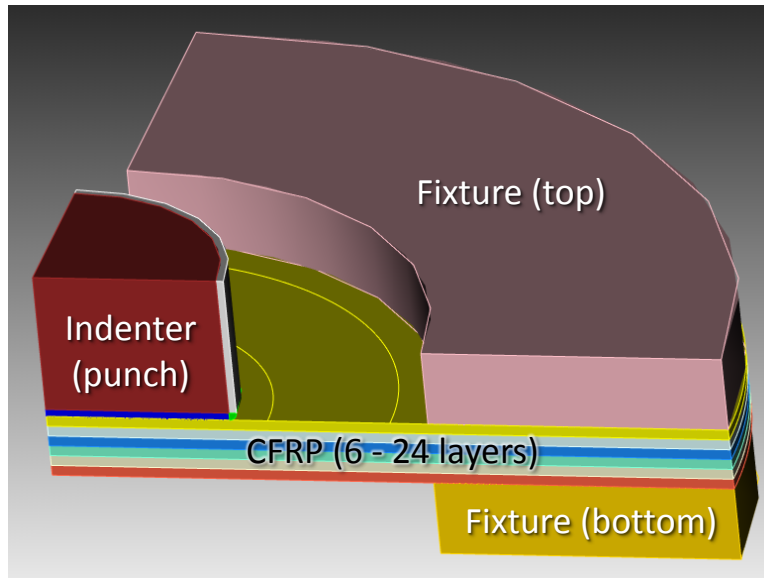


Figure 10. Example CUBIT specified geometry.

3.1.2. Material properties

Four different materials are used in the finite element model corresponding to these different regions:

- Indenter – hardened steel (isotropic),
- Fixture – 6061 aluminum¹ (isotropic),
- Carbon-fiber reinforced polymer – 8HS 3K AS4 fiber with UF3362 resin (orthotropic),
- Interlaminar region – UF3362 resin (isotropic).

The material properties for the isotropic materials are listed in Table 3. For the orthotropic CFRP, material properties are listed in Table 4.

Table 3. Isotropic material properties.

Material	Young's modulus (E) (MPa)	Poisson's ratio (ν)	Density (tonnes/mm ³)
Hardened steel	200,000	0.24	7.80×10^{-9}
6061 aluminum	68,900	0.33	2.70×10^{-9}
UF3362 resin	3,450	0.35	1.85×10^{-9}

¹ Fixture is erroneously modeled as hardened steel in the finite element analyses conducted herein. However, this is verified to have minimal impact on results presented in this document.

Table 4. Orthotropic CFRP material properties.

E ₁₁ (MPa)	63,900
E ₂₂ (MPa)	62,700
E ₃₃ (MPa)	8,585
G ₁₂ (MPa)	3,463
G ₁₃ (MPa)	3,265
G ₂₃ (MPa)	3,250
v ₁₂	0.048
v ₁₃	0.4075
v ₂₃	0.4080
Density (tonnes/mm ³)	1.52 × 10 ⁻⁹

3.1.3. Boundary conditions and loading

Boundary conditions in the finite element model are illustrated in Figure 11. The top and bottom fixtures are fixed in the y -direction (the out-of-plane direction), an x -symmetry boundary condition is placed on the $x = 0$ plane, and a z -symmetry boundary condition is placed on the $z = 0$ plane.

Rather than loading the indenter directly, load is induced by applying a displacement to the top of the indenter. This displacement varies from model to model, depending on the total displacement exhibited on the force/displacement curve before the proportional limit is reached in testing. Finite element models are conducted with indenter displacements ranging from 0.5 mm in the SPR = 2 models to 2 mm in the SPR = 8, N = 12 model. While delamination is not a major factor in the force/displacement response of the SPR = 8, N = 6 model, an elastic model is run on this configuration to a total indenter displacement of 8 mm.

In all models, the total displacement is subdivided into 100 time steps to track the force/displacement response as displacement increased. Field variables and history variables are tracked and recorded at each time step. To analyze the stress and strain state of the model at initiation of delamination failure, the average applied force at delamination initiation is calculated for each model geometry based on test results. Then, state variables are linearly interpolated at this force and each failure criterion is calculated using these interpolated values. Table 5 lists the applied force at delamination initiation for each model geometry.

Table 5. Applied force to CFRP at delamination initiation.

Model	Force (N)	Standard Deviation (N)
SPR = 2, N = 6	3,819	254
SPR = 2, N = 12	8,362	204
SPR = 2, N = 24	19,878	197
SPR = 8, N = 6	4,995*	3*
SPR = 8, N = 12	7,847	177
SPR = 8, N = 24	18,000	221

*Force to point A in Figure 8 (initial punch-through of indenter and delamination adjacent to regions of punch-through failure).

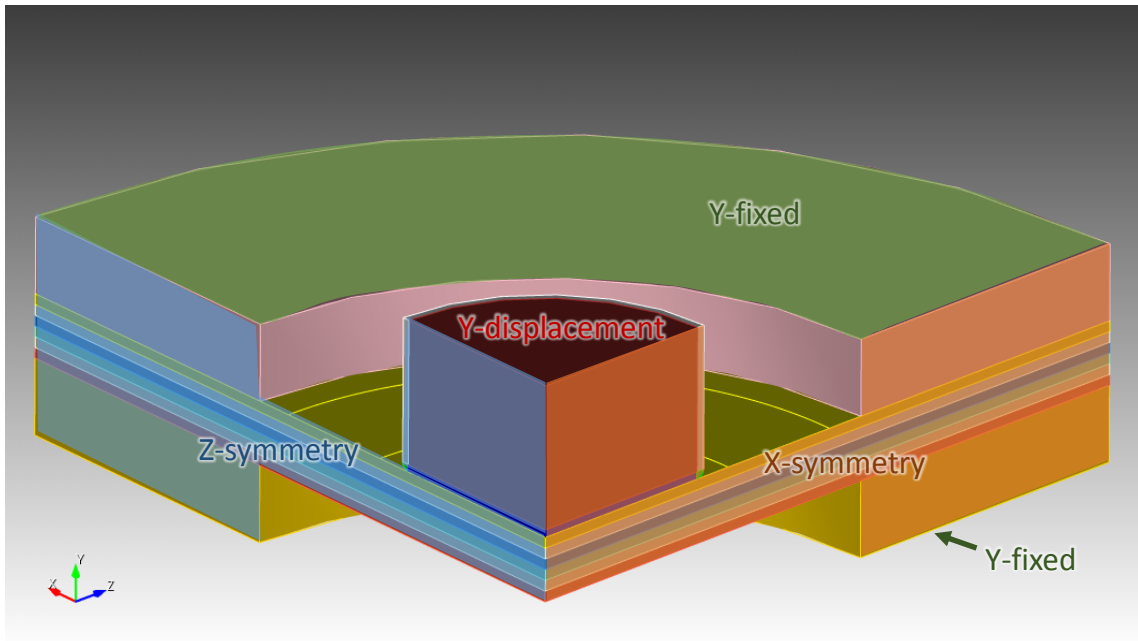


Figure 11. Boundary conditions in the finite element model.

Interactions between the indenter, the CFRP, and the fixture are modeled using contact. In general, master surfaces are selected on the fixture and the indenter, while slave surfaces are created on the composite. Friction between surfaces is enabled, with a coefficient of friction of 0.3 in all contact relationships. Additionally, frictionless general contact is enabled to limit interpenetration in interlaminar localization elements (these elements are described in the following section).

3.1.4. Element type

With the exception of interlaminar regions, all elements are eight node hexahedral elements with reduced integration. In the interlaminar region, localization elements [9] are used. These elements are similar to cohesive zone elements in that they both are initially zero volume and have length scale defined through an additional field variable. However, localization elements provide fully populated stress and strain tensors and a complete constitutive relationship. In contrast, cohesive zone elements only require a traction-separation relationship in the element. In all analyses, an interlaminar thickness of 0.0127 mm is presumed [10]. To test the effect of interlaminar thickness, models with a presumed interlaminar thickness of 0.127 mm are also analyzed. These models demonstrate lower overall stiffness compared to test results.

3.1.5 Constitutive model

A Kirchhoff material is assumed for the lamina. This is considered an appropriate choice for large deformation, small strain materials, which is how the CFRP specimens are expected to deform. This constitutive relationship is of the form

$$\mathbf{S} = \mathbf{C}:\mathbf{E}$$

where \mathbf{S} is the 2nd Piola-Kirchhoff stress and \mathbf{E} is the Green-Lagrange strain. \mathbf{C} is a 4th order tensor of material constants, which are defined similarly to the small deformation, linear elastic 4th order tensor of elastic moduli.

While the constitutive model is based on \mathbf{S} and \mathbf{E} , delamination initiation criteria are measured in terms of the unrotated Cauchy stress ($\hat{\boldsymbol{\sigma}} = \mathbf{R}^T \boldsymbol{\sigma} \mathbf{R}$) and the unrotated log strain ($\hat{\boldsymbol{\varepsilon}} = \ln \sqrt{\mathbf{F}^T \mathbf{F}}$). These quantities can be transformed via the following relationships:

$$\mathbf{S} = J\mathbf{U}^{-1}\hat{\boldsymbol{\sigma}}\mathbf{U}^{-T} \quad \text{and} \quad \mathbf{E} = \frac{1}{2}\left((e^{\hat{\boldsymbol{\varepsilon}}})^2 - \mathbf{I}\right)$$

where \mathbf{F} is the deformation gradient, J is the determinant of the deformation gradient, and \mathbf{U} is the right stretch tensor. Since small strains are assumed in these analyses, the difference between stress and strain measures used in this document versus the standard Kirchhoff material measures are anticipated to be minimal.

3.1.6. Mesh refinement

Discretization errors are quantified through mesh refinement studies on the SPR = 2, N = 6 model. Three different levels of mesh refinement are tested, and interlaminar out-of-plane stresses from various points in the model, as well as maximum/minimum interlaminar out-of-plane (y-direction) stresses in each of the three models, are listed in Table 6. Since the models are elastic, the models are compared after exactly 50% of the total indenter displacement has been applied (0.25 mm). Meshes of the CFRP material are illustrated for all three mesh refinements in Figure 12.

Table 6. Mesh refinement study on interlaminar regions of SPR = 2, N = 6 geometry.

Location	Least refinement (MPa)	Medium refinement (MPa)	Most refinement (MPa)
σ_{yy} , max (@ bottom layer)	13.583	13.450	13.361
σ_{yy} , min (@ top layer, under indenter)	-10.631	-11.586	-11.639
σ_{yy} , top layer just outside indenter	-5.444	-6.198	-6.417
σ_{yy} , top layer, center	-0.346	-0.377	-0.407
σ_{yy} , bottom layer, just outside indenter	12.955	12.867	12.888

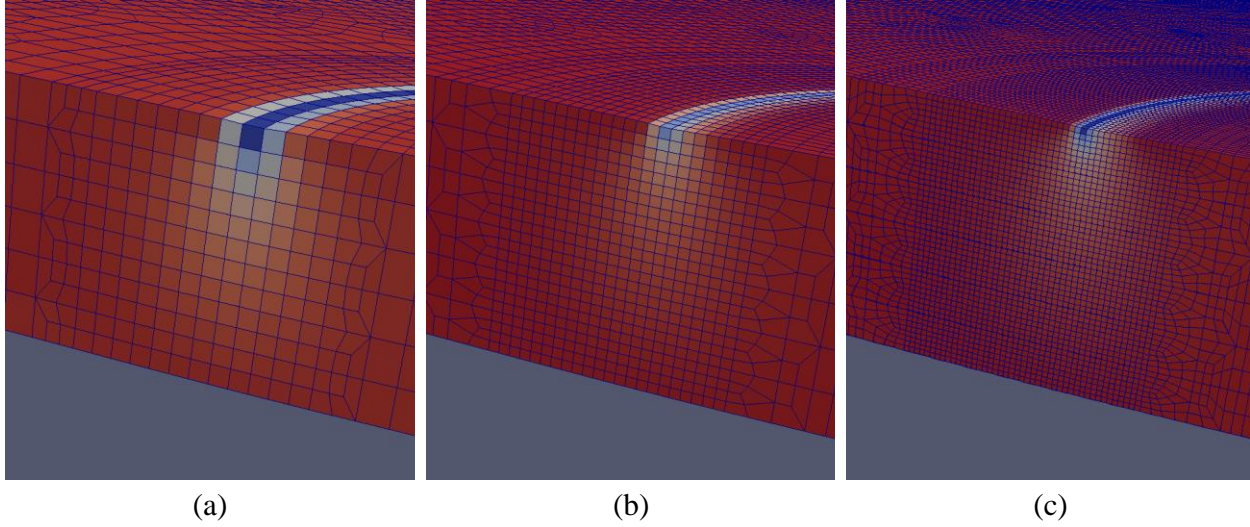


Figure 12. Three levels of CFRP mesh refinement tested.

Figure 13 illustrates relative discretization error versus relative mesh size. Relative mesh size is measured as the relative length of the sides of one of the elements. For example, a value of unity represents the “Most refinement” mesh, while a value of two would indicate an element with twice the length on each dimension (“Medium refinement”), and an overall volume eight times larger. The rate of mesh convergence for a uniform mesh refinement factor r and metrics for each mesh refinement f , is given as

$$p = \frac{\ln\left(\frac{f_3 - f_1}{f_2 - f_1}\right)}{\ln(r)}.$$

Then the percent relative discretization error (RDE) is estimated by

$$\%RDE = \frac{f_k - f_{exact}}{f_{exact}} \times 100\%,$$

where the exact value is estimated from Richardson’s extrapolation as

$$f_{exact} \approx f_1 + \frac{f_1 - f_2}{r^p - 1}.$$

In the measurement of out-of-plane stress at the bottom of the composite specimen, a consistent trend is not observed with increasing mesh refinement. Since all three measurements of stress varied 0.6% at most, stresses measured here are considered to be mesh insensitive and the error is small.

While the “Least refinement” mesh is able to capture some of the stress values relatively accurately, the “Medium refinement” mesh is needed to capture more accurate stresses in the vicinity of the indenter – where the stress gradient is the highest. Additional refinement in the

“Most refinement” mesh demonstrates relative accuracy (and adequacy) of the “Medium refinement” mesh. Stress values in the highly refined mesh are nearly identical to the mesh with medium refinement, even in the regions under the indenter. Figure 13 demonstrates these trends more quantitatively. In Figure 13, a maximum RDE of 16% is observed in the points sampled on the medium refinement mesh. However, this point (the top of the composite sample, under the punch) has relatively small stresses leading to small changes in stress giving large discretization errors. Furthermore, even the “Most refinement” mesh demonstrated 7% RDE in stresses measured at this point. In all other points sampled, RDE is under 5% for both the medium and most refined meshes.

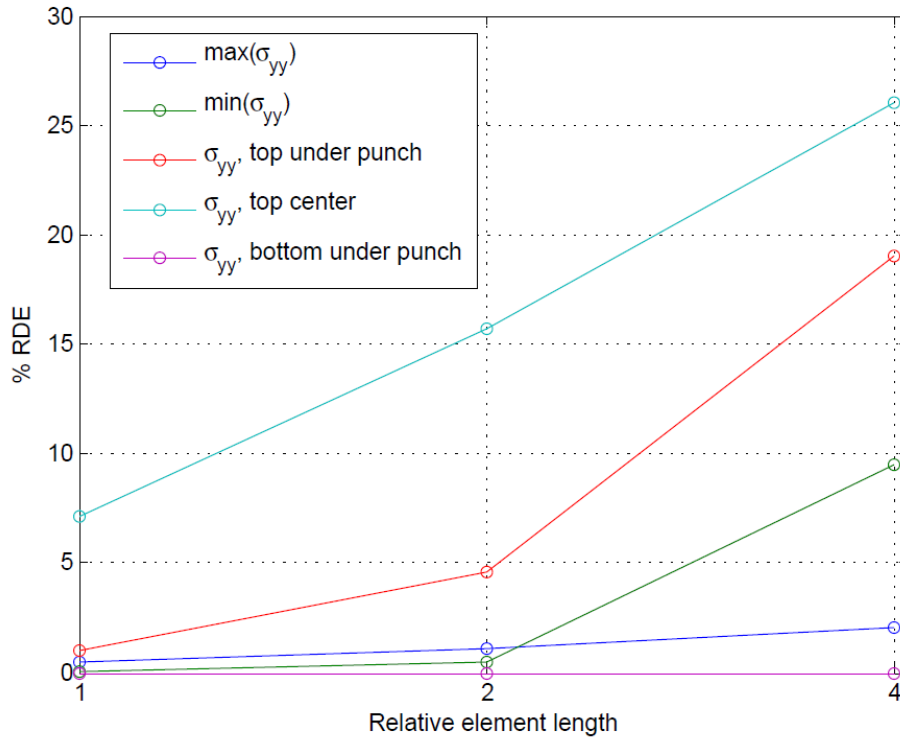


Figure 13. Stress convergence with mesh refinement.

3.2. Results

From the finite element analysis results, indenter force/displacement curves are created and compared to test results in Figure 14 through Figure 19. In the SPR = 2, N = 12 and SPR = 2, N = 24 models, the FEA results match test results very well. FEA of the remaining test geometries match somewhat well, but FEA exhibited stiffness up to 17 percent higher than stiffness from test results. Test specimens that did not match FEA were generally model geometries which contained relatively high in-plane tensile stresses. To better match test results, the in-plane stiffness of the lamina or the stiffness of the interlaminar region could be modified, or the contact relationship could be modified to reduce friction between the clamp and the CFRP specimen. However, since no specific information as to which parameter should be modified is available, none of these parameters were changed in this report.

In the $SPR = 2, N = 6$ geometry, stiffness “ramps” up before a constant rate of stiffness is obtained at a displacement of approximately 0.04 mm. This is caused by a preload applied to the test specimen. Had no preload been applied, the stiffness would have been linear at the initiation of the test. However, the observed linear force/displacement relationship after ramp up has completed is the same regardless of whether or not a preload is applied. To eliminate the effect of the preload in the analysis, the proportional limit of the geometry is selected based on applied load, rather than displacement.

The FEA model of the $SPR = 8, N = 24$ geometry is very large, and the analysis could not be completed to the desired indenter displacement. Therefore, the results that are available will be linearly extrapolated to the desired location on the force/displacement curve. Stresses and strains will be extrapolated similarly. Based on the nearly constant stiffness in the force/displacement curve both in test results and the analysis results that are available, minimal error is expected from this approximation. Specifically, the model is run to 6776 N of load on the indenter and an indenter displacement of 0.31 mm.

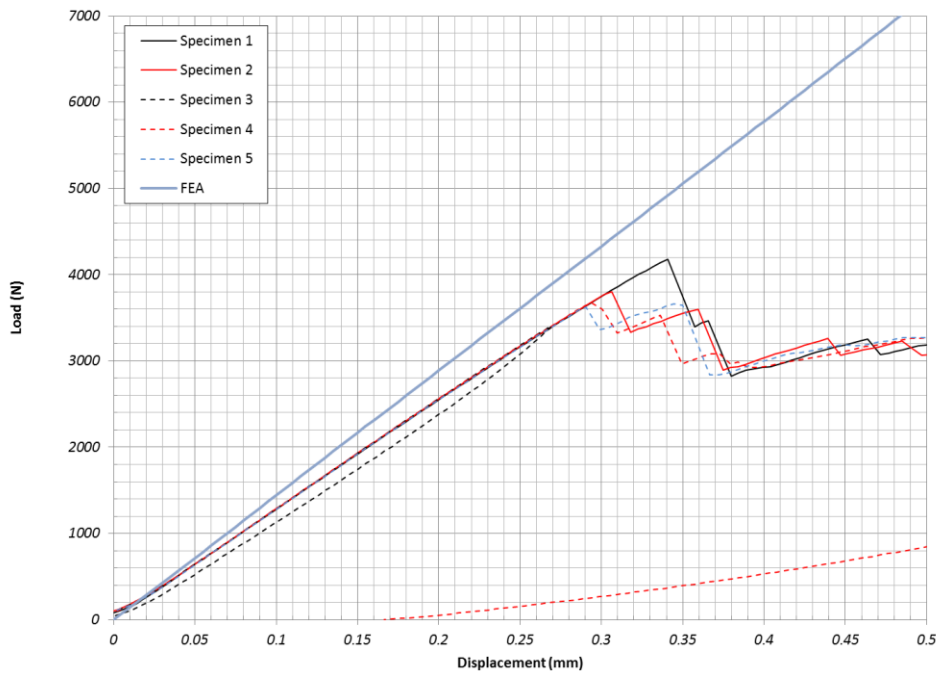


Figure 14. Force/displacement curve in FEA and test results for $SPR = 2, N = 6$ geometry.

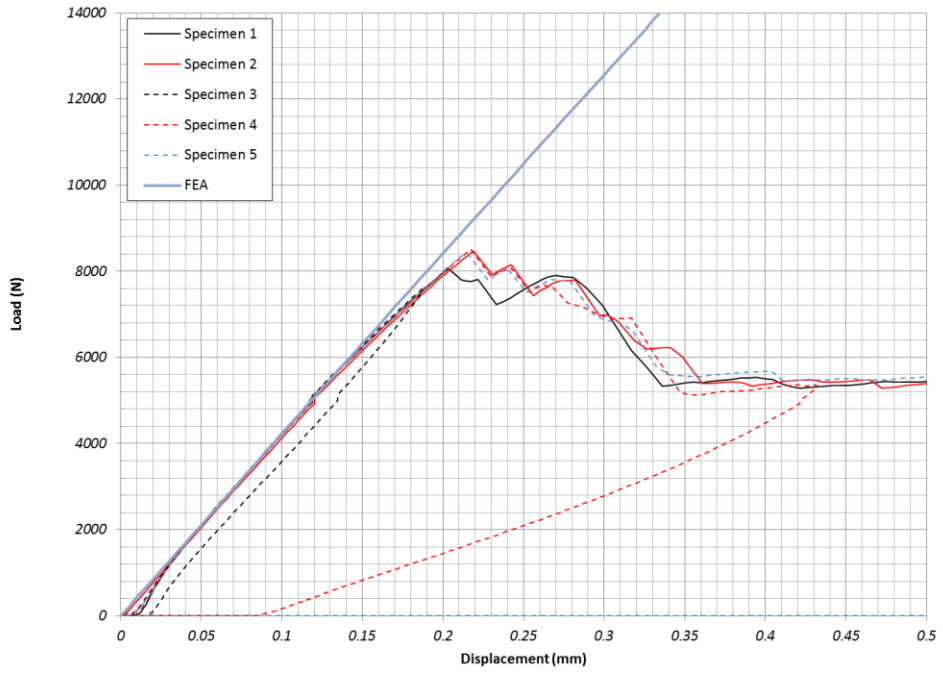


Figure 15. Force/displacement curve in FEA and test results for SPR = 2, N = 12 geometry.

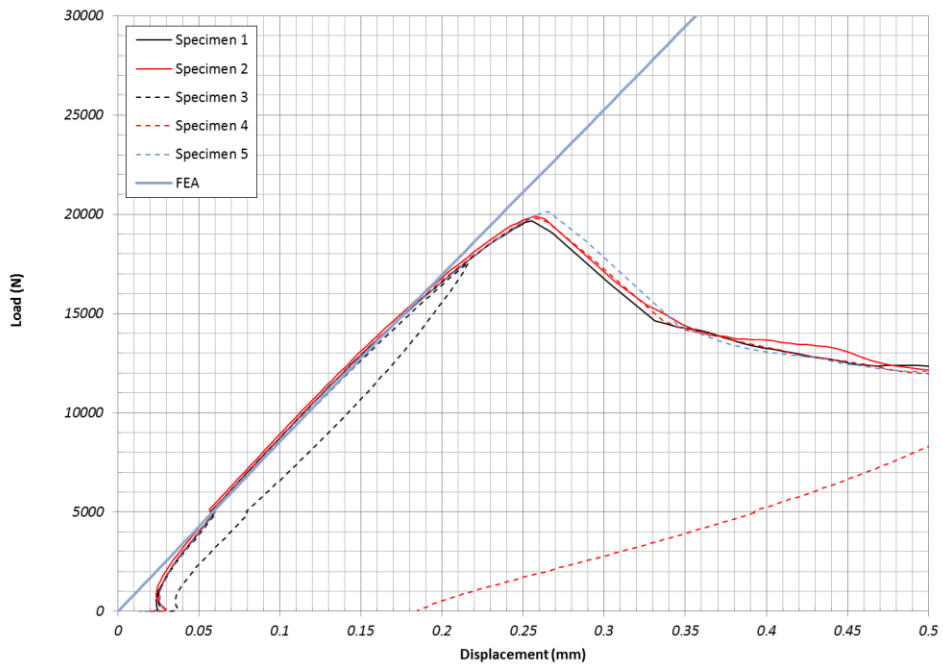


Figure 16. Force/displacement curve in FEA and test results for SPR = 2, N = 24 geometry.

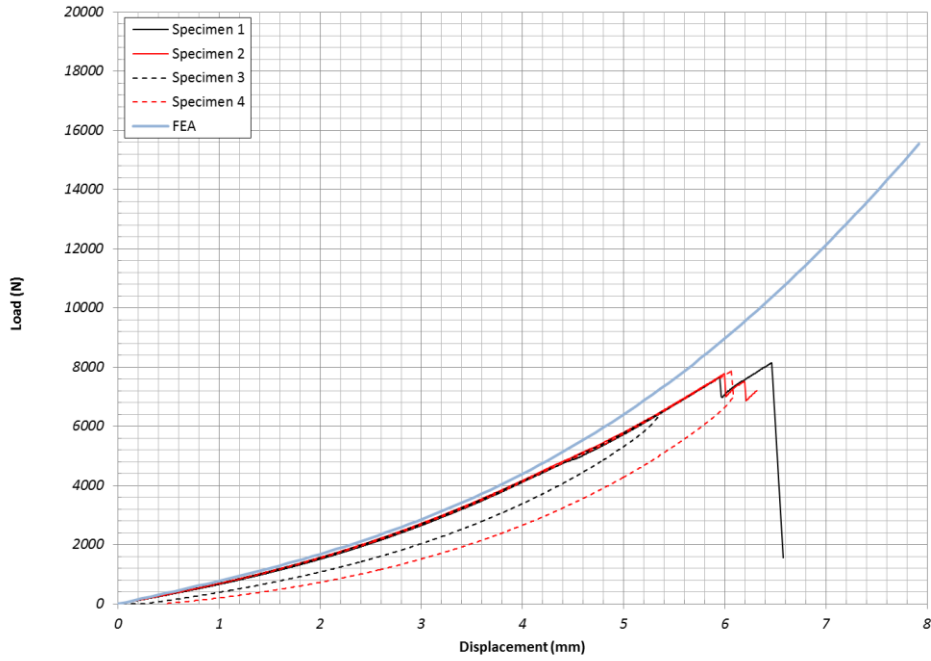


Figure 17. Force/displacement curve in FEA and test results for SPR = 8, N = 6 geometry.

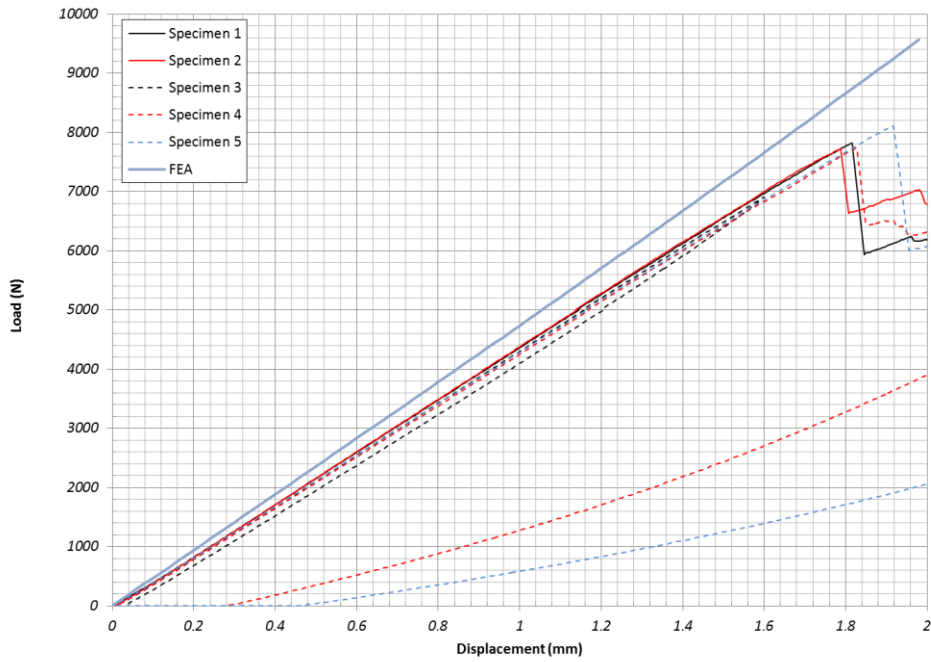


Figure 18. Force/displacement curve in FEA and test results for SPR = 8, N = 12 geometry.

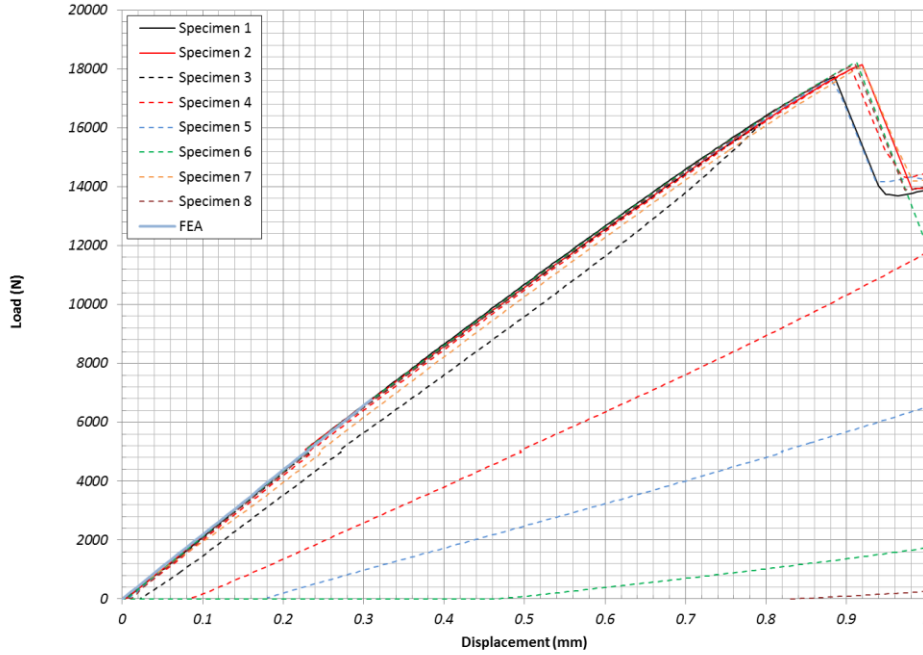


Figure 19. Force/displacement curve in FEA and test results for SPR = 8, N = 24 geometry.

3.3. Failure criteria analysis

In this section, various failure criteria are analyzed for suitability in predicting initiation of delamination in each of the test geometries. All test geometries except for the SPR = 8, N = 6 case, are analyzed at the proportional limit of loading (the load where delamination is believed to begin). The SPR = 8, N = 6 geometry is analyzed at point A in Figure 8, which is the point where delamination is first presumed to appear. As mentioned previously, results from the SPR = 8, N = 24 geometry is linearly extrapolated to the stress and strain at the proportional limit of loading. As a reminder of this, the SPR = 8, N = 6 geometry is marked with a star (*) and the SPR = 8, N = 24 geometry is marked with a double star (**) in the figures below.

Localization elements provide full stress and strain tensors; however, due to general contact to limit element interpenetration, these tensors underestimate out-of-plane stresses and strains. As a result, in-plane stresses and out-of-plane strains are calculated from in-plane strain and out-of-plane stress values, which are assumed to be more accurate. Accurate out-of-plane stresses can be calculated as the sum of contact stresses in the normal direction (T_n) and out-of-plane stress from the stress tensor (σ_{yy}). In plane, strains are assumed to follow from the deformation of the lamina, and are therefore presumed to be more accurate than stresses, which are influenced by Poisson effects on the constraint induced by the lamina. From these three quantities, out of plane strain and in-plane stress are calculated to be:

$$\varepsilon_{yy} = \frac{(\bar{\sigma}_{yy} - \lambda\varepsilon_{xx} - \lambda\varepsilon_{zz})}{E + 2\lambda\nu}$$

$$\sigma_{xx} = \frac{E}{(1+\nu)(1-2\nu)} ((1-\nu)\varepsilon_{xx} + \nu\varepsilon_{yy} + \nu\varepsilon_{zz})$$

$$\sigma_{zz} = \frac{E}{(1+\nu)(1-2\nu)} (\nu\varepsilon_{xx} + \nu\varepsilon_{yy} + (1-\nu)\varepsilon_{zz})$$

where

$$\lambda = \frac{\nu E}{(1+\nu)(1-2\nu)} \quad \text{and} \quad \bar{\sigma}_{yy} = \sigma_{yy} + T_n.$$

In the following failure criteria, stresses and strains are calculated using these formulas.

While localization elements are used here (which provide full stress and strain tensors), ultimately, cohesive zone elements are planned to be used to model interlaminar regions. With cohesive zone elements, only a traction/separation relationship is defined. Therefore, failure criteria which do not require full stress/strain tensors will be preferred.

3.3.1. von Mises stress criterion

While a single stress parameter has been deemed insufficient in characterizing initiation of delamination [1], the von Mises stress criterion provides insight into the state of stress at the proportional limit of loading.

von Mises stress is calculated as:

$$\sigma_{VM} = \sqrt{\frac{1}{2} \left[(\sigma_{xx} - \bar{\sigma}_{yy})^2 + (\sigma_{yy} - \sigma_{zz})^2 + (\sigma_{zz} - \sigma_{xx})^2 + 6(\sigma_{xy}^2 + \sigma_{yz}^2 + \sigma_{xz}^2) \right]}.$$

The maximum von Mises stresses, and their location within each model, are listed in Table 7. Figure 20 illustrates the relative values of maximum von Mises stress at initiation of delamination. As the table and figure show, the von Mises stress is not consistent from geometry to geometry, demonstrating that von Mises stress alone is not sufficient to predict delamination initiation. While the von Mises stress value is not consistent, the location of maximum von Mises stress remained in the top interlaminar region, under the indenter in all model geometries. Since all test specimens loaded past the proportional limit experienced delamination in this region, this is a plausible region of delamination initiation.

Table 7. Maximum von Mises stress value and location at delamination initiation.

Model	Max von Mises stress (MPa)	Location
SPR = 2, N = 6	108	top interlaminar region, under indenter
SPR = 2, N = 12	138	top interlaminar region, under indenter
SPR = 2, N = 24	216	top interlaminar region, under indenter
SPR = 8, N = 6	135	top interlaminar region, under indenter
SPR = 8, N = 12	152	top interlaminar region, under indenter
SPR = 8, N = 24	210	top interlaminar region, under indenter

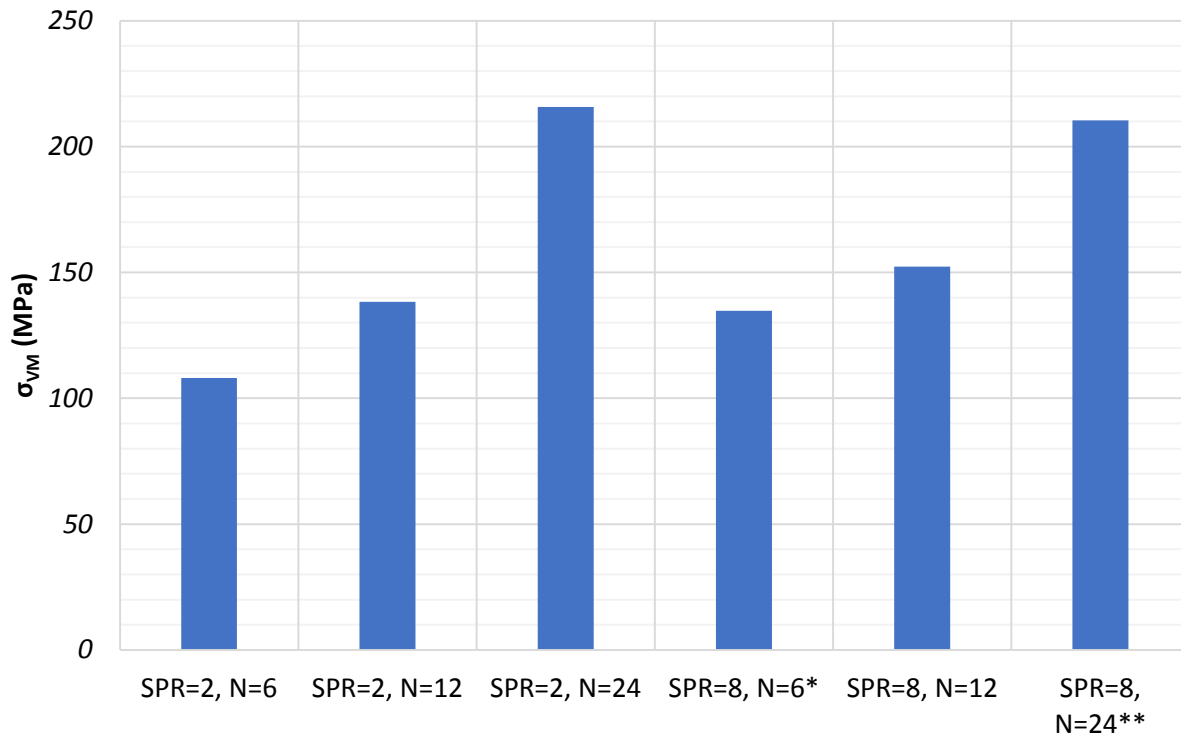


Figure 20. Maximum von Mises stress at delamination initiation.

3.3.2. Maximum principal stress and strain criterion

Similar to the von Mises failure criterion, this criterion uses a single parameter to characterize failure. However, while von Mises characterizes failure by measuring distortion energy, the principal stress and strain simply measures the maximum tensile stress and strain value. The maximum principal stresses in each geometry at delamination initiation are listed in Table 8 and illustrated in Figure 21. The maximum principal strains are in Table 9 and Figure 22.

Table 8. Maximum principal stress value, location, and direction at delamination initiation.

Model	Max principal stress (MPa)	Layer/location	Direction (x, y, z)
SPR = 2, N = 6	56	center/just outside indenter radius	(0.702, 0.712, -0.0289)
SPR = 2, N = 12	55	center/just outside indenter radius	(0.519, 0.689, 0.506)
SPR = 2, N = 24	71	top/under indenter radius	(0.708, 0.707, 0.00182)
SPR = 8, N = 6	81	bottom/just outside indenter radius	(-0.539, -0.0296, 0.842)
SPR = 8, N = 12	55	2 below center/just outside indenter radius	(0.495, 0.687, 0.532)
SPR = 8, N = 24	57	top/under indenter radius	(0.706, 0.708, 0.00209)

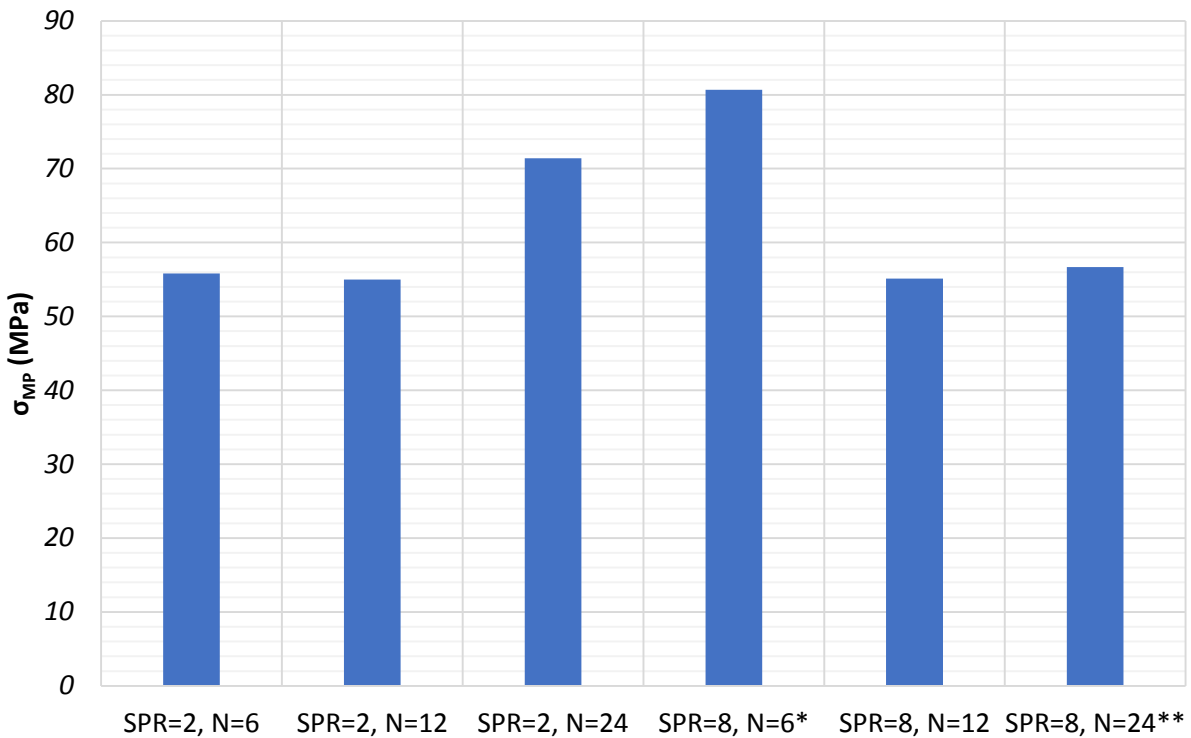


Figure 21. Maximum principal stress at delamination initiation.

The maximum principal stress measure illustrates several interesting trends regarding the state of stress in each geometry at initiation of delamination. These trends are summarized below.

1. Four of the test specimens had maximum principal stresses of around 55 MPa at initiation of delamination failure. This stress occurred at roughly the center interlaminar layer, and corresponded to out-of-plane shear (based on direction vector). Based on this, combined with inspection of test specimens, out-of-plane

shear in center interlaminar regions are expected to be the dominant failure mode that leads to delamination in these geometries.

2. In the SPR = 2, N = 24 model, the top interlaminar region has the highest principal stress at loss of proportionality in the force/displacement curve. As in the previous four specimens, the dominant stress is out-of-plane shear. As explained in the previous paragraph, out-of-plane shear stress is a stress that seems to correlate well with delamination initiation. Therefore, it is possible in this specimen that small-scale delamination initiated in the top layers without causing the proportional limit of loading to be reached. Inspection of ultrasonic imaging before the proportional limit of loading is reached seems to support this hypothesis (see Figure A10). Further, the center interlaminar region has a maximum principal stress of 53 MPa when proportional loading ceases – much closer to the principal stress exhibited in the previous four specimens analyzed.
3. In the SPR = 8, N = 6 model, the maximum principal stress occurs in the bottom interlaminar region, and is due to in-plane stresses. However, test specimens exhibited no damage in this region, suggesting that in-plane stress is not as crucial of a stress component when compared to out-of-plane stresses.

Table 9. Maximum principal strain value, location, and direction at delamination initiation.

Model	Max principal strain (mm/mm)	Layer/location	Direction (x, y, z)
SPR = 2, N = 6	0.0221	center/just outside indenter radius	(0.704, 0.710, -0.000)
SPR = 2, N = 12	0.0273	top/under indenter radius	(-0.013, 0.690, 0.723)
SPR = 2, N = 24	0.0423	top/under indenter radius	(-0.025, 0.691, 0.723)
SPR = 8, N = 6	0.0267	top/under indenter radius	(-0.498, -0.695, 0.519)
SPR = 8, N = 12	0.0291	top/under indenter radius	(-0.496, -0.708, 0.504)
SPR = 8, N = 24	0.0404	top/under indenter radius	(0.723, 0.691, 0.001)

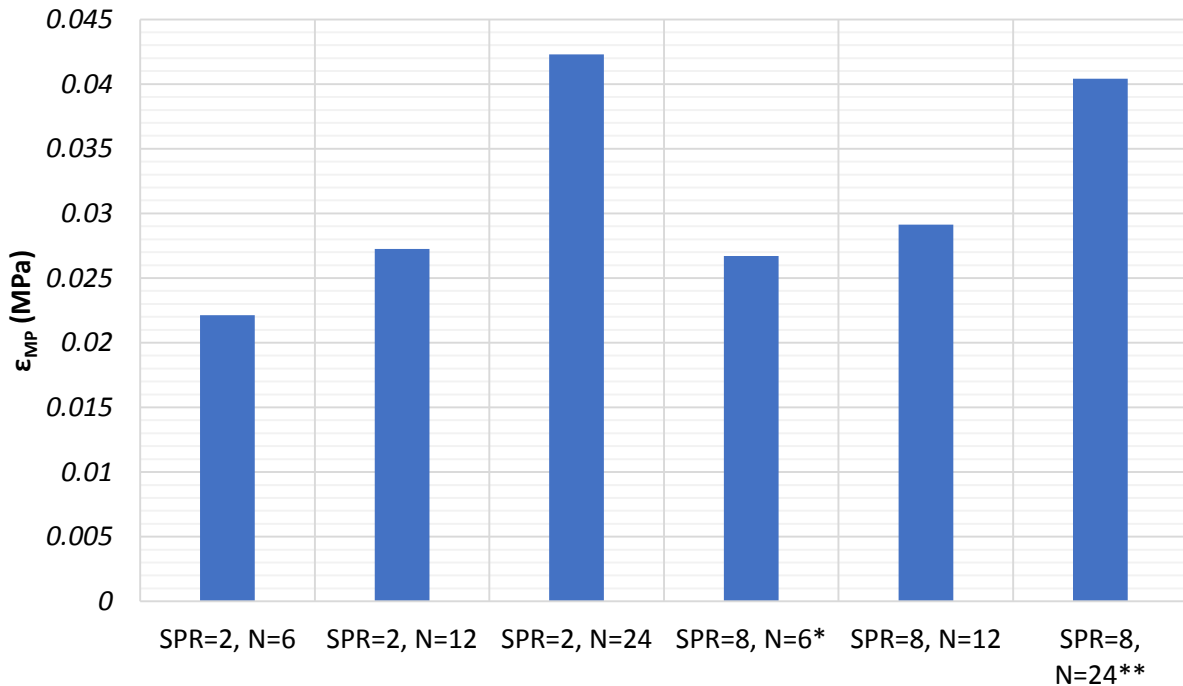


Figure 22. Maximum principal strain at delamination initiation.

Overall, trends in maximum principal strain are not as clear as in maximum principal stress. Out-of-plane tensile strains are much higher than out-of-plane stresses under the indenter. These strains are postulated to be a consequence of the higher stiffness in the lamina when compared to the interlaminar regions. As a result, maximum principal strains tend to occur in higher interlaminar regions, directly under the indenter.

3.3.3. Hashin/Rotem quadratic criterion

An approach to handle multiple failure parameters is to formulate each independently, then combine them quadratically to deal with mixed parameter failure. This approach is followed by Hashin and Rotem in their quadratic stress criterion, which can be stated as [17]:

$$\begin{aligned} \left(\frac{\sigma_{yy}}{S^+_{yy}}\right)^2 + \left(\frac{\sigma_{xy}}{S_{xy}}\right)^2 + \left(\frac{\sigma_{yz}}{S_{yz}}\right)^2 &\leq 1 \quad \text{if } \sigma_{yy} > 0, \\ \left(\frac{\sigma_{yy}}{S^-_{yy}}\right)^2 + \left(\frac{\sigma_{xy}}{S_{xy}}\right)^2 + \left(\frac{\sigma_{yz}}{S_{yz}}\right)^2 &\leq 1 \quad \text{if } \sigma_{yy} < 0. \end{aligned}$$

Here, out-of-plane stress components are presumed to contribute to failure. Specifically, four separate failure parameters are considered in this failure criterion: compressive and tensile out-of-plane stresses (S^-_{yy} and S^+_{yy} , respectively) and out-of-plane shear stresses (S_{xy} and S_{yz}). Unlike the von Mises and principal stress/strain failure criteria, this criterion does not require a full stress/strain tensor, and can therefore be implemented with cohesive zone elements.

Critical values of out-of-plane stresses are set as follows:

- S_{xy} and S_{yz} – these values are assumed to be equal, and set by max principal stress values from Section 3.3.2. Based on those results, S_{xy} and S_{yz} are assumed to be 57 MPa.
- S^+_{yy} – Limited data is available for setting this failure parameter. Therefore, based on the assumption of no in-plane strains and a von Mises failure criterion (see Section 3.3.4 for details), S^+_{yy} is assumed to be 50 MPa.
- S^-_{yy} – As with S^+_{yy} , limited data is available to calibrate this parameter since pure compression did not result in any failures in test specimen. Based on parametric studies, larger values for S^-_{yy} provide a better fit to the data. Therefore, this parameter is assumed to be infinite, and this term is eliminated from the failure criterion.

Based on these parameters, the Hashin/Rotem failure criterion was calculated in each FEA model, and the results are shown below both in Table 10 and Figure 23.

Table 10. Maximum Hashin/Rotem failure criterion and location at delamination initiation.

Model	Max Hashin/Rotem FC (MPa)	Location
SPR = 2, N = 6	1.19	top interlaminar region, under indenter
SPR = 2, N = 12	1.96	top interlaminar region, under indenter
SPR = 2, N = 24	4.75	top interlaminar region, under indenter
SPR = 8, N = 6	1.86	top interlaminar region, under indenter
SPR = 8, N = 12	2.38	top interlaminar region, under indenter
SPR = 8, N = 24	1.65	top interlaminar region, under indenter

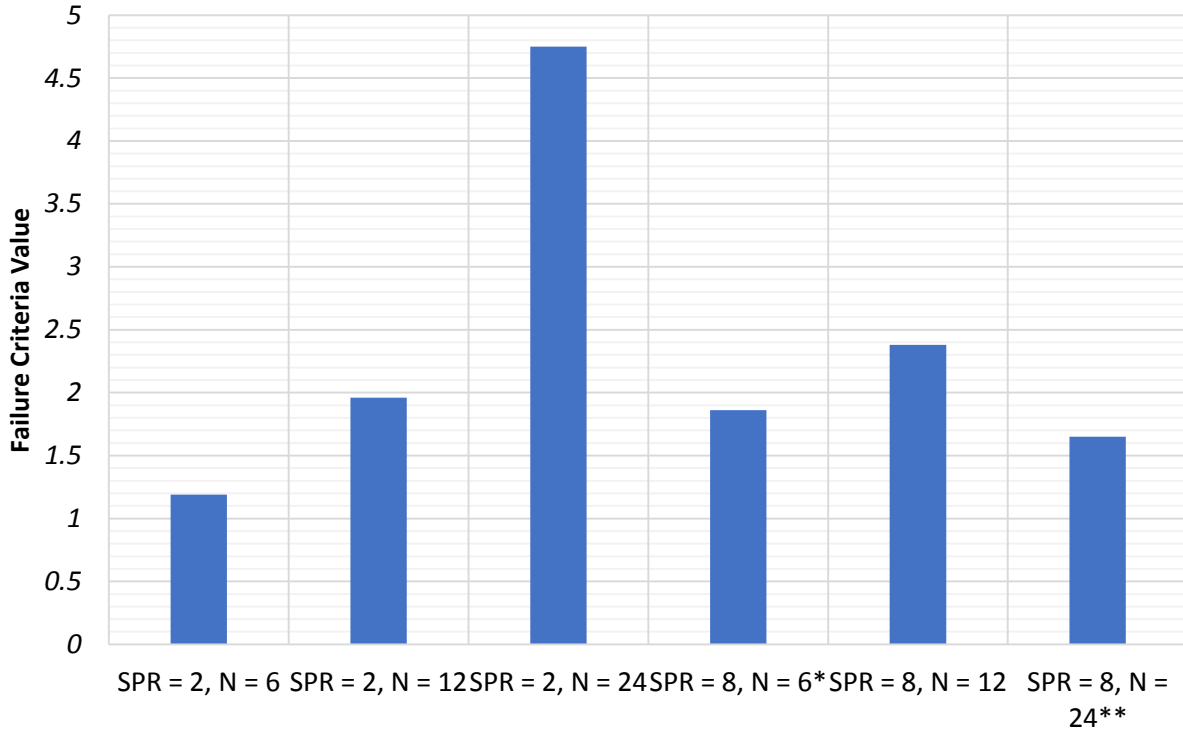


Figure 23. Maximum Hashin/Rotem failure criteria at delamination initiation.

In general, the Hashin/Rotem failure criteria does not sufficiently predict delamination initiation in the geometries tested. At center lamina (where out-of-plane compression is negligible), the failure criteria is near unity for all geometries tested, suggesting that out-of-plane compression enhances the ability of the test specimens to resist delamination. Therefore, a failure criteria which takes this effect into account is anticipated to improve the results observed.

3.3.4. Yen/Caiazzo quadratic stress criterion

This stress-based delamination initiation criterion is

$$FC_{YC} = \left(\frac{\langle \sigma_{yy} \rangle}{S_{yy}} \right)^2 + \left(\frac{\sigma_{xy}}{S_{xy} + S_{com}} \right)^2 + \left(\frac{\sigma_{yz}}{S_{yz} + S_{com}} \right)^2 \leq 1,$$

where:

- $\langle x \rangle = \begin{cases} x & \text{if } x > 0 \\ 0 & \text{if } x \leq 0 \end{cases}$ denotes Macaulay brackets,
- S_{yy} is the out-of-plane tensile strength,
- S_{xy} and S_{yz} are the out-of-plane shear strengths,
- and $S_{com} = \langle -\sigma_{yy} \rangle \tan \varphi$ is an interlaminar shear strength modifier based on Mohr-Columb theory, which acts to increase shear strength with increased compressive out-of-plane force.

This failure initiation criterion is similar to the Hashin/Rotem criterion except for one very important difference. Here, S_{com} acts to increase shear strength with increased out-of-plane compressive force, mitigating the shortcoming present in the Hashin/Rotem criterion. As with the Hashin/Rotem initiation criterion, the Yen/Caiazzo criterion is compatible with cohesive zone elements.

Uniaxial tensile strength values are available for UF3362 in [10]. There, a value of S_{yy} is given as 68.95 MPa. Assuming a von Mises type yield criterion, this is equivalent to a pure shear of 39.8 MPa. However, these values assume the material is undergoing either pure tensile stress or pure shear, and are therefore invalid for this situation. In order to apply this failure criterion, values of S_{xy} , S_{yz} , S_{yy} , and φ will need to be developed.

First, S_{xy} and S_{yz} are assumed to be equal, based on the symmetry of the CFRP. Bounds on S_{xy} will be set based on the SPR = 2, N = 6 model, whose maximum failure criterion occurs in regions dominated by shear. Based on this geometry, a shear strength of $S_{xy} = S_{yz} = 57$ MPa is deemed reasonable. Unfortunately, out-of-plane tensile stresses did not occur in appreciable quantities in regions of delamination failure, making calibration of this quantity difficult. As a first-order estimate, the uniaxial tensile strength of UF3362 can be transformed into a von Mises yield criterion assuming all in-plane strains are zero. This is a reasonable assumption for a thin interlaminar region surrounded by lamina with much higher stiffness. First, the zero in-plane strain assumption gives in-plane stress values of

$$\sigma_{xx} = \sigma_{zz} = \frac{2\nu}{(1 + \nu)(1 - 2\nu)} \sigma_{yy}.$$

Now, assuming a von Mises yield criterion, the critical out-of-plane stress is

$$S_{yy} = \left| 1 - \frac{2\nu}{(1 + \nu)(1 - 2\nu)} \right| \sigma_{yy}.$$

With the assumed values for ν and uniaxial tensile strength for UF3362, S_{yy} is estimated as 50 MPa.

Calibration of the final parameter, φ , turns out to be a more difficult task. In the PST geometry, regions of large compressive stress are limited to regions of the test specimen under the edges of the indenter. Furthermore, these are also regions of very high shear. Therefore, increasing the angle φ acts to shift the location of initial failure from under the indenter down to interlaminar layers at the center of the test specimen, where relatively high shear persists but compressive stress is nearly nonexistent. Once the location of initial failure has shifted from the top of the

test specimen to the center of it, additional increases of φ have no effect on the maximum value of the failure criterion. However, increasing φ in this situation would further reduce the value of the failure criterion in regions directly beneath the indenter.

The effect of modifying φ on the maximum value of FC_{YC} is demonstrated in Figure 24. As the figure demonstrates, no single value of φ gives a maximum value of unity in all test geometries. Excluding the SPR = 2, N = 24 and SPR = 8, N = 24 models, $\varphi = 30^\circ$ gives a reasonable maximum value for this failure criterion in most of the test geometries. If the SPR = 2, N = 24 model is included, $\varphi = 57^\circ$ gives a somewhat reasonable maximum value for failure criteria in all test geometries. However, with such a large angle chosen for φ , regions near the indenter in non-SPR = 2, N = 24 models have very low values for FC_{YC} , which is not realistic when compared to test results.

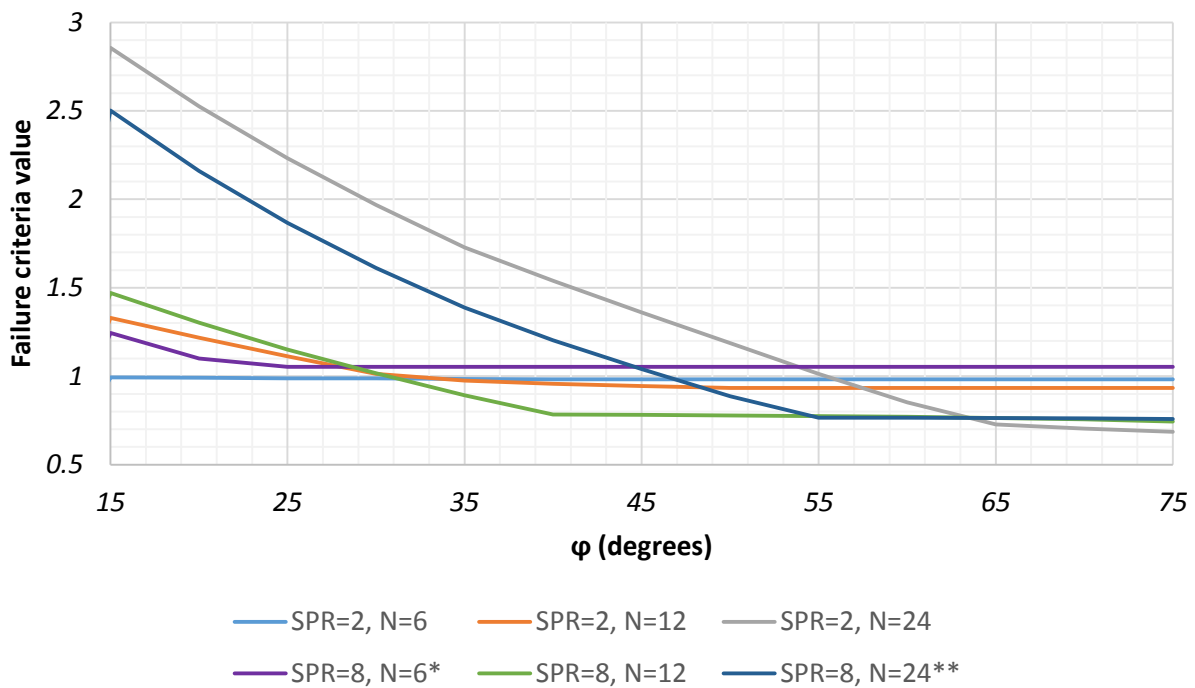


Figure 24. Yen/Caiazzo failure criterion value as a function of φ .

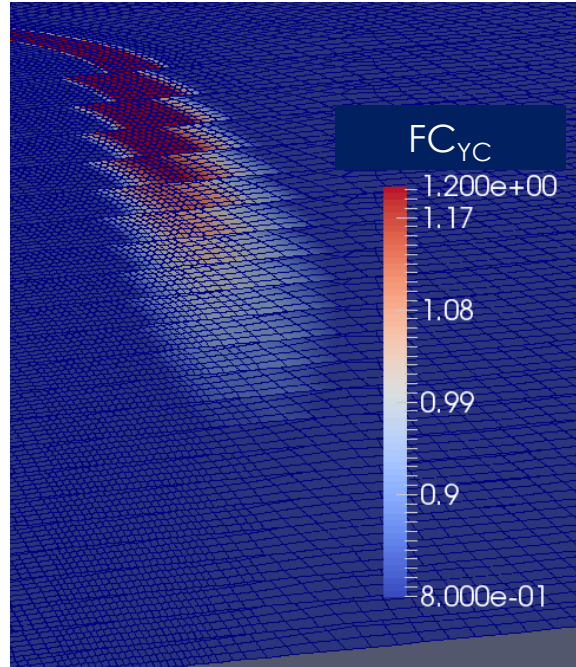


Figure 25. Yen/Caiazzo failure criterion in SPR = 2, N = 24 model with $\phi = 30^\circ$.

Examining values of FC_{YC} in the SPR = 2, N = 24 and SPR = 8, N = 24 models with $\phi = 30^\circ$ demonstrates that regions of delamination predicted are small, and limited to the first four to five interlaminar layers immediately surrounding the indenter (see Figure 25 for SPR = 2, N = 24 geometry). Furthermore, ultrasonic images from Specimen 3 of the SPR = 2, N = 24 test geometry (see Figure A10) and Specimen 3 of the SPR = 8, N = 24 geometry (see Figure A21) indicate that some damage likely occurs before the proportional limit is reached in these test geometries. Small-scale delamination in the top layers (with no other failure modes present) would be consistent with the damage observed in Figure A10 and Figure A21.

Based on this analysis, the model parameters in Table 11 are assumed for the Yen/Caiazzo failure criterion. The resulting maximum values for FC_{YC} are plotted in Figure 26. Maximum values for FC_{YC} and their locations are listed in Table 12. The resulting failure surface, along with the location of each test geometry on it, are illustrated in Figure 27.

Table 11. Assumed model parameters for the Yen/Caiazzo failure criterion.

Parameter	Assumed value	Source
S_{xy}	57 MPa	max shear strain at delamination initiation in SPR = 2, N = 6 model
S_{yz}	57 MPa	max shear strain at delamination initiation in SPR = 2, N = 6 model
S_{yy}	50 MPa	estimated from constraint modified ultimate tensile strength
ϕ	30°	parametric studies

Table 12. Maximum Yen/Caiazzo failure criterion value at delamination initiation.

Model	Max FC_{YC}	Interlaminar layer & location
SPR = 2, N = 6	0.99	center, just outside indenter radius
SPR = 2, N = 12	1.01	top, at indenter radius
SPR = 2, N = 24	1.97	top, at indenter radius
SPR = 8, N = 6	1.05	center, just outside indenter radius
SPR = 8, N = 12	1.02	top, at indenter radius
SPR = 8, N = 24	1.61	top, at indenter radius

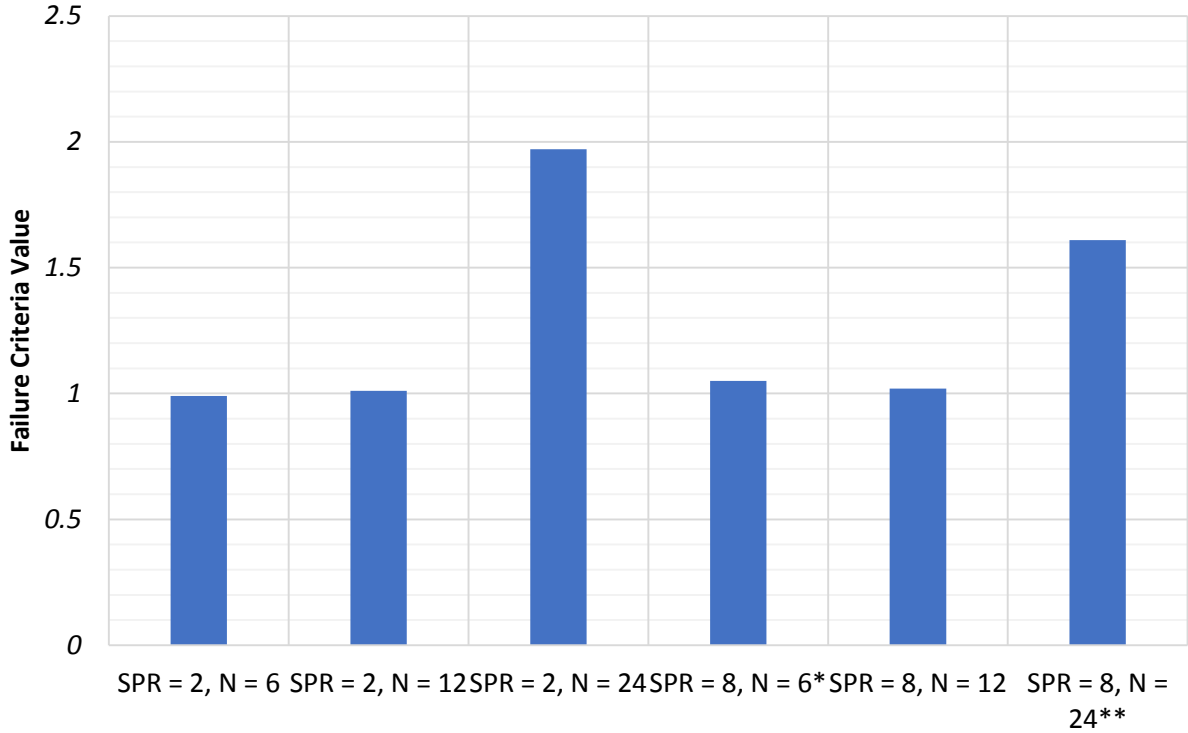


Figure 26. Maximum Yen/Caiazzo stress failure criteria at delamination initiation.

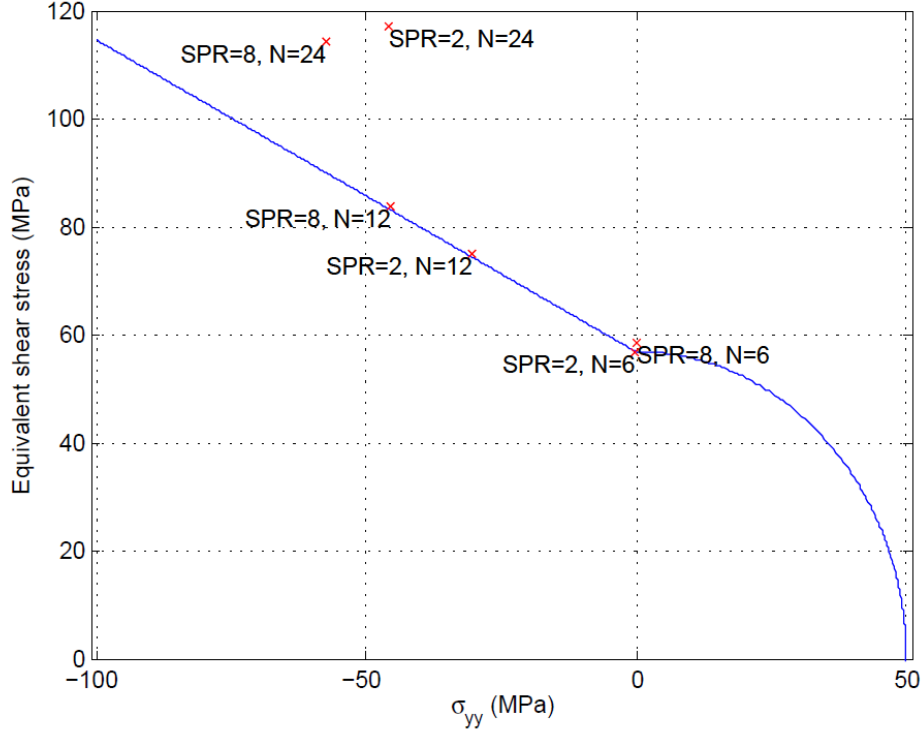


Figure 27. Yen/Caiazzo failure surface with max FC_{YC} in each geometry plotted.

3.3.5. Yen/Caiazzo quadratic strain criterion

In Reference [7], the Yen/Caiazzo stress-based criterion is transformed into a strain-based criterion by substituting the critical stresses with one-dimensional constitutive relationships. The resulting strain-based delamination initiation criterion is

$$FC_{YC} = \left(\frac{\langle E_y \varepsilon_{yy} \rangle}{S_{yy}} \right)^2 + \left(\frac{G_{xy} \varepsilon_{xy}}{S_{xy} + S_{com}} \right)^2 + \left(\frac{G_{yz} \varepsilon_{yz}}{S_{yz} + S_{com}} \right)^2 \leq 1,$$

where:

- $\langle x \rangle = \begin{cases} x & \text{if } x > 0 \\ 0 & \text{if } x \leq 0 \end{cases}$ denotes Macaulay brackets,
- S_{yy} is the out-of-plane tensile strength,
- S_{xy} and S_{yz} are the out-of-plane shear strengths,
- and $S_{com} = \langle -E_y \varepsilon_{yy} \rangle \tan \varphi$ is an interlaminar shear strength modifier based on Mohr-Columb theory, which acts to increase shear strength with increased compressive out-of-plane force.

At first glance, this failure criterion is very similar to the one introduced in Section 3.3.3; however, due to Poisson effects, there are profound differences between the two. In the top interlaminar layer under the indenter, very little out-of-plane stress is present², but tensile out-of-plane strains are present (due to greater compliance in the interlaminar regions compared to the

² While out-of-plane stress is very high under the edge of the indenter, under the center of the indenter, very little out-of-plane stress occurs.

lamina). This causes failure initiation (based on this criterion) to occur in the top interlaminar layer in all test geometries and the parameter S_{com} to have reduced impact when compared to the stress based Yen/Caiazzo criterion.

Keep in mind that using cohesive zone elements to model interlaminar regions results in no difference between stress-based and strain-based criteria. Since this is eventually the method that will be used to model these interlaminar regions, the differences between the stress-based and strain-based failure criteria will eventually be moot. However, since localization elements provide full stress and strain tensors, such a comparison is warranted, and can provide insight into whether stresses or strains ultimately control delamination failure.

The stress-based parameters in the model are chosen as before, and the elastic moduli value are the same as used in Section 3.1.2. The shear modulus is calculated assuming an isotropic material, giving a value of 2556 MPa. The resulting values for the strain based Yen/Caiazzo failure criterion are given in Table 13 and illustrated in Figure 28. The failure criterion versus φ is plotted in Figure 29.

Table 13. Maximum Yen/Caiazzo strain failure criterion value at delamination initiation.

Model	Max FC_{YC}	Interlaminar layer & location
SPR = 2, N = 6	1.00	top, at indenter radius
SPR = 2, N = 12	1.47	top, at indenter radius
SPR = 2, N = 24	3.15	top, at indenter radius
SPR = 8, N = 6	1.57	top, at indenter radius
SPR = 8, N = 12	1.93	top, at indenter radius
SPR = 8, N = 24	2.93	top, at indenter radius

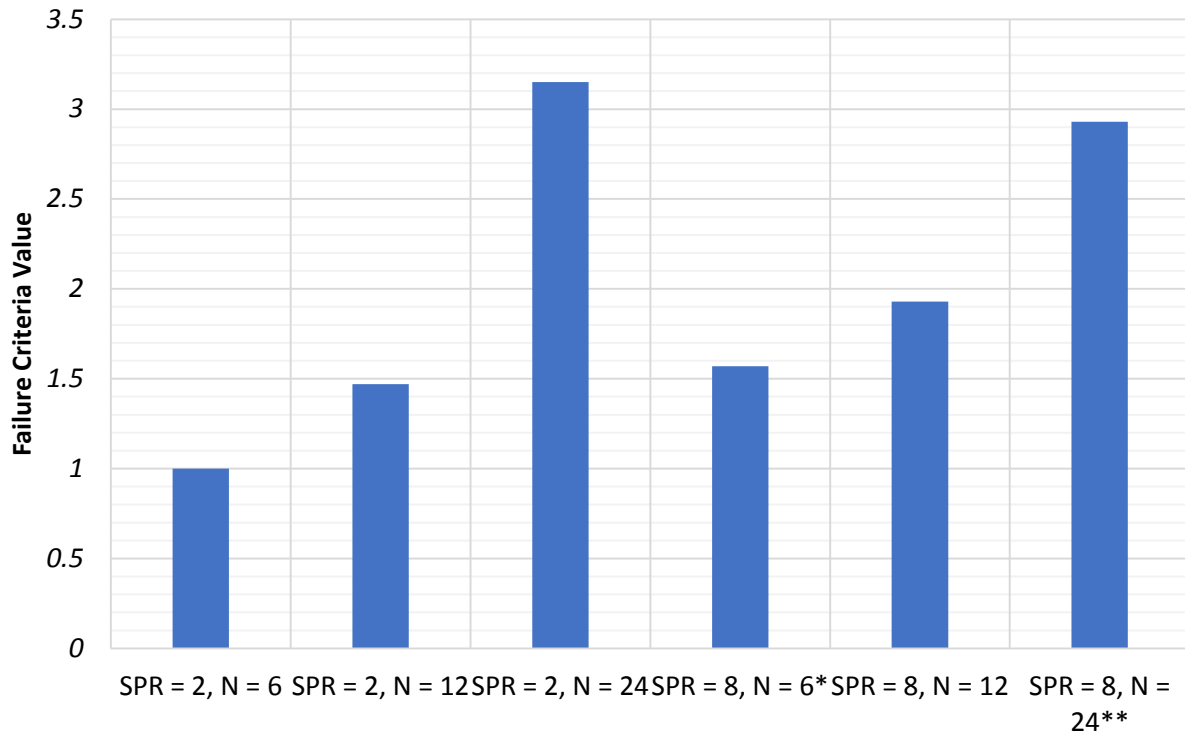


Figure 28. Maximum Yen/Caiazzo strain failure criteria at delamination initiation.

The strain-based Yen/Caiazzo delamination initiation criterion did not match the data as well as the stress-based version. A strain-based criteria that better matches these observed test results would need to take into account increased out-of-plane strains under the indenter. As this particular modeling effort progresses, cohesive zone elements will negate the difference between stress-based and strain-based criteria. However, in these analyses, it remains to be seen how out-of-plane stresses or strains under the indenter will affect the initiation criteria.

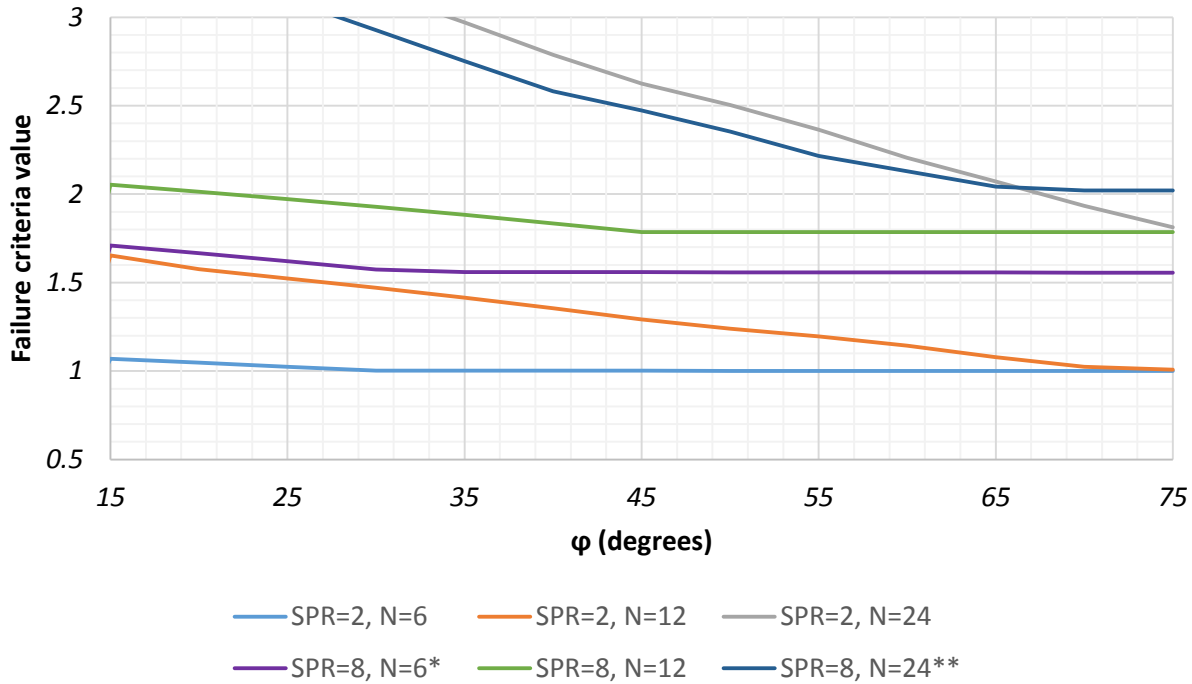


Figure 29. Yen/Caiazzo strain failure criterion value as a function of ϕ .

3.4. Discussion

In this section, a number of delamination initiation criteria are demonstrated on quasi-static punch-shear tests in six different specimen geometries. The criteria tested included von Mises stress, maximum principal stress/strain, a yield surface developed by Hashin and Rotem, and a yield surface developed by Yen/Caiazzo in both stress-based and strain-based varieties.

Of all failure criteria tested, the stress-based Yen/Caiazzo criterion produced the best results, with nearly all test specimens falling neatly on the failure surface at the proportional limit of loading. The exceptions to this rule are the SPR = 2, N = 24 and SPR = 8, N = 24 geometries. However, as ultrasonic imaging demonstrates, delamination directly underneath the indenter before the proportional limit has been reached is a realistic possibility. The failed region (determined by $FC_{YC} > 1$) roughly matches the limits of the damaged region highlighted by ultrasonic imaging. Additionally, this delamination criterion indicates delamination initiation occurs at around 5 kN of loading in the SPR = 8, N = 6 model. This is likely where out-of-plane matrix failure and localized delamination begin in this geometry.

Compared to the stress-based Yen/Caiazzo delamination criterion, the von Mises yield criterion and max principal stress/strain criteria prove to be too simplistic. Each stress component leading to delamination failure requires its own, unique ultimate stress value. Furthermore, yield in out-of-plane compression differs from yield in out-of-plane tension. These shortcomings are addressed in the Hashin and Rotem failure criterion, yet this model also falls short in predicting delamination. Here, the issue is related to increased shear strength when out-of-plane compressive stress occurs simultaneously. The Yen/Caiazzo model accounts for this shortcoming.

Since strain-based yield criteria have more physical meaning in polymer materials, such as UF3362, the strain-based Yen/Caiazzo model was anticipated to provide a plausible failure surface for the observed test results. However, the stress-based Yen/Caiazzo model proved to provide the best fit for the observed test results. As mentioned previously, when using cohesive zone elements in the interlaminar region, the stress-based and strain-based Yen/Caiazzo model will give the same results. However, localization elements generally should give a more accurate snapshot of actual stresses and strains present in the interlaminar region. Since the Yen/Caiazzo strain-based criteria is not able to produce a failure surface which matched test results, perhaps other strain-based failure surfaces may be worth developing.

4. CONCLUSION

In this document, failure in carbon-fiber reinforced polymers is investigated. Quasi-static punch shear testing was performed and the resulting force/displacement curves and non-destructive test results were analyzed. Based on these results, finite element analysis was performed to match the proportional portion of the load/displacement curve. At the proportional limit of the load/displacement curve, a variety of delamination initiation criteria were tested on the interlaminar regions of the finite element model. These initiation criteria were tested at this point since large-scale delamination is the mode of failure that results in reduced load-carrying capacity in the majority of specimen geometries tested.

Based on the examination of force/displacement curves and non-destructive test results, a sequence of failure was determined in each test specimen geometry. Two separate sequences of failure were observed among all the test geometries. In the SPR = 8, N = 6 geometry, the first mode of failure observed is matrix damage, followed by fiber failure. Small delamination occurred around damaged regions, but delamination had little effect on the overall shape of the force-displacement curve. In the remaining test geometries, matrix damage and large-scale delamination occur at the proportional limit of loading. Then, loading increases as higher strength fibers begin to accumulate load. Eventually, these fibers fail and the specimen's load carrying capacity is drastically reduced.

Based on the assumed location of initiation of delamination (the proportional limit in most specimen geometries), a number of different delamination initiation criteria are tested. The criterion that best matches test data is a stress-based Yen/Caiazzo failure surface. This failure surface takes into account out-of-plane tension, compression, and shear. Tension and shear act as terms in a quadratic failure surface, while compression acts as to increase shear strength.

The next goal in this project is to develop an interactive failure criteria for the fibers and the matrix of the lamina, then run analyses that integrate all modes of failure and develop a full force/displacement response for each test specimen geometry. The interactive failure criteria will be mesh size dependent, so a non-local method will likely be needed to build a convergent finite element model. Investigation of integrating non-local methods with a continuum damage mechanics model will be the next specific step taken toward realizing the ultimate goal of the project.

5. REFERENCES

1. J. C. Brewer and P.A. Lagace, Quadratic stress criterion for initiation of delamination, in *Journal of Composite Materials*, vol. 22, pp. 1141-1155, 1988.
2. R. Y. Kim and S. R. Soni, Experimental and analytical studies on the onset of delamination in laminated composites, in *Journal of Composite Materials*, vol. 18, pp. 70-80, 1984.
3. C. F. Yen and A. Caiazzo, *Innovative Processing of Multifunctional Composite Armor for Ground Vehicles*, ARL-CR-484. U.S. Army Research Laboratory, Aberdeen Proving Ground, MD, 2001.
4. S. J. deTeresa, D. C. Freeman, and S. E. Groves, The effects of through-thickness compression on the interlaminar shear response of laminated fiber composites, in *Journal of Composite Materials*, vol. 38, pp. 681-697, 2004.
5. J. R. Xiao and J. W. Gillespie Jr., A phenomenological Mohr-Coulomb failure criterion for composite laminates under interlaminar shear and compression, in *Journal of Composite Materials*, vol. 41, pp. 1295-1309, 2007.
6. J. M. Whitney and C. E. Browning, On short-beam shear tests for composite materials, in *Experimental Mechanics*, vol. 25, pp. 294-300, 1985.
7. J. R. Xiao, B. A. Gama, and J. W. Gillespie Jr., Progressive damage and delamination in plain weave S-2 glass/SC-15 composites under quasi-static punch-shear loading, in *Composite Structures*, vol. 78, pp. 182-196, 2007.
8. SIERRA Solid Mechanics Team, *Sierra/SolidMechanics 4.36 User's Guide*, SAND2015-2199, Sandia National Laboratories, Albuquerque, NM, March 2015.
9. Q. Yang, A. Mota, and M. Ortiz., A class of variational strain-localization finite elements, in *International Journal for Numerical Methods in Engineering*, vol. 62, pp. 1013-1037, 2005.
10. T.M. Briggs, *Developing a multiscale test approach for characterizing polymer composites*, SAND2012-7988, Sandia National Laboratories, Albuquerque, NM, September 2012.
11. A. Matzenmiller, J. Lubliner, R. L. Taylor, A constitutive model for anisotropic damage in fiber-composites, in *Mechanics of Materials*, vol. 20, pp. 125-152, 1995.
12. R. M. Christensen, Stress based yield/failure criteria for fiber composites, in *International Journal of Solids and Structures*, vol. 34, pp. 529-543, 1997.
13. E. Martín-Santos, P. Maimí, E. V. González, P. Cruz, A continuum constitutive model for the simulation of fabric-reinforced composites, in *Composite Structures*, vol. 111, pp. 122-129, 2014.
14. R. M. Christensen, Tensor transformations and failure criteria for the analysis of fiber composite materials, in *Journal of Composite Materials*, vol. 22, pp. 874-897, 1988.
15. T. M. Briggs, S. A. English and S. M. Nelson, "Quasi-Static Indentation Analysis of Carbon-Fiber Laminates," Sandia National Laboratories SAND2015-XXXX, 2015.
16. W. S. Rasband, ImageJ, U.S. National Institutes of Health, Bethesda, Maryland, USA, <http://imagej.nih.gov/ij/>, 1997-2014.
17. Z. Hashin and A. Rotem, A fatigue failure criterion for fiber reinforced materials, in *Journal of Composite Materials*, vol. 7, pp. 448-464, 1973.

APPENDIX A: NON-DESTRUCTIVE EVALUATION OF TEST SPECIMENS

Determining the location of delamination initiation in test specimens is aided by the use of CT scans and ultrasonic imaging. These evaluations, along with force/displacement curves obtained during testing, allow a sequence of failure to be postulated for each of the test geometries. Since testing continued beyond initiation of delamination, the applications of the failure sequences detailed here extend beyond the scope of the current work. The process of determining each failure sequence is detailed in this Appendix. The images and discussion presented in this Appendix parallel and are partially derived from a companion SAND report [15].

A.1. Testing and evaluation

As described in Section 2 of the report, the majority of tests are run to different points on the force/displacement curve (rather than complete specimen failure). As a result, these test specimens with varying degrees of damage provide insight into the sequence of failure in each test geometry. The three pieces of information that are used to develop a failure sequence are the force/displacement curves, CT scans, and ultrasonic images. The force/displacement curves are pictured in Figure 2 through Figure 7 of Section 2. The ultrasonic images are pictured in the sections that follow. Also, descriptions of each lamina and interlaminar region from CT scan imagery are described in the sections that follow. Illustrative images of CT scans are shown in Section A.2.

CT scans are stored in .avi file format and are manipulated using ImageJ version 1.49 [16]. CT scans are conducted in the three principle axes, with the XY and XZ scan directions being in-plane and the YZ scan direction being out-of-plane. The following types of damage were observed in the CT scans:

- **Out-of-plane lamina matrix damage** – This failure type is most clearly identified in the out-of-plane scans. Permanent deformation causes lamina regions adjacent to the indenter to appear in scans taken at higher or lower planes than expected. As matrix damage progresses, in-plane scans demonstrate “cliffs” around the location of the indenter.
- **Out-of-plane fiber damage** – Closely related to matrix damage, fiber damage is primarily visible through “cliffs” in in-plane scans around the location of the indenter, with a discontinuity in the lamina clearly present (visibility is often enhanced by delamination around the indenter).
- **Lamina cracking** – Identified as cracks visible in the out-of-plane direction (generally initiating from the indenter).
- **Delamination** – Sometimes identifiable as distinct layers in the in-plane directions, but usually recognized as darkened regions of out-of-plane scans. Generally, if permanent lamina damage is present then this failure mode is more easily recognizable in CT scans. Without permanent damage in the lamina, delaminations tend to be too small to be seen in CT scans. Therefore, estimations of delamination from CT imaging alone may underestimate the true extent of delamination in each test specimen.

Layer-by-layer evaluation of each specimen is attempted in the sections that follow. This is accomplished by interpolating frames of the out-of-plane .avi file and examining each layer of the in-plane .avi file. Since some approximation is involved in this method of analysis, the layer-by-layer evaluations are meant to present an overall trend of the state of each specimen, rather than a precise description of each layer.

A.1.1. $SPR = 2, N = 6$ specimens

For convenience, Figure 2 is repeated below (in Figure A1). Specifically, Specimen 3, Specimen 4, and Specimen 5 will be evaluated in this section. Based on evaluation of these samples, the following damage is observed:

- Specimen 3 (loaded until before proportional limit was reached) – no damage
- Specimen 4 (loaded past proportional limit, until first region of damage occurs) – ultrasonic imaging clearly indicates a damaged region slightly larger than twice the radius of the indenter; CT scans demonstrate matrix damage around the indenter in the top lamina and delamination about two-thirds through the specimen
- Specimen 5 (loaded to maximum load, immediately preceding complete failure of the test specimen) – ultrasonic imaging demonstrates a damaged region slightly larger than Specimen 4; CT scans illustrate matrix and fiber damage in the first three layers of lamina and a delamination region about two times the size of the indenter propagating through all layers

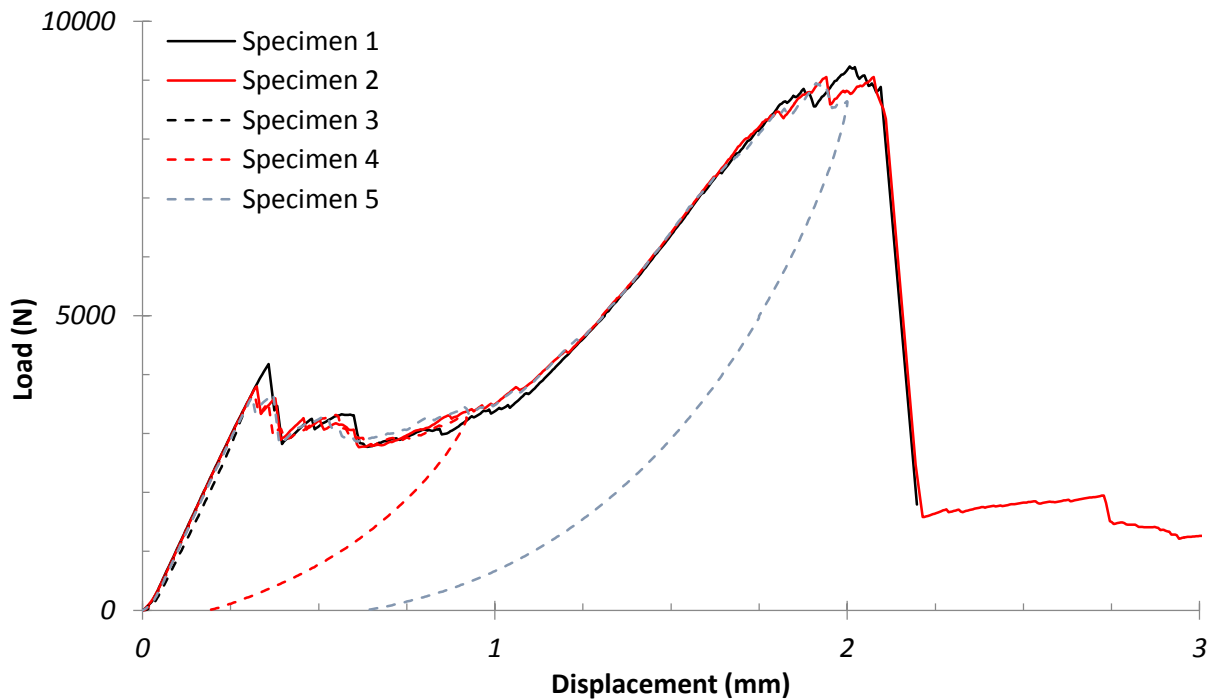


Figure A1. Force/displacement curves for $SPR = 2, N = 6$ test specimens.

A.1.1.1. Specimen 3

Specimen 3 is not loaded past the proportional limit of the force/displacement curve. Accordingly, no visible damage is incurred on the test specimen. Ultrasonic imaging (Figure A2) and a description of each lamina/interlaminar region (Table A1) follow.

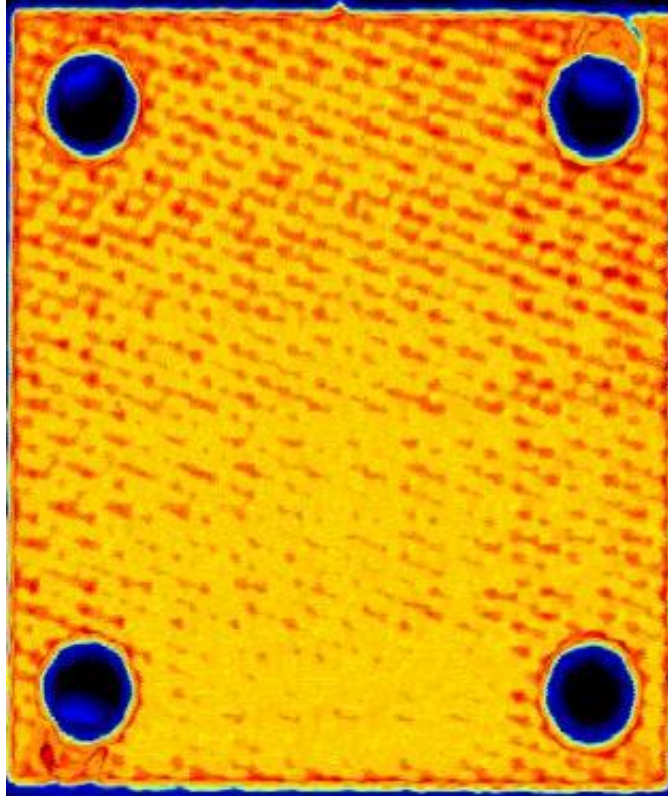


Figure A2. Ultrasonic imaging for SPR = 2, N = 6 test specimen 3. Yellow/orange regions indicate no damage.

Table A1. Damage in each layer of SPR = 2, N = 6 specimen 3 based on CT scans.

Lamina	Lamina damage	Interlaminar layer	Interlaminar damage
1	no damage	1	no damage
2	no damage	2	no damage
3	no damage	3	no damage
4	no damage	4	no damage
5	no damage	5	no damage
6	no damage		

A.1.1.2. Specimen 4

Specimen 4 is loaded past the proportional limit of the force/displacement curve, to the first region of damage. Out-of-plane matrix damage and delamination is observed in this specimen. Ultrasonic imaging (Figure A3) and a description of each lamina/interlaminar region (Table A2) follow.

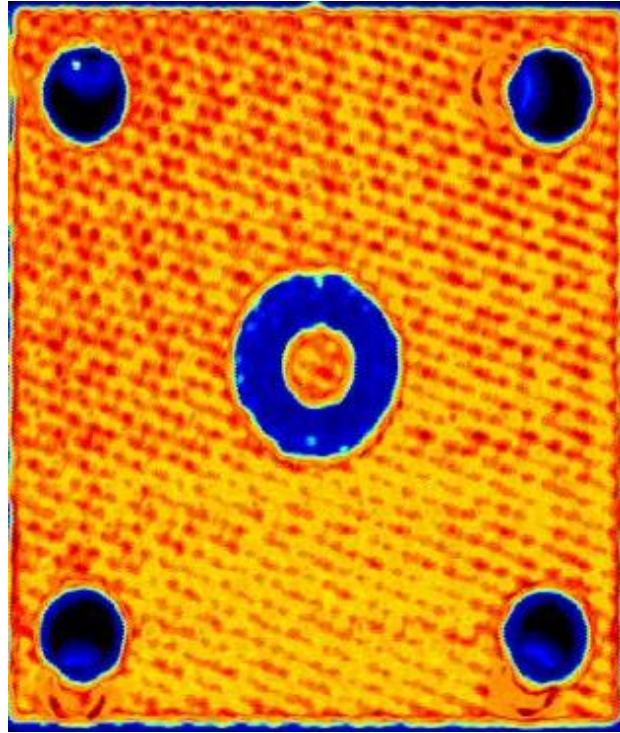


Figure A3. Ultrasonic imaging for SPR = 2, N = 6 test specimen 4. Yellow/orange regions indicate no damage.

Table A2. Damage in each layer of SPR = 2, N = 6 specimen 4 based on CT scans.

Lamina	Lamina damage	Interlaminar layer	Interlaminar damage
1	out-of-plane matrix damage around punch	1	delamination around punched region
2	no damage	2	region of delamination about 1.5x radius of punch
3	no damage	3	region of delamination about 2x radius of punch
4	no damage	4	region of delamination about 2x radius of punch
5	no damage	5	no damage
6	no damage		

A.1.1.3. Specimen 5

Specimen 5 is loaded to roughly the point of maximum load carrying capacity of the specimen. Matrix and fiber damage and delamination are observed in this specimen. Ultrasonic imaging (Figure A4) and a description of each lamina/interlaminar region (Table A3) follow.

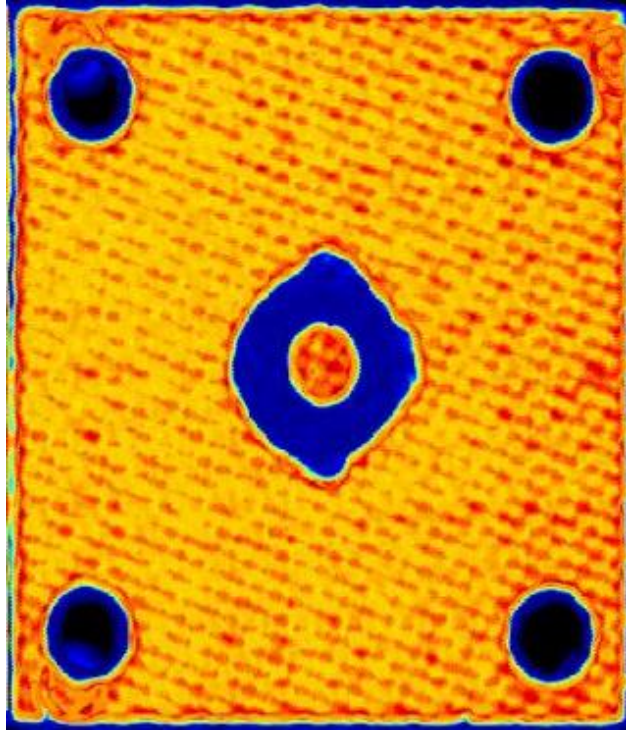


Figure A4. Ultrasonic imaging for SPR = 2, N = 6 test specimen 5. Yellow/orange regions indicate no damage.

Table A3. Damage in each layer of SPR = 2, N = 6 specimen 5 based on CT scans.

Lamina	Lamina damage	Interlaminar layer	Interlaminar damage
1	punch-through failure around punch	1	region of delamination about 2x radius of punch
2	punch-through failure around punch	2	region of delamination about 2x radius of punch
3	punch-through failure around punch	3	region of delamination about 2x radius of punch
4	matrix damage around punch	4	region of delamination about 2x radius of punch
5	permanent deformation around punch (some possible matrix damage)	5	region of delamination about 2x radius of punch
6	permanent deformation around punch (some possible matrix damage)		

A.1.2. SPR = 2, N = 12 specimens

For convenience, Figure 3 is repeated below (in Figure A5). Specifically, Specimen 3, Specimen 4, and Specimen 5 will be evaluated in this section. Based on evaluation of these samples, the following damage is observed:

- Specimen 3 (loaded until before proportional limit was reached) – no damage
- Specimen 4 (loaded past proportional limit, within “valley” of force/displacement curve) – ultrasonic imaging clearly indicates a damaged region slightly larger than twice the radius of the indenter; CT scans demonstrate matrix crushing around the indenter in the top lamina and likely delamination from the top to two-thirds through the specimen
- Specimen 5 (loaded to maximum load, immediately preceding complete failure of the test specimen) – ultrasonic imaging demonstrates a diamond-shaped damaged region slightly larger than Specimen 4; CT scans illustrate punch-through failure (caused by fiber and matrix damage) in the first 5 layers of lamina and delamination propagating around the indenter through all interlaminar regions of the specimen

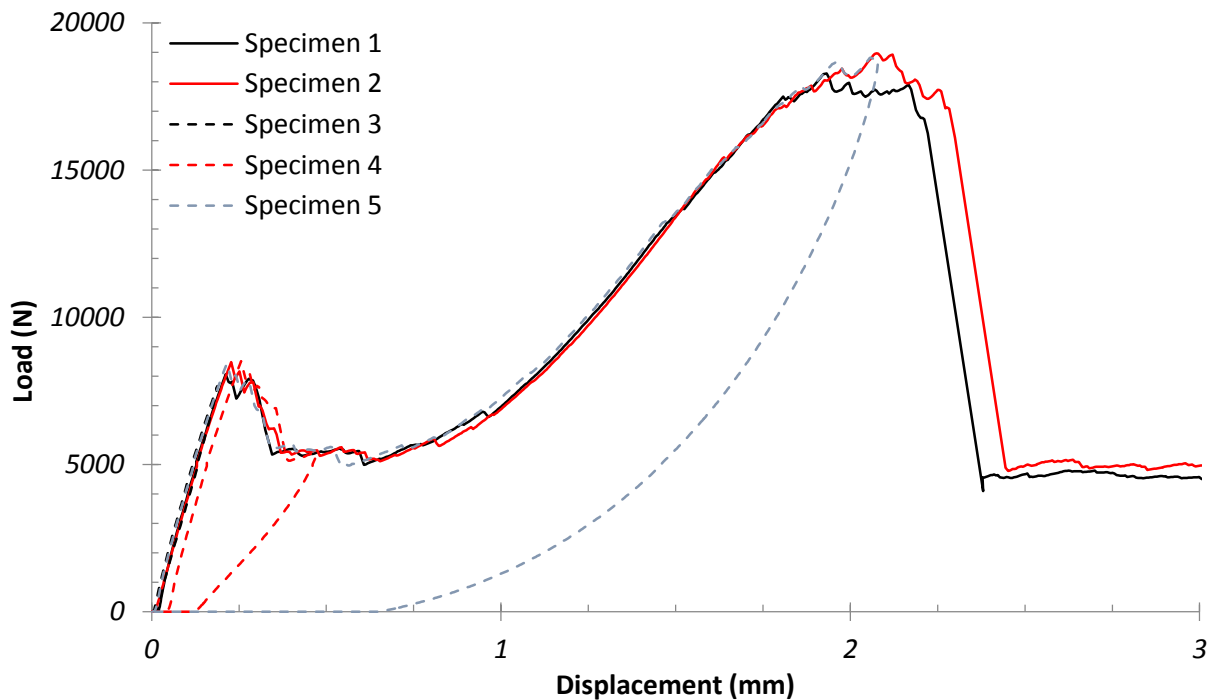


Figure A5. Force/displacement curves for SPR = 2, N = 12 test specimens.

A.1.2.1. Specimen 3

Specimen 3 is not loaded past the proportional limit of the force/displacement curve. Accordingly, no visible damage is incurred on the test specimen. Ultrasonic imaging (Figure A6) and a description of each lamina/interlaminar region (Table A4) follow.

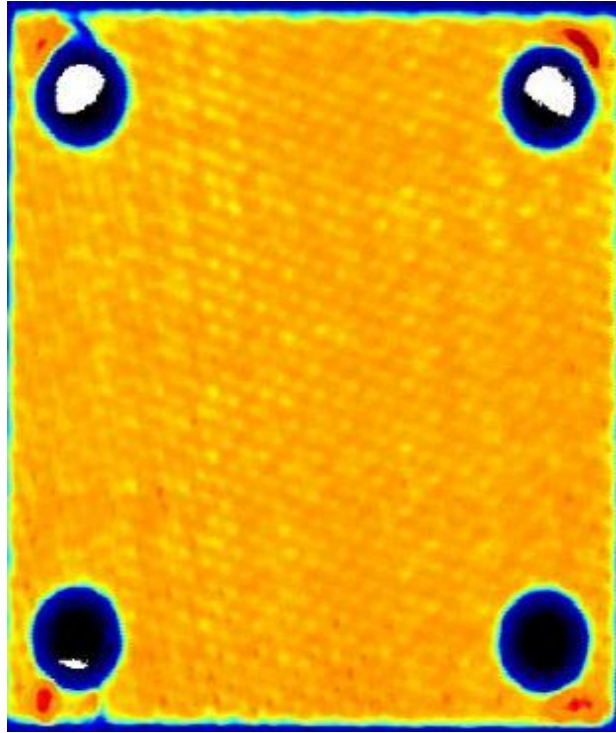


Figure A6. Ultrasonic imaging for SPR = 2, N = 12 test specimen 3. Yellow/orange regions indicate no damage.

Table A4. Damage in each layer of SPR = 2, N = 12 specimen 3 based on CT scans.

Lamina	Lamina damage	Interlaminar layer	Interlaminar damage
1	no damage	1	no damage
2	no damage	2	no damage
3	no damage	3	no damage
4	no damage	4	no damage
5	no damage	5	no damage
6	no damage	6	no damage
7	no damage	7	no damage
8	no damage	8	no damage
9	no damage	9	no damage
10	no damage	10	no damage
11	no damage	11	no damage
12	no damage		

A.1.2.2. Specimen 4

Specimen 4 is loaded past the proportional limit, to the bottom of the “valley” that occurs after this point. Out-of-plane matrix damage and delamination are observed on this test specimen.

Ultrasonic imaging (Figure A7) and a description of each lamina/interlaminar region (Table A5) follow.

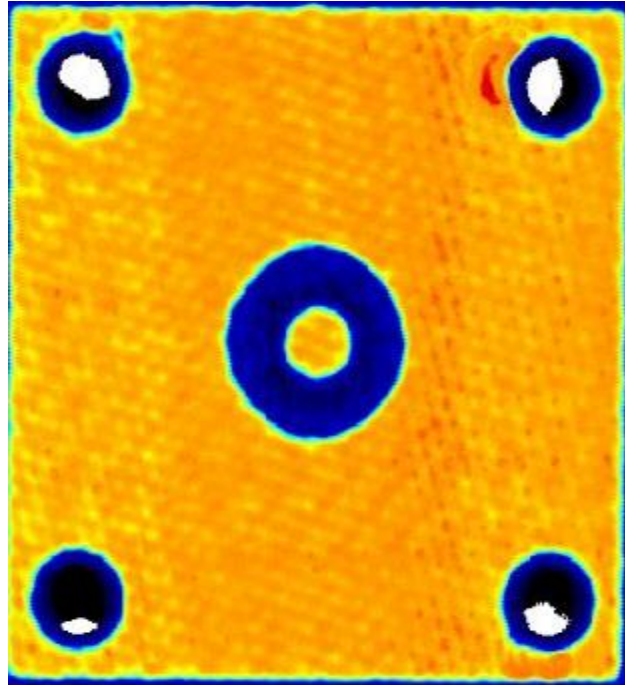


Figure A7. Ultrasonic imaging for SPR = 2, N = 12 test specimen 4. Yellow/orange regions indicate no damage.

Table A5. Damage in each layer of SPR = 2, N = 12 specimen 4 based on CT scans.

Lamina	Lamina damage	Interlaminar layer	Interlaminar damage
1	out-of-plane matrix damage around punch	1	minimal delamination around punch
2	minimal out-of-plane matrix damage around punch	2	minimal delamination around punch
3	no damage	3	region of delamination about 1.2x radius of punch
4	no damage	4	likely delamination about 1.4x radius of punch
5	no damage	5	possible delamination about 1.4x radius of punch
6	no damage	6	possible delamination about 1.4x radius of punch
7	no damage	7	possible delamination about 1.4x radius of punch
8	no damage	8	possible delamination about 1.4x radius of punch
9	no damage	9	possible delamination about 1.4x radius of punch

10	no damage	10	no damage
11	no damage	11	no damage
12	no damage		

A.1.2.3. Specimen 5

Specimen 5 is loaded to roughly the maximum load carrying capacity of the test geometry. Out-of-plane fiber and matrix damage and delamination are observed on this test specimen. Ultrasonic imaging (Figure A8) and a description of each lamina/interlaminar region (Table A6) follow.

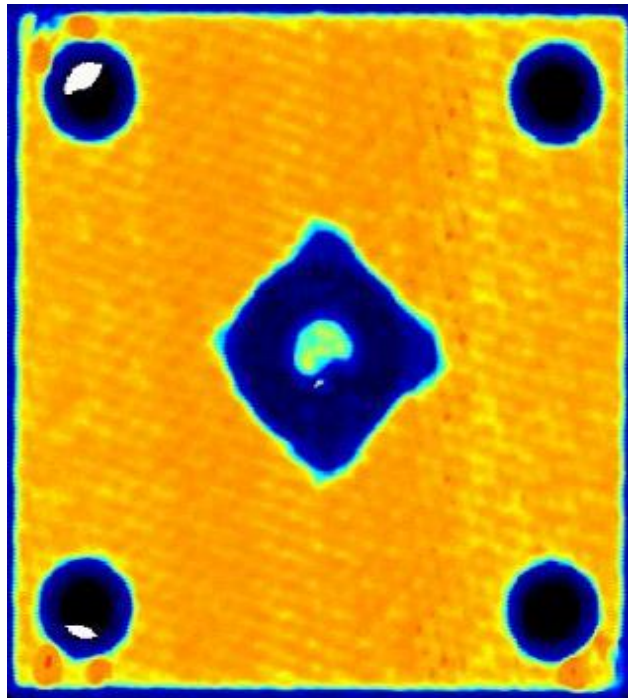


Figure A8. Ultrasonic imaging for SPR = 2, N = 12 test specimen 5. Yellow/orange regions indicate no damage.

Table A6. Damage in each layer of SPR = 2, N = 12 specimen 5 based on CT scans.

Lamina	Lamina damage	Interlaminar layer	Interlaminar damage
1	punch-through failure around punch (fiber damage)	1	delamination in the immediate vicinity of the punch
2	punch-through failure around punch (fiber damage)	2	region of delamination about 2x radius of punch
3	punch-through failure around punch (fiber damage)	3	region of delamination about 2.2x radius of punch
4	punch-through failure around punch (fiber damage)	4	region of delamination about 2.2x radius of punch
5	punch-through failure around	5	region of delamination about 2.2x

	punch (fiber damage)		radius of punch
6	out-of-plane matrix damage around punch	6	region of delamination about 2.2x radius of punch
7	minimal out-of-plane matrix damage around punch	7	region of delamination about 2x radius of punch
8	no damage	8	region of delamination about 2x radius of punch
9	no damage	9	region of delamination about 2x radius of punch
10	no damage	10	region of delamination about 2x radius of punch
11	no damage	11	region of delamination about 1.7x radius of punch
12	no damage		

A.1.3. $SPR = 2$, $N = 24$ specimens

For convenience, Figure 4 is repeated below (in Figure A9). Specifically, Specimen 3, Specimen 4, and Specimen 5 will be evaluated in this section. Based on evaluation of these samples, the following damage is observed:

- Specimen 3 (loaded until before proportional limit was reached) – ultrasonic imaging indicates a small, slightly damaged region around the indenter (possible delamination); CT scans did not show any damage
- Specimen 4 (loaded past proportional limit, within “valley” of force/displacement curve) – ultrasonic imaging clearly indicates a damaged region two to three times the radius of the indenter; CT scans demonstrate matrix damage around the indenter in the top lamina and likely delamination through every interlaminar region of the specimen
- Specimen 5 (loaded to maximum load, immediately preceding complete failure of the test specimen) – ultrasonic imaging demonstrates a diamond-shaped damaged region about 1.75 times larger than the damaged region in Specimen 4; CT scans illustrate fiber damage and matrix damage in all layers of lamina and a region of delamination slightly larger than twice the size of the indenter propagating through all interlaminar regions

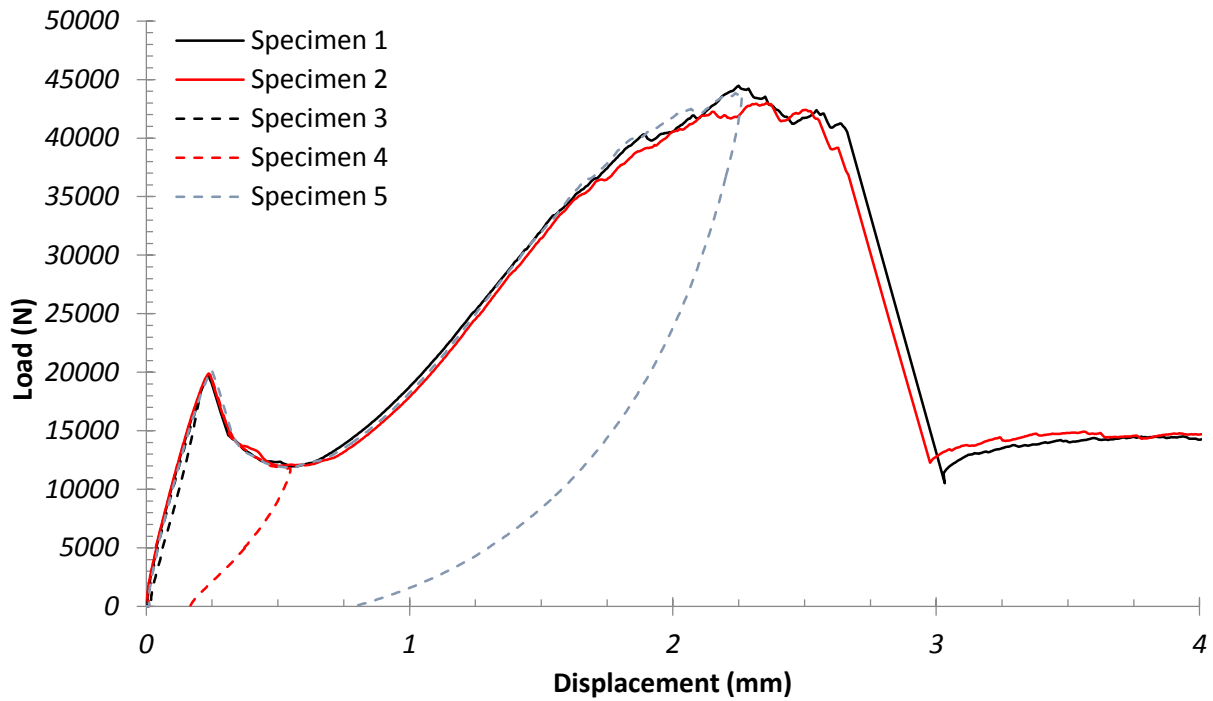


Figure A9. Force/displacement curves for SPR = 2, N = 24 test specimens.

A.1.3.1. Specimen 3

Specimen 3 is loaded to before the proportional limit for this geometry. CT scans of the test specimen indicate no damage; however, ultrasonic imaging shows a small, somewhat damaged region around the indenter. Ultrasonic imaging (Figure A10) and a description of each lamina/interlaminar region (Table A7) follow.

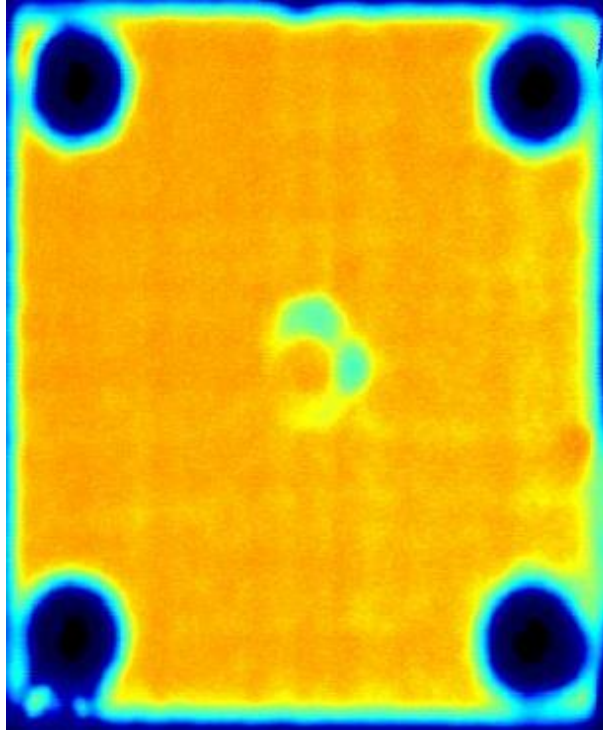


Figure A10. Ultrasonic imaging for SPR = 2, N = 24 test specimen 3. Yellow/orange regions indicate no damage.

Table A7. Damage in each layer of SPR = 2, N = 24 specimen 3 based on CT scans.

Lamina	Lamina damage	Interlaminar layer	Interlaminar damage
1	no damage	1	no damage
2	no damage	2	no damage
3	no damage	3	no damage
4	no damage	4	no damage
5	no damage	5	no damage
6	no damage	6	no damage
7	no damage	7	no damage
8	no damage	8	no damage
9	no damage	9	no damage
10	no damage	10	no damage
11	no damage	11	no damage
12	no damage	12	no damage
13	no damage	13	no damage
14	no damage	14	no damage
15	no damage	15	no damage
16	no damage	16	no damage
17	no damage	17	no damage

18	no damage	18	no damage
19	no damage	19	no damage
20	no damage	20	no damage
21	no damage	21	no damage
22	no damage	22	no damage
23	no damage	23	no damage
24	no damage		

A.1.3.2. Specimen 4

Specimen 4 is loaded past the proportional limit, to the bottom of the “valley” that occurs after this point. Punch-through failure on the top lamina and delamination are observed on this test specimen. Ultrasonic imaging (Figure A11) and a description of each lamina/interlaminar region (Table A8) follow.

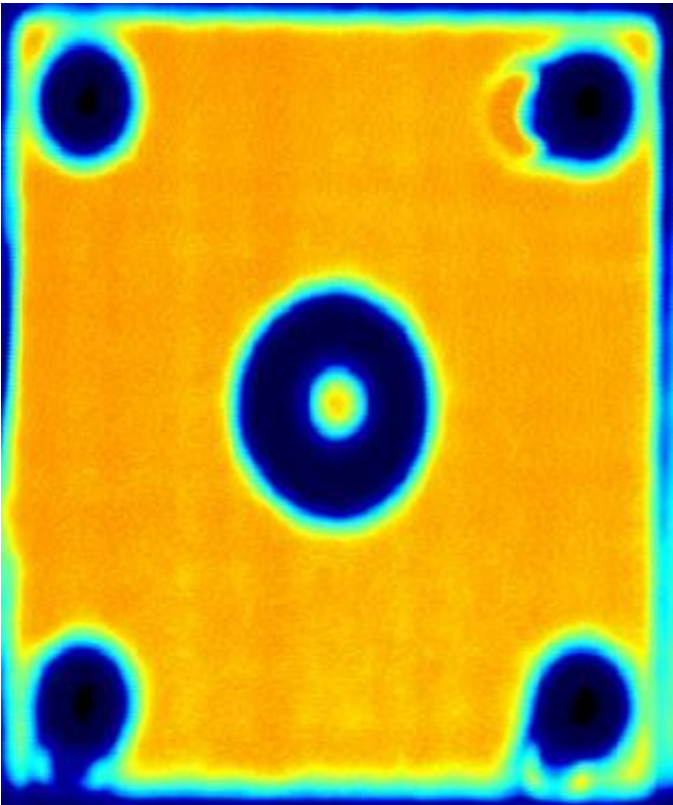


Figure A11. Ultrasonic imaging for SPR = 2, N = 24 test specimen 4. Yellow/orange regions indicate no damage.

Table A8. Damage in each layer of SPR = 2, N = 24 specimen 4 based on CT scans.

Lamina	Lamina damage	Interlaminar layer	Interlaminar damage
1	matrix (and possible fiber) damage and small cracks around punch	1	delamination in the immediate vicinity around the punch
2	out-of-plane matrix damage around punch	2	region of delamination about 1.4x radius of punch
3	minimal out-of-plane matrix damage around punch	3	region of delamination about 1.5x radius of punch
4	no damage	4	region of delamination about 1.5x radius of punch
5	no damage	5	region of delamination about 1.5x radius of punch
6	no damage	6	region of delamination about 1.5x radius of punch
7	no damage	7	region of delamination about 1.5x radius of punch
8	no damage	8	region of delamination about 1.6x radius of punch
9	no damage	9	region of delamination about 1.7x radius of punch
10	no damage	10	region of delamination about 1.7x radius of punch
11	no damage	11	region of delamination about 1.7x radius of punch
12	no damage	12	region of delamination about 1.7x radius of punch
13	no damage	13	region of delamination about 1.7x radius of punch
14	no damage	14	region of delamination about 1.7x radius of punch
15	no damage	15	region of delamination about 1.8x radius of punch
16	no damage	16	region of delamination about 1.8x radius of punch
17	no damage	17	region of delamination about 1.8x radius of punch
18	no damage	18	region of delamination about 1.8x radius of punch
19	no damage	19	region of delamination about 1.9x radius of punch
20	no damage	20	region of delamination about 1.9x radius of punch
21	no damage	21	region of delamination about 1.9x radius of punch

22	no damage	22	region of delamination about 1.9x radius of punch
23	no damage	23	likely delamination about 2x radius of punch
24	no damage		

A.1.3.3. Specimen 5

Specimen 5 is loaded to roughly the maximum load carrying capacity of the test geometry. Out-of-plane punch-through failure, fiber crushing, lamina cracking, and delamination are observed on this test specimen. Ultrasonic imaging (Figure A12) and a description of each lamina/interlaminar region (Table A9) follow.

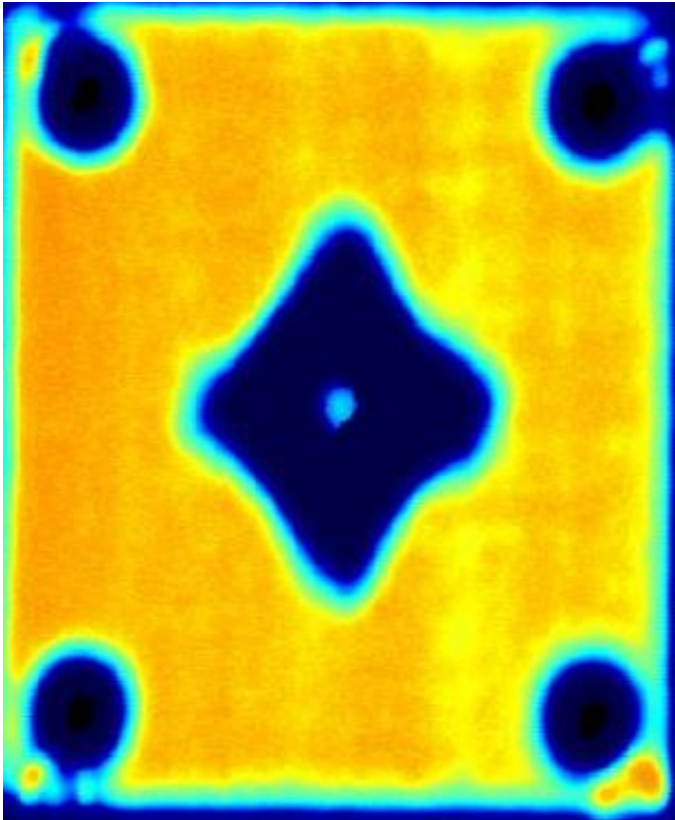


Figure A12. Ultrasonic imaging for SPR = 2, N = 24 test specimen 5. Yellow/orange regions indicate no damage.

Table A9. Damage in each layer of SPR = 2, N = 24 specimen 5 based on CT scans.

Lamina	Lamina damage	Interlaminar layer	Interlaminar damage
1	punch-through failure around punch (matrix and fiber damage)	1	delamination in the immediate vicinity around the punch
2	punch-through failure around punch (matrix and fiber damage)	2	delamination in the immediate vicinity around the punch
3	punch-through failure around punch (matrix and fiber damage)	3	region of delamination about 1.3x radius of punch
4	punch-through failure around punch (matrix and fiber damage)	4	region of delamination about 1.7x radius of punch
5	punch-through failure around punch (matrix and fiber damage)	5	region of delamination about 2x radius of punch
6	punch-through failure around punch (matrix and fiber damage)	6	region of delamination about 2x radius of punch
7	punch-through failure around punch (matrix and fiber damage)	7	region of delamination about 2.2x radius of punch
8	punch-through failure around punch (matrix and fiber damage)	8	region of delamination about 2.2x radius of punch
9	punch-through failure around punch (matrix and fiber damage)	9	region of delamination about 2.3x radius of punch
10	minimal out-of-plane matrix damage around punch; square cracking about 1.2x radius of punch	10	region of delamination about 2.3x radius of punch
11	square cracking about 1.2x radius of punch	11	region of delamination about 2.3x radius of punch
12	square cracking about 1.2x radius of punch	12	region of delamination about 2.3x radius of punch
13	square cracking about 1.2x radius of punch	13	region of delamination about 2.3x radius of punch
14	square cracking about 1.4x radius of punch	14	region of delamination about 2.3x radius of punch
15	square cracking about 1.4x radius of punch	15	region of delamination about 2.3x radius of punch
16	square cracking about 1.6x radius of punch	16	region of delamination about 2.3x radius of punch

17	square cracking about 1.7x radius of punch	17	region of delamination about 2.3x radius of punch
18	square cracking about 1.7x radius of punch	18	region of delamination about 2.3x radius of punch
19	square cracking about 1.7x radius of punch	19	region of delamination about 2.3x radius of punch
20	square cracking about 1.8x radius of punch	20	region of delamination about 2.3x radius of punch
21	square cracking about 1.9x radius of punch	21	region of delamination about 2.3x radius of punch
22	square cracking about 2x radius of punch	22	region of delamination about 2.3x radius of punch
23	square cracking about 2x radius of punch	23	region of delamination about 2.3x radius of punch
24	square cracking about 2.1x radius of punch		

A.1.4. SPR = 8, N = 6 specimens

For convenience, Figure 5 is repeated below (in Figure A13). Specifically, Specimen 3 and Specimen 4 will be evaluated in this section. Based on evaluation of these samples, the following damage is observed:

- Specimen 3 (displaced to about 80% of ultimate failure displacement) – ultrasonic imaging gives a small region of damage near the indenter; CT scans demonstrate some punch-through (fiber and matrix damage) and delamination immediately around the punch
- Specimen 4 (displaced to about 92% of ultimate failure displacement) – ultrasonic imaging demonstrates a slightly larger region of damage compared to Specimen 3; CT scans demonstrate fiber and matrix damage beginning to propagate through all lamina as well as delamination in regions around the punch

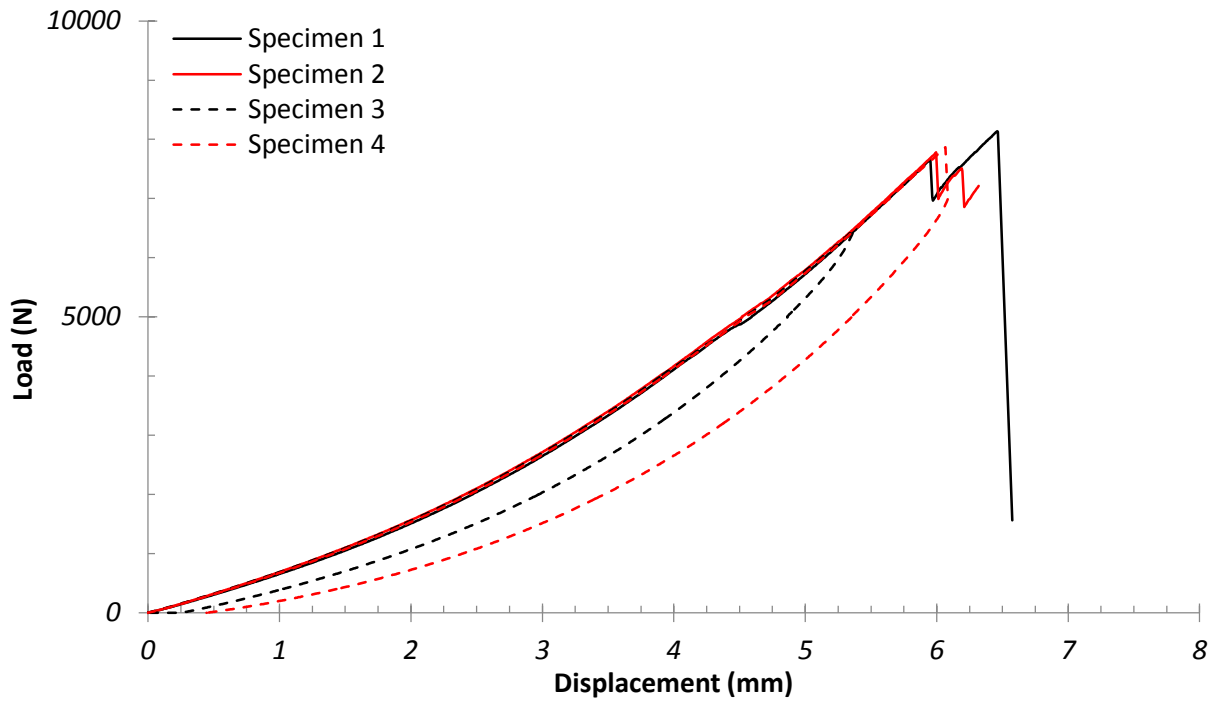


Figure A13. Force/displacement curves for SPR = 8, N = 6 test specimens.

A.1.4.1. Specimen 3

Specimen 3 is loaded to approximately 80% of ultimate failure deformation for this geometry. Punch-through, fiber crushing, and delamination are visible on the test specimen. Ultrasonic imaging (Figure A14) and a description of each lamina/interlaminar region (Table A10) follow.

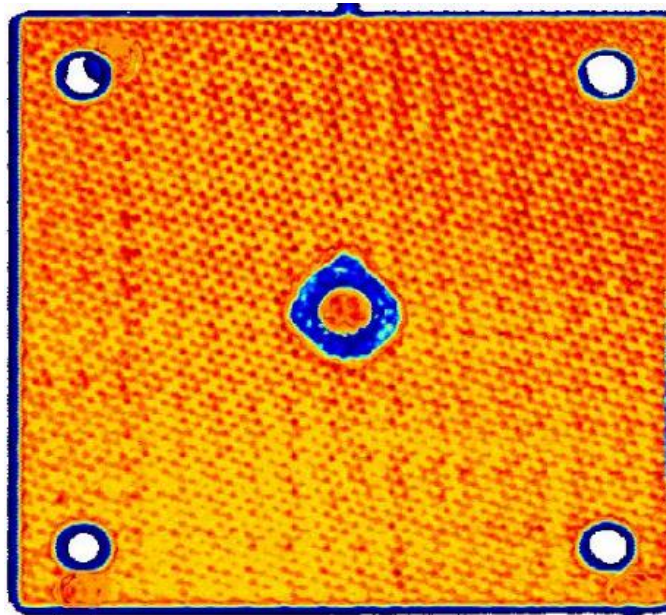


Figure A14. Ultrasonic imaging for SPR = 8, N = 6 test specimen 3. Yellow/orange regions indicate no damage.

Table A10. Damage in each layer of SPR = 8, N = 6 specimen 3 based on CT scans.

Lamina	Lamina damage	Interlaminar layer	Interlaminar damage
1	punch-through failure, matrix/fiber damage	1	delamination around cracked/punched region
2	slight out-of-plane matrix damage	2	delamination around cracked/punched region
3	slight out-of-plane matrix damage	3	region of delamination about 1.5x size of punch
4	no damage	4	region of delamination about 1.5x size of punch
5	no damage	5	no damage
6	no damage		

A.1.4.2. Specimen 4

Specimen 4 is loaded to 92% of the ultimate failure displacement for this geometry. Punch-through (caused by fiber and matrix damage) and delamination are observed in this specimen. Ultrasonic imaging (Figure A15) and a description of each lamina/interlaminar region (Table A11) follow.

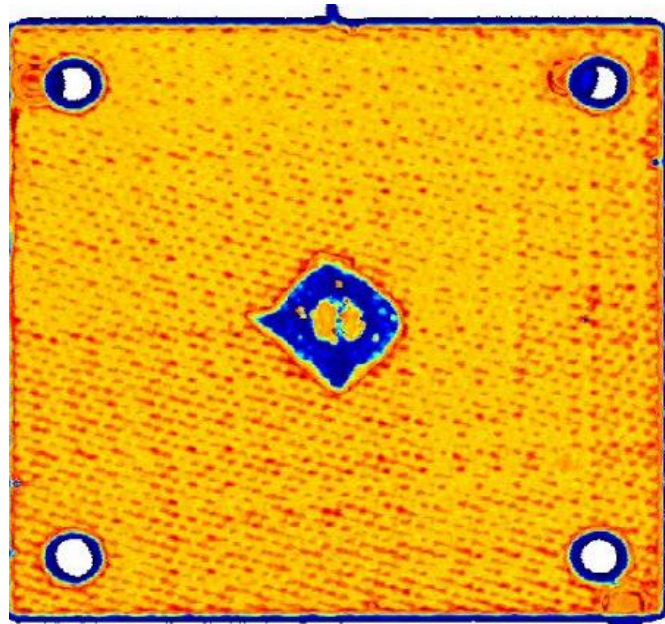


Figure A15. Ultrasonic imaging for SPR = 8, N = 6 test specimen 4. Yellow/orange regions indicate no damage.

Table A11. Damage in each layer of SPR = 8, N = 6 specimen 4 based on CT scans.

Lamina	Lamina damage	Interlaminar layer	Interlaminar damage
1	fiber and matrix damage, lamina cracking	1	delamination around cracked/punched region
2	matrix damage, lamina cracking	2	delamination around cracked/punched region
3	slight matrix damage and lamina cracking	3	region of delamination about 1.5x size of punch
4	no damage	4	region of delamination about 1.65x size of punch
5	some out-of-plane damage to matrix/fiber	5	possible delamination region about 2x size of punch
6	out-of-plane fiber/matrix failure around punch, appears to be some indication of fiber pullout		

A.1.5. SPR = 8, N = 12 specimens

For convenience, Figure 6 is repeated below (in Figure A16). Specifically, Specimen 3, Specimen 4, and Specimen 5 will be evaluated in this section. Based on evaluation of these samples, the following damage is observed:

- Specimen 3 (loaded until before proportional limit was reached) – ultrasonic imaging indicates a small, slightly damaged region around the radius of the indenter; CT scans indicate no damage
- Specimen 4 (displaced past proportional limit, ultimately to 33 percent of failure displacement) – ultrasonic imaging clearly indicates a damaged region slightly larger than twice the radius of the indenter; CT scans demonstrate fiber and matrix damage around the indenter in the top lamina and likely delamination from the top to two-thirds through the specimen
- Specimen 5 (displaced to approximately 60 percent of failure displacement for the test geometry) – ultrasonic imaging demonstrates a diamond-shaped damaged region slightly larger than Specimen 4; CT scans illustrate punch-through failure (fiber/matrix damage) in the first 5 layers of lamina and delamination propagating around the indenter through all interlaminar regions of the specimen

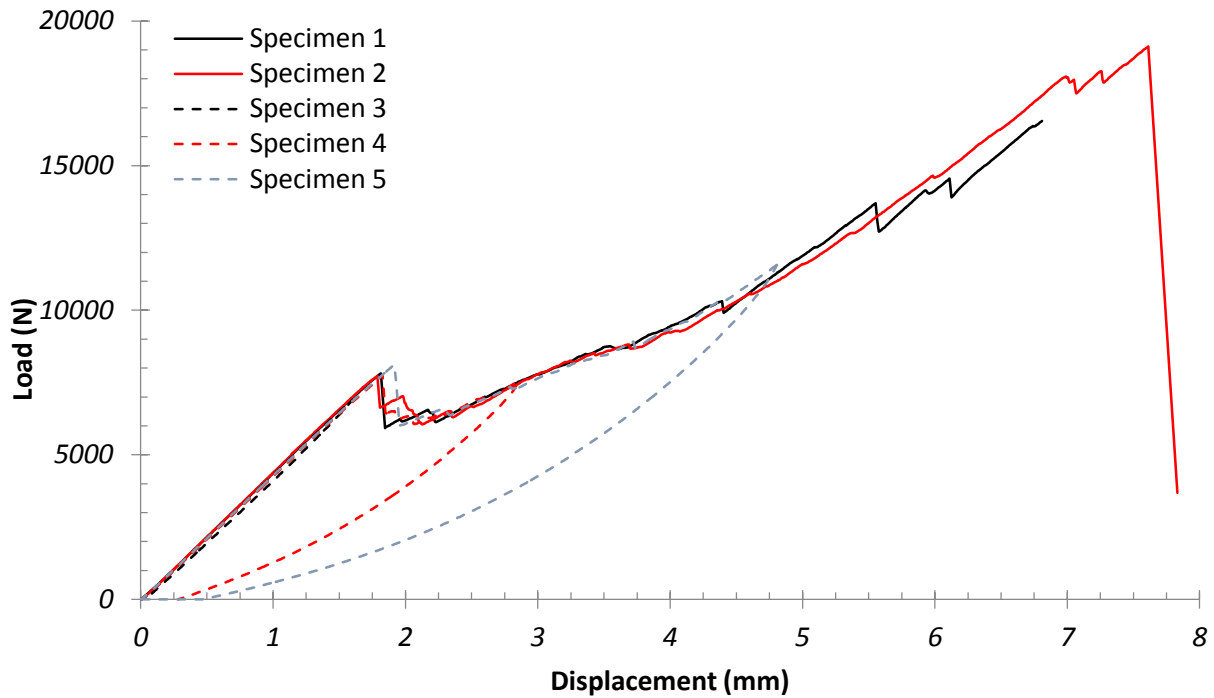


Figure A16. Force/displacement curves for SPR = 2, N = 12 test specimens.

A.1.5.1. Specimen 3

Specimen 3 is not loaded past the proportional limit of the force/displacement curve. CT scans show no damage in the specimen; however ultrasonic imaging indicates some damage. Ultrasonic imaging (Figure A17) and a description of each lamina/interlaminar region (Table A12) follow.

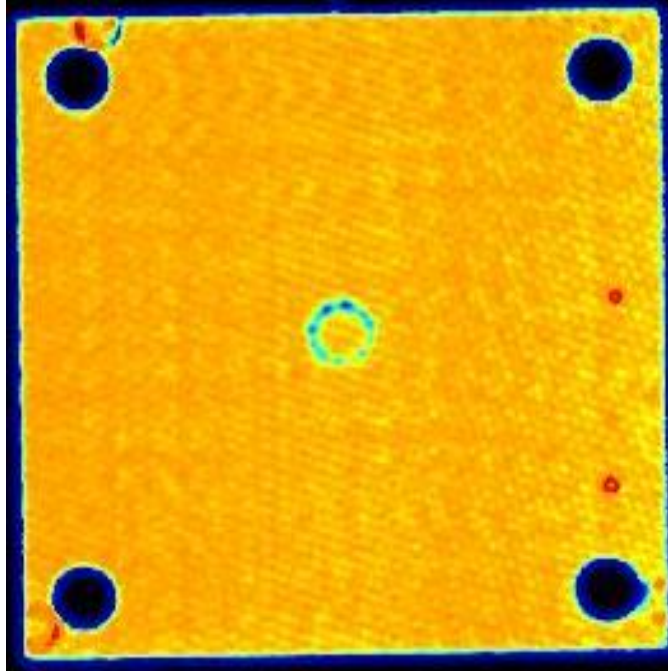


Figure A17. Ultrasonic imaging for SPR = 8, N = 12 test specimen 3. Yellow/orange regions indicate no damage.

Table A12. Damage in each layer of SPR = 8, N = 12 specimen 3 based on CT scans.

Lamina	Lamina damage	Interlaminar layer	Interlaminar damage
1	no damage	1	no damage
2	no damage	2	no damage
3	no damage	3	no damage
4	no damage	4	no damage
5	no damage	5	no damage
6	no damage	6	no damage
7	no damage	7	no damage
8	no damage	8	no damage
9	no damage	9	no damage
10	no damage	10	no damage
11	no damage	11	no damage
12	no damage		

A.1.5.2. Specimen 4

Specimen 4 is loaded past the proportional limit, just after the bottom of the “valley” of the force/displacement curve. Out-of-plane matrix/fiber damage, lamina cracking, and delamination are observed on this test specimen. Ultrasonic imaging (Figure A18) and a description of each lamina/interlaminar region (Table A13) follow.

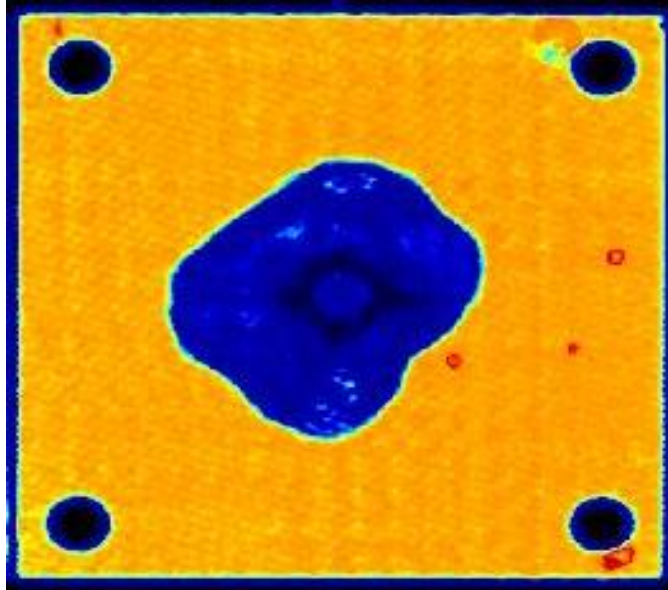


Figure A18. Ultrasonic imaging for SPR = 8, N = 12 test specimen 4. Yellow/orange regions indicate no damage.

Table A13. Damage in each layer of SPR = 8, N = 12 specimen 4 based on CT scans.

Lamina	Lamina damage	Interlaminar layer	Interlaminar damage
1	out-of-plane matrix/fiber damage, matrix/fiber cracking	1	delamination around cracked/punched region
2	out-of-plane matrix/fiber damage, matrix/fiber cracking	2	delamination around cracked/punched region
3	slight out-of-plane matrix damage	3	region of delamination about 1.25x size of punch
4	no damage	4	region of delamination about 1.5x size of punch
5	no damage	5	region of delamination about 2x size of punch
6	no damage	6	region of delamination about 2x size of punch
7	no damage	7	region of delamination about 3x size of punch
8	no damage	8	region of delamination about 2.5x size of punch
9	no damage	9	no damage
10	no damage	10	no damage
11	no damage	11	no damage
12	no damage		

A.1.5.3. Specimen 5

Specimen 5 is loaded to roughly 60 percent of the maximum displacement for the test geometry before ultimate failure occurs. Out-of-plane matrix/fiber damage, lamina cracking, and delamination are observed on this test specimen. Ultrasonic imaging (Figure A19) and a description of each lamina/interlaminar region (Table A14) follow.

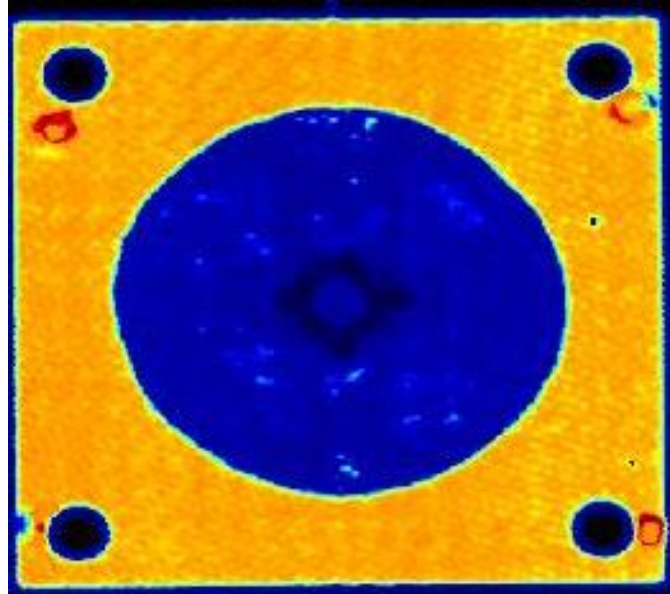


Figure A19. Ultrasonic imaging for SPR = 8, N = 12 test specimen 5. Yellow/orange regions indicate no damage.

Table A14. Damage in each layer of SPR = 8, N = 12 specimen 5 based on CT scans.

Lamina	Lamina damage	Interlaminar layer	Interlaminar damage
1	punch-through around punch (matrix/fiber damage), lamina cracking	1	delamination around cracked/punched region
2	punch-through around punch (matrix/fiber damage), lamina cracking	2	delamination around cracked/punched region, about 1.4x size of punch
3	matrix damage, some fiber damage possible	3	region of delamination about 1.5x size of punch
4	no damage	4	region of delamination about 1.5x size of punch
5	no damage	5	region of delamination about 2x size of punch, growing region of delamination below punch
6	no damage	6	large region of delamination about 5x size of punch
7	no damage	7	large region of delamination about 7x

			size of punch
8	no damage	8	large region of delamination about 7x size of punch
9	no damage	9	possible region of delamination, about 5x size of punch
10	no damage	10	no damage
11	no damage	11	no damage
12	no damage		

A.1.6. SPR = 8, N = 24 specimens

For convenience, Figure 7 is repeated below (in Figure A20). Specifically, Specimen 3, Specimen 4, Specimen 5, Specimen 6, Specimen 7, and Specimen 8 will be evaluated in this section. Based on evaluation of these samples, the following damage is observed:

- Specimen 3 (loaded until before proportional limit was reached) – ultrasonic imaging shows small region of damage around indenter; no damage visible on CT scans
- Specimen 4 (displaced to past proportional limit, up to 15 percent of ultimate failure displacement) – ultrasonic imaging clearly indicates a damaged region four times the radius of the indenter; CT scans demonstrate fiber and matrix damage around the indenter in the two to three top lamina, a relatively small region of delamination surrounding the indenter, and a larger, cross-shaped region of delamination about half way through the depth of the specimen
- Specimen 5 (displaced to past proportional limit, up to 25 percent of ultimate failure displacement) – ultrasonic imaging demonstrates a damaged region six to seven times the radius of the indenter; CT scans demonstrate fiber and matrix damage around the indenter in the top two to three lamina and a region of delamination surrounding the indenter evolving into a larger, cross-shaped region of delamination about half way through the depth of the specimen
- Specimen 6 (displaced to past proportional limit, up to 40 percent of ultimate failure displacement) – ultrasonic imaging demonstrates a circular damaged region six times the radius of the indenter; CT scans demonstrate fiber and matrix damage around the indenter in the top four lamina, lamina cracking, and a region of delamination surrounding the indenter evolving into a larger region of delamination (6x indenter radius) about half way through the depth of the specimen
- Specimen 7 (displaced to past proportional limit, up to 45 percent of ultimate failure displacement) – ultrasonic imaging demonstrates a damaged region seven times the radius of the indenter; CT scans demonstrate fiber and matrix damage around the indenter in the top four lamina, lamina cracking, and a region of delamination surrounding the indenter evolving into a larger, cross-shaped region of delamination about half way through the depth of the specimen and finally a large, circular region of delamination toward the bottom of the specimen
- Specimen 8 (displaced to past proportional limit, up to 75 percent of ultimate failure displacement) – ultrasonic imaging demonstrates a circular, damaged region seven times the radius of the indenter; CT scans demonstrate fiber and matrix around the indenter in the top four lamina, lamina cracking, and a region of delamination surrounding the indenter evolving into a larger, cross-shaped region of delamination about half way through the depth of the specimen and finally a large, circular region of delamination toward the bottom of the specimen

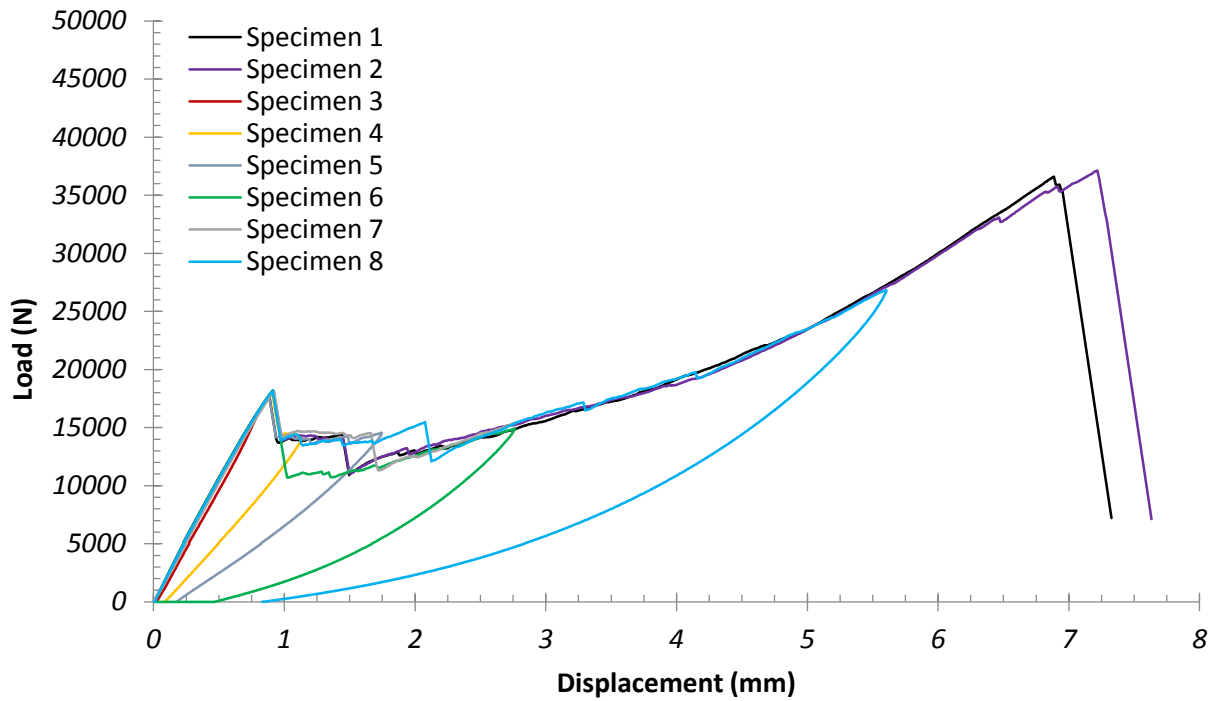


Figure A20. Force/displacement curves for SPR = 8, N = 24 test specimens.

A.1.6.1. Specimen 3

Specimen 3 is loaded to before the proportional limit for this geometry. No damage is observed on this test specimen in the CT scans, though ultrasonic imaging indicates some damage around the indenter. Ultrasonic imaging (Figure A21) and a description of each lamina/interlaminar region (Table A15) follow.

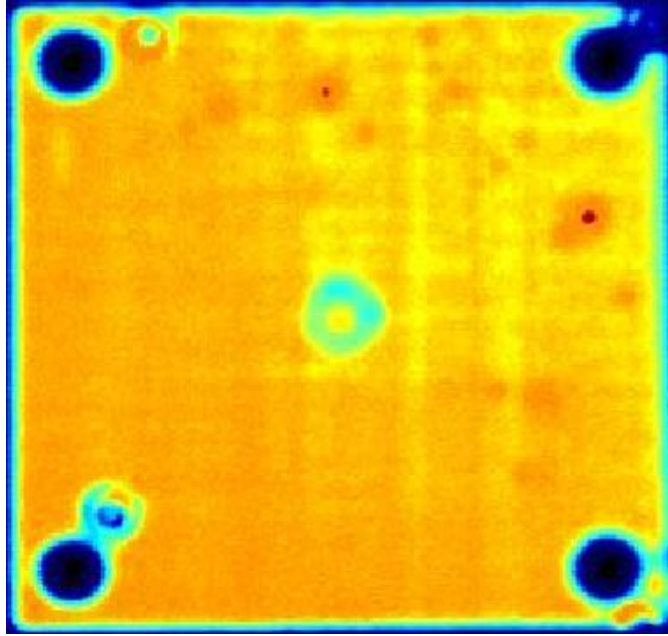


Figure A21. Ultrasonic imaging for SPR = 8, N = 24 test specimen 3. Yellow/orange regions indicate no damage.

Table A15. Damage in each layer of SPR = 8, N = 24 specimen 3 based on CT scans.

Lamina	Lamina damage	Interlaminar layer	Interlaminar damage
1	no damage	1	no damage
2	no damage	2	no damage
3	no damage	3	no damage
4	no damage	4	no damage
5	no damage	5	no damage
6	no damage	6	no damage
7	no damage	7	no damage
8	no damage	8	no damage
9	no damage	9	no damage
10	no damage	10	no damage
11	no damage	11	no damage
12	no damage	12	no damage
13	no damage	13	no damage
14	no damage	14	no damage
15	no damage	15	no damage
16	no damage	16	no damage
17	no damage	17	no damage
18	no damage	18	no damage
19	no damage	19	no damage
20	no damage	20	no damage

21	no damage	21	no damage
22	no damage	22	no damage
23	no damage	23	no damage
24	no damage		

A.1.6.2. Specimen 4

Specimen 4 is loaded past the proportional limit, to 15 percent the ultimate failure displacement of the test specimen. Punch-through failure (matrix/fiber damage) in the top two lamina and delamination are observed on this test specimen. Ultrasonic imaging (Figure A22) and a description of each lamina/interlaminar region (Table A16) follow.

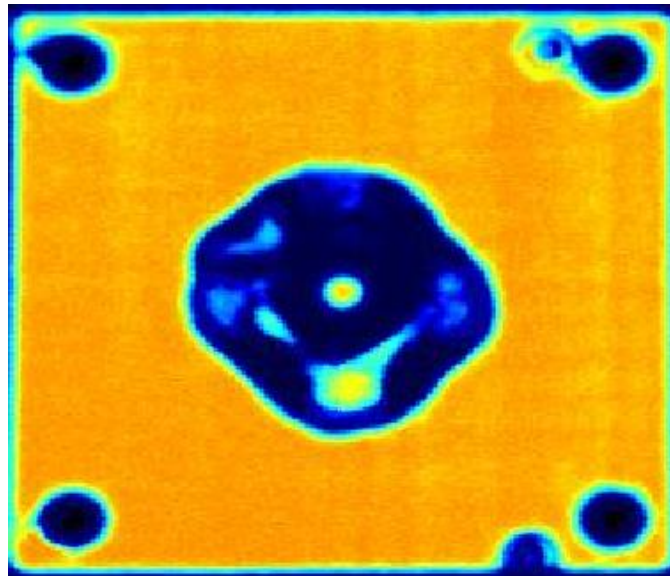


Figure A22. Ultrasonic imaging for SPR = 8, N = 24 test specimen 4. Yellow/orange regions indicate no damage.

Table A16. Damage in each layer of SPR = 8, N = 24 specimen 4 based on CT scans.

Lamina	Lamina damage	Interlaminar layer	Interlaminar damage
1	matrix/fiber damage around punch	1	delamination immediately around punch radius
2	matrix/fiber damage around punch	2	region of delamination about 1.2x radius of punch
3	possible matrix/fiber damage	3	region of delamination about 1.3x radius of punch
4	no damage	4	region of delamination about 1.3x radius of punch
5	no damage	5	region of delamination about 1.4x radius of punch
6	no damage	6	region of delamination about 1.4x

			radius of punch
7	no damage	7	region of delamination about 1.7x radius of punch
8	no damage	8	region of delamination about 1.7x radius of punch
9	no damage	9	possible region of delamination about 1.7x radius of punch
10	no damage	10	no damage
11	no damage	11	possible cross-shaped region of delamination about 3x radius of punch
12	no damage	12	possible cross-shaped region of delamination about 3x radius of punch
13	no damage	13	possible cross-shaped region of delamination about 3x radius of punch
14	no damage	14	no damage
15	no damage	15	no damage
16	no damage	16	no damage
17	no damage	17	no damage
18	no damage	18	no damage
19	no damage	19	no damage
20	no damage	20	no damage
21	no damage	21	no damage
22	no damage	22	no damage
23	no damage	23	no damage
24	no damage		

A.1.6.3. Specimen 5

Specimen 5 is loaded past the proportional limit, to 25 percent the ultimate failure displacement of the test specimen. Punch-through failure (matrix/fiber damage) in the top three lamina, lamina cracking, and delamination are observed on this test specimen. Ultrasonic imaging (Figure A23) and a description of each lamina/interlaminar region (Table A17) follow.

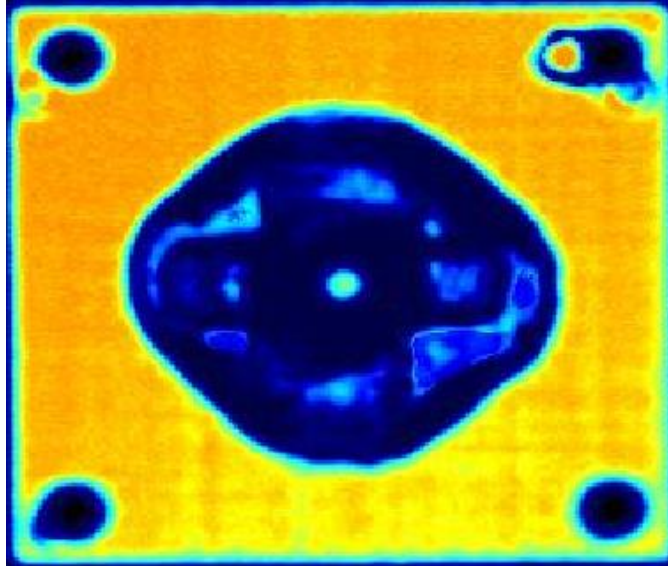


Figure A23. Ultrasonic imaging for SPR = 8, N = 24 test specimen 5. Yellow/orange regions indicate no damage.

Table A17. Damage in each layer of SPR = 8, N = 24 specimen 5 based on CT scans.

Lamina	Lamina damage	Interlaminar layer	Interlaminar damage
1	matrix/fiber damage around punch, lamina cracking	1	delamination immediately around punch radius
2	matrix/fiber damage around punch, lamina cracking	2	region of delamination about 1.5x radius of punch
3	possible matrix/fiber damage	3	region of delamination about 1.7x radius of punch
4	no damage	4	region of delamination about 2x radius of punch
5	no damage	5	region of delamination about 2x radius of punch
6	no damage	6	region of delamination about 2.1x radius of punch
7	no damage	7	region of delamination about 2.5x radius of punch
8	no damage	8	region of delamination up to about 3x radius of punch
9	no damage	9	region of delamination up to about 3x radius of punch
10	no damage	10	region of delamination up to about 3.5x radius of punch
11	no damage	11	cross-shaped region of delamination

			about 5x radius of punch
12	no damage	12	cross-shaped region of delamination about 7x radius of punch
13	no damage	13	cross-shaped region of delamination about 7x radius of punch
14	no damage	14	cross-shaped region of delamination about 7x radius of punch
15	no damage	15	possible cross-shaped region of delamination about 7x radius of punch
16	no damage	16	possible cross-shaped region of delamination about 7x radius of punch
17	no damage	17	possible region of delamination about 7x radius of punch
18	no damage	18	possible region of delamination about 7x radius of punch
19	no damage	19	no damage
20	no damage	20	no damage
21	no damage	21	no damage
22	no damage	22	no damage
23	no damage	23	no damage
24	no damage		

A.1.6.4. Specimen 6

Specimen 6 is loaded past the proportional limit, to 40 percent the ultimate failure displacement of the test specimen. Punch-through failure (matrix/fiber damage) in the top three lamina, lamina cracking, and delamination are observed on this test specimen. Ultrasonic imaging (Figure A24) and a description of each lamina/interlaminar region (Table A18) follow.

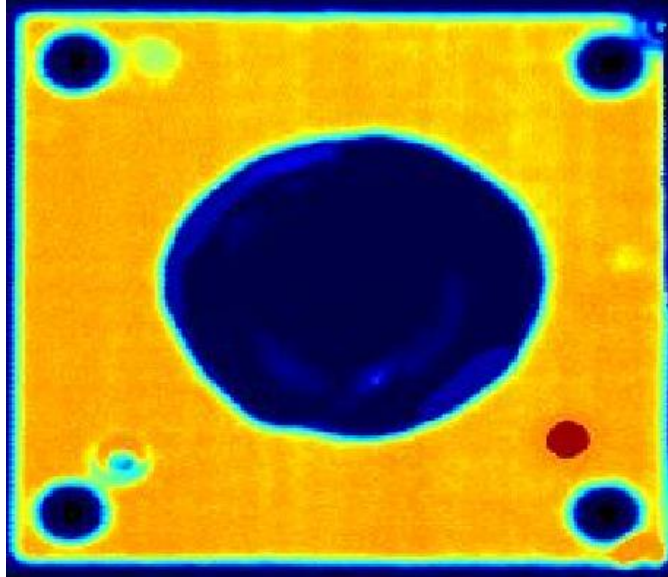


Figure A24. Ultrasonic imaging for SPR = 8, N = 24 test specimen 6. Yellow/orange regions indicate no damage.

Table A18. Damage in each layer of SPR = 8, N = 24 specimen 6 based on CT scans.

Lamina	Lamina damage	Interlaminar layer	Interlaminar damage
1	matrix/fiber damage around punch, lamina cracking 2x punch radius	1	delamination immediately around punch radius
2	matrix/fiber damage around punch, lamina cracking 2.5x punch radius	2	region of delamination about 3x radius of punch
3	matrix/fiber damage around punch, lamina cracking 2.5x punch radius	3	region of delamination about 3x radius of punch
4	slight matrix damage	4	region of delamination about 3.2x radius of punch
5	no damage	5	region of delamination about 3.2x radius of punch
6	no damage	6	region of delamination about 3.5x radius of punch
7	no damage	7	region of delamination about 3.5x radius of punch
8	no damage	8	region of delamination about 3.7x radius of punch
9	no damage	9	region of delamination about 4x radius of punch
10	no damage	10	region of delamination about 4.2x radius of punch

11	no damage	11	region of delamination about 4.5x radius of punch
12	no damage	12	region of delamination up to about 5x radius of punch
13	no damage	13	region of delamination up to about 5x radius of punch
14	no damage	14	cross-shaped region of delamination about 5x radius of punch
15	no damage	15	cross-shaped region of delamination about 6x radius of punch
16	no damage	16	region of delamination about 6x radius of punch
17	no damage	17	possible region of delamination about 6x radius of punch
18	no damage	18	possible region of delamination about 6x radius of punch
19	no damage	19	region of delamination about 6x radius of punch
20	no damage	20	region of delamination about 6x radius of punch
21	no damage	21	possible region of delamination about 6x radius of punch
22	no damage	22	no damage
23	no damage	23	no damage
24	no damage		

A.1.6.5. Specimen 7

Specimen 7 is loaded past the proportional limit, to 45 percent the ultimate failure displacement of the test specimen. Punch-through failure (matrix/fiber damage) in the top three lamina, lamina cracking, and delamination are observed on this test specimen. Ultrasonic imaging (Figure A25) and a description of each lamina/interlaminar region (Table A19) follow.

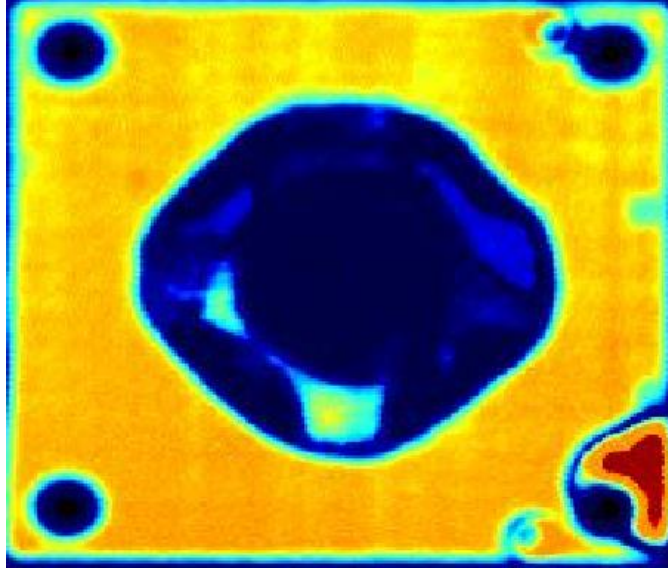


Figure A25. Ultrasonic imaging for SPR = 8, N = 24 test specimen 7. Yellow/orange regions indicate no damage.

Table A19. Damage in each layer of SPR = 8, N = 24 specimen 7 based on CT scans.

Lamina	Lamina damage	Interlaminar layer	Interlaminar damage
1	fiber/matrix damage around punch, lamina cracking 2x punch radius	1	region of delamination about 1.5x radius of punch
2	fiber/matrix damage around punch, lamina cracking 3x punch radius	2	region of delamination about 2.5x radius of punch
3	fiber/matrix damage around punch, lamina cracking 3x punch radius	3	region of delamination about 3x radius of punch
4	slight out-of-plane fiber crushing	4	region of delamination about 3x radius of punch
5	no damage	5	region of delamination about 3.2x radius of punch
6	no damage	6	region of delamination about 3.5x radius of punch
7	no damage	7	region of delamination about 3.5x radius of punch
8	no damage	8	region of delamination about 4x radius of punch
9	no damage	9	region of delamination about 4x radius of punch
10	no damage	10	region of delamination about 4.2x radius of punch

11	no damage	11	cross-shaped region of delamination about 8x radius of punch
12	no damage	12	cross-shaped region of delamination about 8x radius of punch
13	no damage	13	cross-shaped region of delamination about 8x radius of punch
14	no damage	14	cross-shaped region of delamination about 8x radius of punch
15	no damage	15	cross-shaped region of delamination about 8x radius of punch
16	no damage	16	region of delamination about 8x radius of punch
17	no damage	17	possible region of delamination about 5x radius of punch
18	no damage	18	possible region of delamination about 6x radius of punch
19	no damage	19	region of delamination about 5.5x radius of punch
20	no damage	20	region of delamination about 6x radius of punch
21	no damage	21	possible region of delamination about 5x radius of punch
22	no damage	22	no damage
23	no damage	23	no damage
24	no damage		

A.1.6.3. Specimen 8

Specimen 8 is loaded past the proportional limit, to 75 percent the ultimate failure displacement of the test specimen. Punch-through failure (matrix/fiber damage) in the top three lamina, lamina cracking, and delamination are observed on this test specimen. Ultrasonic imaging (Figure A26) and a description of each lamina/interlaminar region (Table A20) follow.

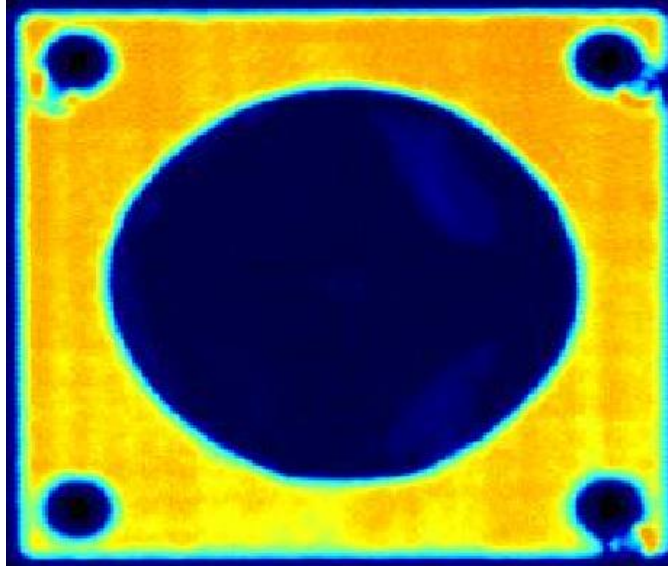


Figure A26. Ultrasonic imaging for SPR = 8, N = 24 test specimen 8. Yellow/orange regions indicate no damage.

Table A20. Damage in each layer of SPR = 8, N = 24 specimen 8 based on CT scans.

Lamina	Lamina damage	Interlaminar layer	Interlaminar damage
1	punch-through failure (matrix/fiber damage) around punch, lamina cracking 5.5x punch radius	1	region of delamination about 1.2x radius of punch
2	punch-through failure (matrix/fiber damage) around punch, lamina cracking 6x punch radius	2	region of delamination about 2.5x radius of punch
3	punch-through failure (matrix/fiber damage) around punch, lamina cracking 6x punch radius	3	diamond shaped region of delamination about 3x radius of punch
4	slight out-of-plane matrix damage	4	region of delamination about 4x radius of punch
5	no damage	5	region of delamination up to about 4.5x radius of punch
6	no damage	6	region of delamination up to about 6.5x radius of punch
7	no damage	7	region of delamination about 6.5x radius of punch
8	no damage	8	region of delamination about 7x radius of punch
9	no damage	9	region of delamination about 7x

			radius of punch
10	no damage	10	region of delamination about 7x radius of punch
11	no damage	11	cross-shaped region of delamination about 8x radius of punch
12	no damage	12	cross-shaped region of delamination about 8x radius of punch
13	no damage	13	cross-shaped region of delamination about 8x radius of punch
14	no damage	14	cross-shaped region of delamination about 8x radius of punch
15	no damage	15	cross-shaped region of delamination about 8x radius of punch
16	no damage	16	cross-shaped region of delamination about 8x radius of punch
17	no damage	17	region of delamination about 7x radius of punch
18	no damage	18	region of delamination about 7x radius of punch
19	no damage	19	region of delamination about 7x radius of punch
20	no damage	20	region of delamination about 6x radius of punch
21	no damage	21	no damage
22	no damage	22	no damage
23	no damage	23	no damage
24	no damage		

A.2. Example CT images

In this section, images of each of the types of damage observed in CT scans are presented. Lamina punch-through failure and lamina cracking are presented in Figure A27. Out-of-plane fiber crushing is presented in Figure A28 and delamination is presented in Figure A29.

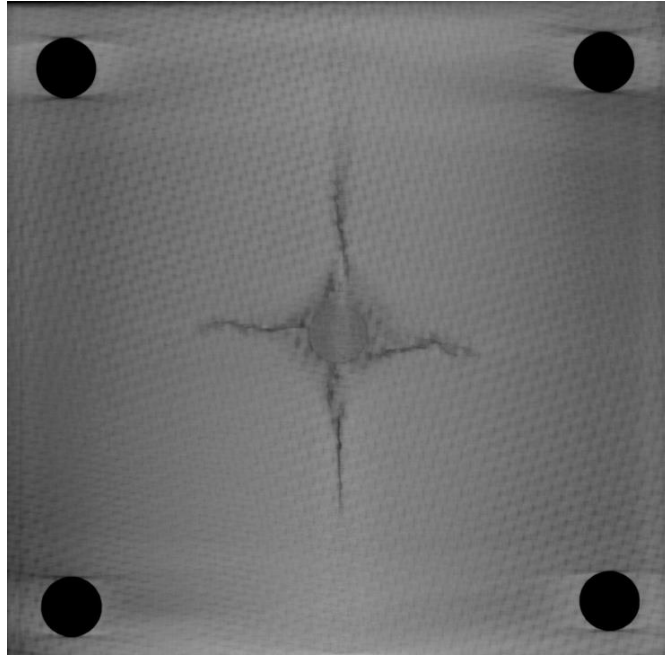


Figure A27. CT scan of out-of-plane lamina punch-through and lamina cracking.

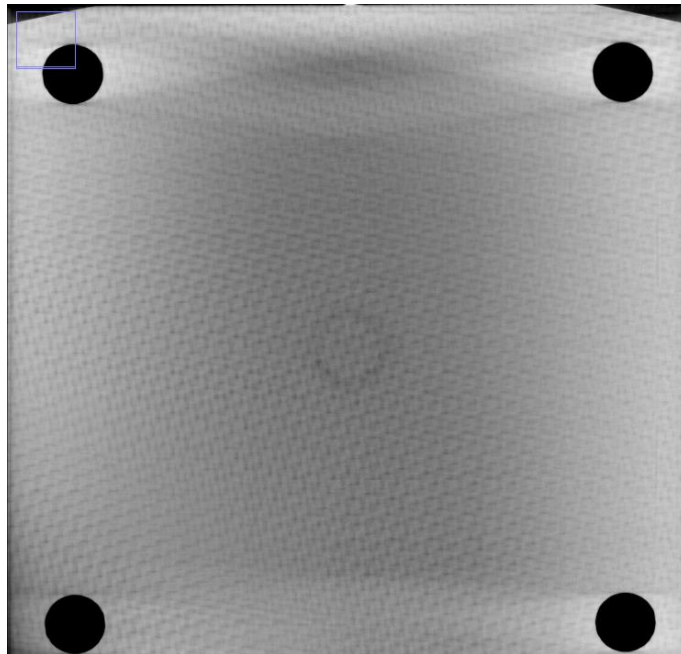


Figure A28. CT scan of out-of-plane fiber crushing (without punch-through).

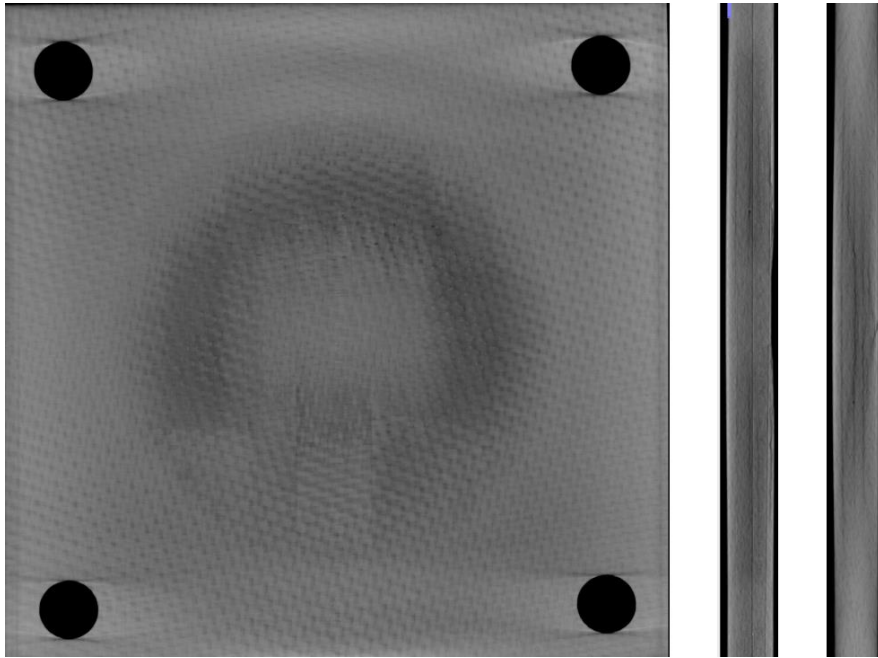


Figure A29. CT scan of delamination (out-of-plane and in-plane scans).

A.3. Observations and Trends

This section presents general observations and trends observed in test results.

- Ultimate failure displacement is only weakly correlated to number of total layers of lamina. The span-to-punch ratio has a much larger effect on the overall displacement of the specimen at ultimate failure.
- In the $SPR = 8, N = 24$ geometry, a cross-like region of delamination is observed roughly half way through the thickness in the majority of test specimens. This feature is exclusive to this test geometry and the prominence of this feature varies from test to test. Tests where the cross-shaped region is prominent contained a second notable “drop” in force in the force/displacement curve. While there are plausible explanations for what is observed, it is unclear what the cause of this phenomena is.

DISTRIBUTION

MS0557	D. Epp	1522 (electronic copy)
MS9042	C. Nilsson	8250 (electronic copy)
MS9042	M. Chiesa	8259 (electronic copy)
MS9106	A. Rohan	8226 (electronic copy)
MS9153	T. Shepodd	8220 (electronic copy)
MS0899	Technical Library	9536 (electronic copy)



Sandia National Laboratories